

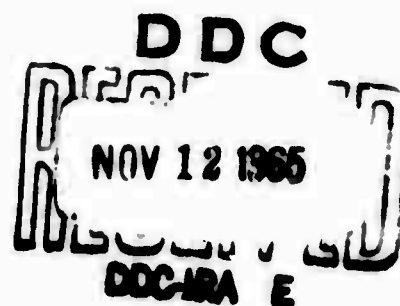
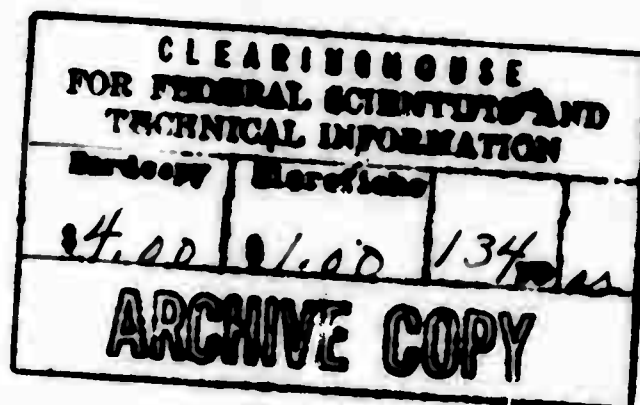
AD623401  
RESEARCH REPORT NO: 64-29

STEADY-STATE ROCKET COMBUSTION OF GASEOUS HYDROGEN  
AND LIQUID OXYGEN. PART II: ANALYSIS FOR  
COAXIAL JET INJECTION

By

L. P. Combs and M. D. Schuman

RESEARCH REPORT



March 1965



**ROCKETDYNE**

A DIVISION OF NORTH AMERICAN AVIATION, INC.  
6833 CANOGA AVENUE, CANOGA PARK, CALIFORNIA


**STEADY-STATE ROCKET COMBUSTION OF GASEOUS HYDROGEN  
AND LIQUID OXYGEN. PART II: ANALYSIS  
FOR COAXIAL JET INJECTION**

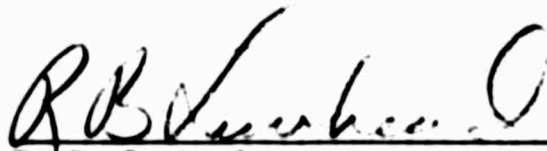
**Research Report 64-29**

**By**

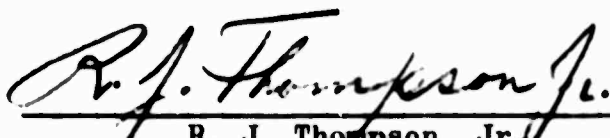
**L. P. Combs and M. D. Schuman**

**Technically Reviewed and Approved By**

  
\_\_\_\_\_  
**T. A. Coultas**  
**Group Scientist**  
**Combustion, Heat Transfer and**  
**Fluid Dynamics**

  
\_\_\_\_\_  
**R. B. Lawhead**  
**Chief**  
**Propulsion Processes & Applications**

**Release Approved By**

  
\_\_\_\_\_  
**R. J. Thompson, Jr.**  
**Vice-President and Director**  
**Research**

**March 1965**



## FOREWORD

The studies reported here were conducted largely under U. S. Air Force Contract AF49(638)-817, monitored by the Air Force Office of Scientific Research, of the Office of Aerospace Sciences. The analytical work was incomplete at the end of that contract. The final formulation of the combustion model was completed with funds from a Rocketdyne Liquid Propellant IR&D program and from Contract NAS 8-19 (J-2 program). The analytical formulation was put into a form useful for predicting combustion characteristics of rocket engines of interest in those programs.

## ACKNOWLEDGMENT

The rudiments of the analytical description for liquid oxygen jet atomization used in this study were suggested by Mr. F. B. Cramer, who also participated in helpful discussions of other parts of the combustion model formulation.



## ABSTRACT

Simultaneous equations describing rocket propellant injection, atomization, mixing, vaporization, and combustion are formulated for a cylindrical liquid oxygen jet surrounded by an annular gaseous hydrogen stream. The formulation is based on division of the combustion chamber into a nonburning region near the injector and a combustion region further downstream. Processes in the nonburning region are required to satisfy certain combustibility criteria before combustion is possible. The propellants then pass through a plane flame front into the combustion region. A simplified treatment of turbulent mixing between unlike reacting gas streams, one of which contains a liquid oxygen spray, characterizes the combustion region model. Solutions of the system of equations, obtained with a digital computer program, are detailed, discussed, and compared favorably with experimental information from Part I.



## CONTENTS

Foreword . . . . .	iii
Abstract . . . . .	v
Summary . . . . .	1
Introduction . . . . .	3
Model Formulation . . . . .	5
Nonburning Injection Region . . . . .	6
Conditions for Combustibility . . . . .	26
Combustion Region . . . . .	28
Calculated Results and Discussion . . . . .	45
Best-Fit Cases . . . . .	45
Model Predictions for Other Mainstage Conditions . . . . .	64
Model Predictions for Prestage Conditions . . . . .	67
Predicted Oscillatory Combustion . . . . .	68
Conclusion . . . . .	69
<u>Appendix A</u>	
Physical, Thermodynamic, and Transport Properties for the Nonburning Region . . . . .	73
<u>Appendix B</u>	
Determination of a Maximum Droplet Size for LOX-Jet Atomization . . . . .	79
<u>Appendix C</u>	
Flammability Limits and Flame Velocities for Fuel-Rich Hydrogen/Oxygen Mixtures . . . . .	83
<u>Appendix D</u>	
Physical, Thermodynamic, and Transport Properties for the Combustion Region . . . . .	87
<u>Appendix E</u>	
Cross-Sectional Areas vs Distance From Injector for Transparent Two-Dimensional Model Rocket . . . . .	91
Nomenclature . . . . .	93
References . . . . .	103
RLR 64-29	vii



## ILLUSTRATIONS

1. Schematic Representation of the Combustion Processes for Coaxial Jet Injection of Gaseous Hydrogen and Liquid Oxygen (Ref. 1)	109
2. Velocity Profiles at Various Distances Downstream From a Coaxial Jet Injection Element (Conceptual)	110
3. Spray Zone Elemental Structure and Gas Flow (Conceptual)	111
4. Calculated Nonburning Region Structure for Condition of Test 417	112
5. Coaxial Jet Injection of Liquid Nitrogen Into Ambient Air (Ref. 14)	113
6. Photograph of Water Jet Atomization From Two Coaxial Jet Elements With Gaseous Nitrogen	114
7. Calculated LOX Spray Characteristics (Nonburning Region)	115
8. Weight Distribution of Spray Being Produced	116
9. LOX-Jet Atomization and Spray Vaporization in the Nonburning Region	117
10. Oxygen Concentration in Gases at the Spray Zone Boundary, Nonburning Region	118
11. Oxygen Concentration Profiles in the Nonburning Spray Zone at Various Distances From the Injector	119
12. Velocities of the Spray Zone Boundary Gases and Selected Droplet Size Groups in the Nonburning Spray Zone	120
13. Spray Element Droplet and Gas Temperatures in the Nonburning Region (Test 417)	121
14. Maximum Equilibrium Oxygen Concentration in Hydrogen-Oxygen Gas Mixtures That Contain LOX Spray	122



15.	Calculated Craya-Curtet Number . . . . .	123
16.	Calculated Combustion Region Characteristics, Test 417 . .	124
17.	Comparison Between Experimental Data and Calculated Velocities and Pressures of the Best-Fit Cases . . . . .	125
18.	Progress of Oxygen Atomization and Reaction in the Combustion Region . . . . .	126
19.	Calculated LOX Spray Characteristics (Combustion Region) .	127
20.	Comparison Between Experimental Data and Calculated Velocities When No Gaseous Mantle Flow was Provided (Test 431) . . . . .	128
B-1.	Calculated Behaviors of Various Sizes of Liquid Oxygen Droplets in a Combustion Gas Flow Field Prescribed From Run 417, PETER, PRA . . . . .	129
B-2.	Calculated Behaviors of Various Sizes of Liquid Oxygen Droplets in a Combustion Gas Flow Field Prescribed From Run 431, PETER, PRA . . . . .	130
C-1.	Burning Velocities for Gaseous Mixtures of Hydrogen and Oxygen (Near Stoichiometric) . . . . .	131
D-1.	Equilibrium, Stagnation Temperature for LOX/H <sub>2</sub> Combustion Product Gases at 550 psia . . . . .	132
D-2.	Equilibrium Molecular Weight and Ratio of Specific Heats for LOX/H <sub>2</sub> Combustion Product Gases at 550 psia . . . .	133
D-3.	Equilibrium Viscosity and Thermal Conductivity for LOX/H <sub>2</sub> Combustion Product Gases at 550 psia . . . . .	134



## SUMMARY

A complete analysis of the steady-state rocket combustion processes attending coaxial jet injection of liquid oxygen and gaseous hydrogen is presented. Programmed for IBM 7094 EDPM solution, a model is formulated that consists of simultaneous equations describing LOX-jet atomization, gas-spray mixing, spray vaporization, spray ballistic behavior, gas stream expansion and deceleration, gas stream combustibility, propellant combustion, turbulent mixing between parallel gas streams, and gas dynamics of the subsonic portions of the combustor. Required model input parameters are those normally known: injector face area, oxidizer and fuel injection areas, flowrates and temperatures, chamber pressure, and combustion chamber geometry.

There are two discrete parts to the model. The first is adjacent to the injector and is characterized by the absence of propellant combustion. A portion of the liquid oxygen jet is atomized and mixed in a controlled manner with the surrounding hydrogen stream; a cylindrically annular, layered spray structure is hypothesized with the earliest formed spray occupying the outer layers. The hydrogen stream is decelerated and expanded radially by diffusion and mixing with the surrounding (stagnant) gases and by momentum exchange with the contained liquid oxygen spray. Spray vaporization effects a gradually increasing oxygen concentration in the hydrogen stream. Recirculation of combustion gases from the combustion region that lies downstream is presumed not to occur; supporting evidence is cited.

The gases in the nonburning region are considered to be combustible if their hydrogen concentration is lower than the upper flammability limit and if their velocity is lower than the local turbulent flame speed.



When these conditions are satisfied, flame spreading is rapid enough that the nonburning region is terminated by a plane flame front standing in the spray-laden gases.

The second part of the model is a combustion region. A portion of the gases in the nonburning spray zone is assumed to be diverted around the flame front and form a fuel-rich gaseous mantle around a central, well-mixed, one-dimensional spray combustion zone. The progress of propellant combustion can be limited by these processes: (1) atomization of the residual liquid oxygen jet that penetrates into the combustion zone, (2) vaporization of liquid oxygen droplets, and (3) turbulent mixing of the gaseous mantle into the spray combustion zone.

Few data exist concerning some of the processes, so the model formulation includes a number of arbitrary constants and assumptions. Selected values for these were modified until a combination was found that would permit the model predictions to reproduce experimental information from two particular transparent model rocket motor tests. The results from those best-fit model calculations are presented in enough detail to characterize prominent features of the model predictions.

Although the best-fit cases agree well with those two tests which had given the most complete experimental data, parametric variations of model chamber pressure, mixture ratio, and propellant injection temperatures gave some predictions that did not agree particularly well with observed trends in other tests which had given incomplete experimental data. These comparisons are discussed in terms of the model's validity and additional definitive measurements that might have been made in the tests.

## INTRODUCTION

This report is the second in a series presenting the results of a combined experimental and analytical study of the processes that transpire during steady-state rocket combustion with liquid oxygen and gaseous hydrogen propellants. The first report in the series detailed the experimental investigation with three injector types and included a qualitative discussion of the combustion processes found to be important with each type (Ref. 1). As noted there, specific experimental information was sought to aid in formulating physically realistic analytical models of the bi-propellant combustion processes. The analysis that has been based on the experimental information concerning coaxial jet injection, in which each injection element consists of a cylindrical liquid oxygen jet surrounded by an annular gaseous hydrogen stream, is the subject of this report.

The experiments, conducted in a transparent-walled model rocket motor, revealed that the liquid oxygen jets penetrated about 3 to 4-1/2 inches downstream of the injector where they rather abruptly ceased to be visible in high-speed motion pictures. At about the same position, streak photography indicated an abrupt increase in the velocity of luminous combustion elements presumed to be representative of combustion product gases. A short distance further downstream, melting of the pyrex combustor walls began. These phenomena were interpreted to result from a flame-front standing at a particular position in the oxygen-spray-laden gas flow surrounding each liquid oxygen jet. A derived schematic representation of the atomization, jet-spreading, and combustion processes for a single coaxial jet injection element is shown in Fig. 1.

The analyses presented and discussed are almost exclusively based on the concepts shown in Fig. 1. Immediately downstream of the injector, the



initial liquid oxygen jet atomization, spray acceleration and evaporation, and hydrogen stream spreading and deceleration are presumed to take place in the absence of direct combustion. Upstream recirculation of combustion gases is assumed either not to occur or to be so weak as to have no appreciable affect on the important processes in this region. A resultant natural division of the model formulation for this injection type into a distinct nonburning injection region and a subsequent, downstream combustion region is used.

A complete, integrated combustion model for the entire combustion chamber, from the injector face to the nozzle throat, was the goal pursued in this investigation. At many points in the model formulation it became necessary to select one approach or assumption from among alternatives. In some instances, review of the experimental data suggested the most realistic choice; in others, peripheral analyses were performed to guide the development. Occasionally, a choice was made that was later abandoned because results were computed which could not be supported by the experimental evidence. The more important of these alternatives are indicated.



## MODEL FORMULATION

Injectors for liquid propellant rocket combustors are usually based on a single fundamental injection concept with only minor modifications or variations to provide for special requirements, such as film-coolant for chamber walls and adequate ignition sources. Thus, a high-thrust rocket engine injector might have several hundred coaxial jet injection elements, all having identical geometric characteristics and ostensibly having identical propellant supply and flow characteristics, uniformly spaced in the available injector face area. In the ensuing formulation, it is assumed that the processes downstream of any one of those elements may be represented by a stream tube which is characteristic of the entire combustion field. The model, therefore, is based on division of the total injection area, chamber cross-sectional area along the chamber length and propellant flowrates by the number of elements to get equivalent values per element. An additional simplification in this vein is the assumption of cylindrical symmetry of the stream tube about the element's axial centerline.

The model formulation consists of determining the important processes and developing analytical or empirical expressions to describe them. Since a large number of interrelated phenomena are accounted for, the system of equations and expressions must be solved numerically. An IBM 7094 EDPM program, written in FORTRAN II and based on simple stepwise progression down the length of the chamber, has been employed; conditions at a plane  $x$  distant from the injector were used to calculate conditions at a plane  $(x + \Delta x)$  distant from the injector. It was assumed that small enough  $\Delta x$  increments could be used to avoid mathematical instability and accumulation of significant errors along the chamber length.



## NONBURNING INJECTION REGION

Under the experimental conditions detailed in Ref. 1, coaxial jet injection of gaseous hydrogen and liquid oxygen was characterized by a relatively low-velocity liquid oxygen stream being completely surrounded by a much higher velocity gaseous hydrogen flow. At injection-end chamber pressures of 450 to 525 psia, liquid oxygen injection velocities ranged from about 50 to 100 ft/sec (depending upon chamber pressure and mixture ratio), while hydrogen injection velocities ranged from about 1000 to 3000 ft/sec (depending upon chamber pressure, mixture ratio, and injection temperature). The hydrogen stream formed a cylindrical barrier, for at least a short distance from the injector, which insulated the contained liquid oxygen stream from the surroundings. The initial liquid jet atomization, spray acceleration, and spray evaporation unquestionably took place in the absence of combustion. This section is concerned with the model formulation for that nonburning region.

### Liquid Oxygen Jet Atomization

Immediately upon leaving the end of its confining tube, an elemental cylindrical plug of liquid oxygen finds its surface exposed to tremendous shear forces from the surrounding high-velocity hydrogen stream. These forces rapidly induce capillary wave motion on the liquid jet surface. Mayer (Ref. 2) has extended an analysis of capillary waves on plane, deep liquids to a formulation for liquid jet atomization processes. He



derived an equation relating a mean droplet diameter produced by wave amplification and crest shedding to the gas and liquid stream properties:\*

$$D_{\text{mean}} = (9)(12)(16)^{\frac{1}{3}} \pi B_A \left[ \frac{\mu_L (\sigma_L \epsilon_c / \rho_L)^{1/2}}{\rho_g U_r^2} \right]^{2/3} \quad (1)$$

where  $B_A$  is a composite numerical factor including a sheltering parameter and a parameter dependent upon the crest configuration at the instant of erosion or shedding. On conceptual grounds, Mayer reasoned that  $B_A$  should be of the order of unity. He made a favorable parametric comparison of his theoretical result with experimental data (Ref. 3) on costream and contrastream atomization of cylindrical molten wax jets and concluded with an empirical evaluation from that data of  $B_A \approx 0.3$ . This was further resolved to indicate that about 1/7 of the wave amplitude is shed as a ligament at the instant of erosion and that about 70 percent of the wave amplitude is sheltered from the gas stream.

Mayer's droplet size expression has been used in the model formulation to calculate the mean LOX droplet diameter being produced in the  $n$ th  $\Delta x$  increment from the injector:\*\*

$$\left( D_{dn_i} \right)_{1-2} = 2719.2 B_A \left[ \frac{\mu_L (\sigma_{L1} / \rho_{L1})^{1/2}}{(\rho_g')_1 (U_r')_1^2} \right]^{2/3} \quad (1a)$$

\*All equations have been modified to be consistent with the units given in the nomenclature. Values of the required properties appear in Appendix A.

\*\*Or of the  $n$ th spray element for instances where the atomization process ceases for a time and is then resumed.



In contrast with Mayer's exposition in Ref. 2, where  $B_A$  was evaluated from the entire spray resulting from complete jet atomization, Eq. 1a clearly denotes a mean drop size for the spray produced in a small local region. For that reason, the value of  $B_A$  was left as an arbitrary constant in the model formulation.

Dickerson and Schuman (Ref. 4) have shown that Mayer's theory can be extended to provide prediction of a spray production rate. Their derivation was in terms of mass atomization rate per unit liquid surface area:

$$\frac{\dot{W}_A}{A_s} = C_A \left[ \frac{\mu_l \rho_l (\rho_g U_r^2)^2}{\sigma_l g_c} \right]^{1/3} \quad (2)$$

where  $C_A$  is a numerical factor related to  $B_A$  in Eq. 1.

For a cylindrical jet segment  $\Delta x$  long, the local spray production rate of the  $n$ th spray group is here taken as:

$$(\dot{W}_{An})_{1-2} = (6.8597 \times 10^{-3}) C_A D_{l1} \Delta x F(n) \left[ \frac{\mu_{l1} \rho_{l1} \left[ (\rho'_g)_1 (U'_r)^2 \right]^2}{\sigma_{l1}} \right]^{1/3} \quad (2a)$$

in which a suppression factor  $F(n)$  has been introduced to account for the combined effects of finite wave buildup time and finite tube wall thickness



in delaying the atomization immediately downstream of the injector. A parabolic form was assumed:

$$F(n) = \left( \frac{c_1}{1 + c_1 + c_2 - n} \right)^2 ; 1 \leq n < c_2 \quad (3)$$

Values of  $c_1$  and  $c_2$  were usually selected to suppress the atomization by 80 to 90 percent at the injector face and continue suppression for about 1/2 inch from the injector.

The mass of an individual droplet was given by

$$w_{dn} = \frac{\pi}{6} \rho_{dn} D_{dn}^3 \quad (4)$$

so the number flowrate of droplets in the  $n$ th spray group was:

$$\dot{N}_{dn} = (\dot{W}_{An})_{1-2} / w_{dni} \quad (5)$$

According to Eq. 1 and 2, local spray droplet size increases and local spray production rate decreases with decreasing relative velocity between the liquid jet and the atomizing gas stream. As will become apparent later, momentum exchange from the high-velocity gas stream to the accelerating spray can cause fairly rapid deceleration of the gases which, in turn, is followed by production of fewer, but larger, droplets. Very large droplets would later be accelerated so slowly, however, that their velocities over much of the chamber length might be lower than the minimum velocities reduced from the experimental streak photographs. Therefore, in the model formulation, a maximum droplet diameter was imposed on the nonburning atomization process; the maximum size was selected by





a peripheral analysis described in Appendix B. Calculation of droplet sizes larger than the assumed maximum was equivalent to cessation of the atomization process; generally, atomization would not be resumed until a position in the chamber was reached where propellant combustion resulted in a relatively high gas velocity.

### Individual Droplet Behavior

The behavior of an individual droplet of liquid oxygen in a convective gas stream is strongly dependent upon the gas stream properties and conditions. Three kinds of behavior were accounted for in the model formulation, viz., ballistics (acceleration or deceleration), heating (droplet temperature changes), and vaporization. Deviations from spherical shape, interference or reagglomeration with neighboring droplets, and aerodynamic breakup of a droplet following its initial formation were not considered to be of significance to the nonburning analysis.

Droplet ballistics were described by the often-used drag equation for a sphere with a low mass evaporation rate:

$$\frac{d U_d}{dt} = \frac{(3)(12) C_D \rho_g U_r |U_r|}{4 \rho_d D_d} \quad (6)$$

Defining a variable  $K_n$  for the nth droplet group,\*

$$K_n = \frac{3 C_{Dnl} \rho_{gnl} \Delta x}{4 \rho_{dnl} D_{dnl}} \quad (7)$$

---

\*Where gas properties are n-subscripted, those gases locally associated with the nth spray group are meant. Refer to the formulation beginning on page 21 for a description of this association.



Eq. 6 was integrated to obtain:

$$U_{dn2} = 0.5 \left\{ (K_n + 1) U_{dn1} - K_n U_{gn1} + \left[ K_n U_{gn1} - (K_n + 1) U_{dn1}^2 + 4 K_n U_{gn1} (U_{gn1} - U_{dn1}) \right]^{1/2} \right\} \quad (8a)$$

For rapidly decelerating droplets, Eq. 8a may have a negative radicand, so the less accurate form, previously used in Ref. 5, was employed when  $U_{gn1} < U_{dn1}$ :

$$U_{dn2} = U_{dn1} + \frac{K_n (U_{gn1} - U_{dn1}) |U_{gn1} - U_{dn1}|}{U_{dn1}} \quad (8b)$$

The composite form of the droplet drag coefficient that accounts for droplet flattening at high droplet Reynolds numbers (Ref. 5) was used:

$$\begin{aligned} C_{Dn1} &= 24 (Re_{dn1})^{-0.84} & , Re_{dn1} < 80 \\ C_{Dn1} &= 0.271 (Re_{dn1})^{0.217} & , 80 \leq Re_{dn1} < 10^4 \\ C_{Dn1} &= 2 & , Re_{dn1} \geq 10^4 \end{aligned} \quad (9)$$

Free-stream gas properties were used in evaluating the Reynolds numbers for drag coefficient calculations.



Changes in droplet bulk temperature were calculated by means of equations resulting from analysis of simultaneous heat transfer to and mass transfer from an evaporating droplet (Ref. 6):

$$T_{dn2} = T_{dn1} + \frac{144 \Delta x}{(c_p)_{dn1} \rho_{dn1} D_{dn1}^2 (U_{dn1} + U_{dn2})} \times$$

$$\left[ \frac{k_{fnl} z_{nl} Nu_{Hnl} (T_{fnl} - T_{dn1})}{3600 (e^{z_{nl}} - 1)} - \right.$$

$$\left. \frac{(144) M_L \sigma_{vnl} H_{vnl} P_1 Nu_{Mnl}}{RT_{fnl}} \log_e \left( \frac{P_1}{P_1 - P_{vnl}} \right) \right] \quad (10)$$

where

$$z_{nl} = \frac{(144)(3600)(c_p)_{vnl} M_L \sigma_{vnl} P_1 Nu_{Mnl}}{R T_{fnl} k_{fnl} Nu_{Hnl}} \log_e \left( \frac{P_1}{P_1 - P_{vnl}} \right) \quad (11)$$

Here the Reynolds, Prandtl, Schmidt, and Nusselt numbers were evaluated using approximations of the droplet film properties based on an arithmetic mean temperature between the droplet and gas temperatures.

For low evaporation rates, the change in liquid droplet mass across an increment is given (Ref. 7) by:

$$w_{dn2} = w_{dn1} - \frac{2\pi M_{O_2} \rho_{gnl} \sigma_{vnl} D_{dn1} Nu_{Mnl} \Delta x}{144 M_{gnl} (U_{dn1} + U_{dn2})} \times$$

$$\left[ \frac{P_{vnl} - X_{O_2 gnl} P_1}{P_1 - P_{vnl}} \right] \quad (12)$$



The term in brackets could become negative if: (1) the droplet temperature (and thus vapor pressure) were very low, (2) the chamber pressure were very high, or (3) the oxygen concentration in the gas stream were high. The digital computer program formulation avoided the implied oxygen condensation by not permitting  $w_{dn2} > w_{dn1}$ . Modifications of Eq. 12 to account for high mass transfer rates (Ref. 7) were not considered to be necessary in the nonburning region.

Evaporation from the liquid oxygen jet was approximated by assuming that its vaporization rate per unit surface area was equal to that of the last-formed spray group.

#### Hydrogen Stream Expansion and Deceleration

At a position just downstream of the injector, the propellant streams may be idealized as two concentric one-dimensional flows. They immediately interact with each other and with the surrounding chamber gases, however, to form an exceedingly complex bipropellant flow system. The atomization process described earlier is a portion of the interaction. Now, the interactions of the hydrogen stream with the exterior surroundings and with the interior liquid oxygen spray will be considered. Occasional reference to Fig. 2 may be helpful in understanding the hypotheses employed.

The outer periphery of the annular gaseous hydrogen stream exerts viscous shear forces on the surrounding chamber gases setting them in motion alongside the high-velocity hydrogen stream. Injection stream turbulence and shear-induced turbulence lead to fairly rapid gas mixing around the hydrogen stream. In that mixing zone, momentum exchanger decelerates the hydrogen and accelerates the chamber gases. The mixing zone becomes thicker, and the hydrogen velocity defect associated with it penetrates

further into the hydrogen stream with increasing distance from the injector. Except for the liquid jet/spray core (which, as discussed later, makes the problem considerably more complex by transferring most of the depletion in hydrogen momentum to the interior), the hydrogen stream behavior may be related to the classical gas dynamic problems of the free (unconfined) turbulent circular jet and the bounded (confined) turbulent circular jet.

With both free and bounded gas jets having essentially rectangular injection velocity profiles (fully developed turbulent flow), the thickening mixing zone involves more and more of the jet stream until, at some finite distance from the injector, it has grown inward to the jet centerline. Denoting that downstream position as  $x_p$ , it is noted that a diminishing core of unmixed jet stream penetrates at injection velocity to  $x_p$  and there vanishes. The gas dynamics downstream of  $x_p$  have been successfully described theoretically for the free jet (Ref. 8) and studied extensively for bounded jets (e.g., Ref. 9). The bounded jet problem has not yet yielded to complete analytical description. Some results for the free jet are (Ref. 8): (1) the maximum jet velocity occurs on the jet centerline and decays inversely with axial distance from the jet source, (2) the jet width increases linearly with that distance, (3) the radial profile of axial velocity has a characteristic shape similar to a Gaussian distribution, and (4) the total volume of fluid in motion increases linearly with distance from  $x_p$ . The bounded jet results differ from the free jet in that: (1) the velocity at large distance downstream from  $x_p$  approaches a constant one-dimensional velocity (prescribed by mass continuity) rather than approaching zero, (2) momentum exchange at the jet boundary ingests gases which are not freely available from the surroundings but are circulated upstream from the neighborhood where the jet fills the boundary channel (thus forming an annular eddy), and (3) the total mass flowrate is limited to the jet injection flowrate.



The phenomena upstream of  $x_p$  are generally well known from experimental studies but have not confirmed a general theoretical treatment. Even without the additional complication of having a liquid core, it is apparent that empirical approximations are required for a flow model formulation beginning at the injector face.

Before stating the approximations used for exterior hydrogen stream expansion, an effect of the gas-liquid interaction should be noted. Momentum exchange between the liquid oxygen spray droplets and hydrogen-rich gases surrounding them accelerates the droplets (Eq. 8a) and decelerates the attendant gases. An increasing interior cross-sectional area is needed to accommodate the decelerated gas flow; the surrounding hydrogen stream and exterior mixing zone must be displaced radially outward by this internal expansion.

In the model formulation, the exterior hydrogen deceleration was assumed to involve increasing mass flowrate of hydrogen by having the velocity defect penetrate to smaller radius:

$$r_{\text{def},2} = r_{\text{def},1} - c_4 \Delta x, \quad x \leq x_p \quad (13)$$

$$\begin{aligned} \left( \dot{w}_{H_2} \right)_{\text{def},2} &= \left( \dot{w}_{H_2} \right)_{\text{def},1} + \\ &\quad \pi \rho_{H_2,1} U_{H_2,1} \left( r_{\text{def},1}^2 - r_{\text{def},2}^2 \right) \end{aligned} \quad (14)$$



a value of  $c_4$  from free-jet experimental results was used. The increase across the  $\Delta x$  increment of the spray zone radius,  $r_{sz}$  (whose evaluation is discussed in a following section), and the decrease in mass flowrate of hydrogen still having injection velocity,  $\dot{w}_{H_2p}$ , were then used to calculate the effect of spray zone expansion on the radius to which the hydrogen stream velocity defect penetrates:

$$r_{def,2} = \left[ \frac{\dot{w}_{H_2p2} (r_{def,1}^2 - r_{sz1}^2)}{\dot{w}_{H_2p1}} + r_{sz2}^2 \right]^{1/2} \quad (15)$$

The maximum hydrogen stream velocity was defined as:

$$\begin{aligned} \left[ (U_{H_2})_2 \right]_{\max} &= U_{H_2i} \quad ; \quad \dot{w}_{H_2p2} > 0 \\ &= U_{gb2} \quad ; \quad \dot{w}_{H_2p2} = 0 \end{aligned} \quad (16)$$

A linear approximation of the Gaussian velocity distribution in the external velocity defect flow was used to estimate the radius of the boundary between the cylindrically symmetric propellant flow system and the surrounding (stagnant) chamber gases:

$$r_{H_2^2} = (r_{H_2})_{def,2} + \left[ \frac{2(\dot{w}_{H_2})_{def,2}}{\pi \rho_{H_2^2} \left[ (U_{H_2})_2 \right]_{\max,2}} \right]^{1/2} \quad (17)$$



Downstream of  $x_p$ , the furthest distance to which hydrogen at injection velocity penetrates,  $\dot{w}_{H_2p2} = 0$ ; continued momentum exchange with the spray and chamber gases must result in deceleration of the entire gas/spray flow system. As noted earlier, the maximum velocity for an unconfined gaseous jet would decay inversely with increasing distance. With the liquid spray core, however, such a rate of deceleration would soon result in gas flow velocities lower than the liquid oxygen spray droplet velocities; droplet deceleration would then transfer momentum back to the hydrogen-rich gases and prevent them from decelerating so rapidly. In the model formulation, therefore, the gas velocity at the boundary between the spray zone and the surrounding flow was assumed to follow:

$$U_{gb2} = U_{gb1} \left( \frac{x_1}{x_2} \right)^{c_6} ; \quad x_1 > x_p \quad (18)$$

Values of the exponent,  $c_6$ , between 0.5 and 1.0 were chosen to obtain deceleration to velocities lower than a calculated turbulent flame speed upstream of the position where the abrupt velocity step occurred on the streak photographs.

A conceptual, schematic cross-section of the axial propellant velocities is shown in Fig. 2. The solid line shows the concentric, one-dimensional liquid oxygen and gaseous hydrogen flows with rectangular velocity





profiles at the injector face. A short distance,  $x_1$ , downstream some spray has been formed, resulting in internal deceleration of hydrogen and radial displacement of the whole structure. Somewhat further downstream, at  $x_p$ , the unmixed hydrogen jet has just been engulfed by the simultaneous momentum requirements of the accelerating spray and the external gas mixing zone. The continued deceleration and expansion even further downstream is shown at a distance  $x_3$  from the injector.

#### Recirculation

Much as the classical bounded circular gas jet induces an annular eddy of gases circulated upstream along the bounding walls and ingested into a mixing zone around the jet, chamber gas circulation must be induced by the coaxial jet gaseous hydrogen injection. Upstream circulation and entrainment of combustion product gases in this manner is usually referred to as recirculation.

Just what gases are circulated upstream, their composition, and temperature may be critically important to the steady-state propellant combustion and precombustion processes. Recirculated combustion product gas would provide, as a portion of its mass, additional gaseous-state oxidant to the coaxial propellant system and would enhance, through its high-temperature thermal content, heat transfer from the hydrogen stream/mixing zone to the liquid oxygen spray. This, in turn, would enhance the spray evaporation rate; conceivably, the propellants' attainment of combustible conditions could be greatly hastened.



Conversely, circulation of uncombusted gases could play little more than a passive role in the combustion chamber processes. Such a circulation was hypothesized from the experimental observations (Ref. 1) and is reflected in the schematic representation of Fig. 1. If the recirculating gases in the annular eddy are pure hydrogen, they can have no appreciable effect on the propellant precombustion processes. If, however, all of the hydrogen stream were drawn into the spray zone upstream of the end of the recirculation eddy, the circulating gases would contain some oxygen; a moderately higher gaseous oxygen concentration throughout the gaseous mixing zone and the spray zone (between  $x_p$  and the downstream end of the eddy) should then be found.

The current model was formulated without accounting for either uncombusted gas circulation or combustion gas recirculation. The chamber volume outside of  $r_{H_2,2}$  (Eq. 17) was simply assumed to be filled with stagnant gases of unspecified nature which decelerated a "mixing zone" portion of the hydrogen stream without actually getting mixed with the hydrogen. These assumptions (synonymous with a constant-mass, constant-momentum eddy) were unavoidable in a model based on a stepwise progression down the chamber length. The assumed structure is very nearly realistic if pure hydrogen gases are circulating.

A criterion for determining whether or not recirculation forms an important part of the flow processes associated with a ducted turbulent gas jet\* has been developed by Becker, et al. (Ref. 10). They defined

---

\*A ducted jet, in general, consists of a gas stream flowing through a duct (ground stream) with a gas jet having higher or lower velocity injected into it, usually in parallel flow. The bounded or confined jet corresponds to the case of no ground stream flow.



a similarity parameter,  $Ct$ , called the Craya-Curtet number and determined experimentally that recirculation occurred in a constant-pressure, isothermal, single-component system only if the value of  $Ct$  was less than  $3/4$ . The smaller the value of this number, the stronger was the recirculation.

For a confined gas jet,  $Ct$  was given as:

$$Ct = U_k \left[ \left( I_j / \pi \rho_j r_w^2 \right) - \frac{1}{2} U_k^2 \right]^{-1/2} \quad (19)$$

The kinematic velocity ( $U_k$ ) in a cylindrical duct is the space mean velocity, which is related through mass continuity to the initial jet velocity, i.e.,  $U_j r_j^2 = U_k r_w^2$ . Substituting this, together with  $I_j = \pi \rho_j r_j^2 U_j^2$ , into Eq. 19 gives:

$$Ct = (r_j/r_w) \left[ 1 - \frac{1}{2} (r_j/r_w)^2 \right]^{-1/2} \quad (20)$$

showing that recirculation or eddy strength for a confined gas jet in a cylindrical duct at constant pressure is dependent only upon system geometry.

The two-phase two-component coaxial injection under consideration here differs from a confined gas jet mainly in that momentum is transferred between the gas stream and the liquid phase. The gas-phase momentum available for inducing circulation is thus a decaying function of distance from the injector. Becker's result expressed in Eq. 19 is here



modified by replacing  $I_j$  with  $(\sum I_g)_2$ . Taking the ratio

$(\sum I_g)_2 / I_{ji} = F_{I2}$ , the Craya-Curtet number, in a form related to

Eq. 20 is:

$$Ct_2 = \left( \frac{r_{H_2}^2 - r_{Lj}^2}{r_w^2} \right)^{1/2} \left( F_{I2} - \frac{r_{H_2}^2 - r_{Lj}^2}{2 r_w^2} \right)^{-1/2} \quad (21)$$

The model calculations included computation of this value of the Craya-Curtet number at each axial position. It was used simply as an indicator of the model's validity: If flammable conditions were reached after  $Ct_2$  exceeded  $3/4$ , the omission of circulation from the model was assumed to be a valid simplification. On the other hand, if flammable conditions were calculated to occur before  $Ct_2$  exceeded  $3/4$ , this was interpreted as a warning that combustion gas recirculation was probable and that the model calculations might be grossly in error.

### Liquid Oxygen Spray Zone

The structure of the liquid oxygen spray zone surrounding each cylindrical liquid oxygen jet is not known with any certainty. Attempts to determine the spray zone diameter as a function of distance from the injector (by direct measurements on the high-speed Fastax motion picture films) gave fairly erratic results; both jet-to-jet diameter variations and frame-to-frame variations on an individual jet/spray system contributed to wide measurement scatter. Further, it is probable that sparse droplet populations in the outermost periphery of the spray were not visible in the photographs. Thus, only general guidelines for the spray zone formulation could be derived from the experimental work.



Certainly the gas velocity in the spray zone is highest at (or near) its outer periphery and is lowest immediately next to the liquid oxygen jet. This is shown in Fig. 2 as a continuously decreasing velocity, from boundary velocity at  $r_{sz}$  to liquid oxygen injection velocity at  $r_{lj}$ .

The radial velocity profile was hypothesized in the model formulation to be similar to that across a boundary layer. Since no experimental or theoretical information was found in the literature for a comparable heterogeneous turbulent boundary layer, it was reasoned that the boundary-layer-thickening velocity-gradient-reducing effects of spray in the gases would be only partially offset by the opposite effects of having cylindrical flow. Consequently, the spray zone velocity profile was assumed to be similar to that for a laminar boundary layer on a flat plate (Ref. 11):

$$\frac{U_{gr} - U_{lj}}{U_{gb} - U_{lj}} = \frac{3}{2} \left( \frac{r - r_{lj}}{r_{sz} - r_{lj}} \right) - \frac{1}{2} \left( \frac{r - r_{lj}}{r_{sz} - r_{lj}} \right)^3 \quad (22)$$

Conceivably, a sufficiently realistic description of the spray zone might result from assumptions that: (1) spray zone gases are homogeneous, (2) all sizes of spray droplets are uniformly mixed with the homogeneous gas flow, and (3) liquid oxygen jet atomization and spray droplet acceleration can be calculated using an appropriate mean gas velocity. After an initial attempt to base a model formulation on these simplifications\*,

---

\*The preceding assumptions were made together with two other assumptions: that the spray could be considered as monodisperse and that the spray zone radius could be prescribed by measurement from the high-speed motion pictures. The calculated results showed this approach to be so oversimplified that the entire line of attack was abandoned. By far, the poorest of the simplifications was the use of a monodisperse spray; probably the next poorest was basing acceleration and evaporation on a mean gas velocity.



it was feared that too many details of the spray evaporation, gaseous oxygen distribution, and hydrogen deceleration processes were being averaged out. A more complex model of the spray zone was thus adopted.

The spray zone structure in the final formulation was hypothesized to consist of thin, cylindrically concentric, annular "shells" of spray, the new spray being shorn from the liquid oxygen jet surface in the  $k^{\text{th}}$   $\Delta x$ -increment from the injector was considered to occupy an annular space immediately adjacent to and surrounding the liquid oxygen jet (Fig. 3a). To make room for this new spray, the spray formed in the  $(k-1)^{\text{th}}$   $\Delta x$ -increment (upstream) had to have been moved out radially into a larger-diameter annulus. Successively older spray elements were presumed to be flowing through annuli lying further and further radially outward from the liquid jet with the earliest-formed spray occupying the outer periphery of the spray zone.

Consider the spray element being formed in the  $k^{\text{th}}$   $\Delta x$ -increment: Since it is new spray, there is no gas flow associated with it; the nearest available gas is that flowing in the  $(k-1)^{\text{th}}$  spray element. The energy for atomizing and the momentum for accelerating the  $k^{\text{th}}$  spray group must be derived from influx of some (or all, or even more than all) of the gas previously surrounding the  $(k-1)^{\text{th}}$  spray droplets. That gas must then surround the  $k^{\text{th}}$  spray element droplets to provide spray momentum; in so doing, the composition, temperature, and velocity of the gas are changed by its association with that new spray.

At the same time, the  $(k-1)^{\text{th}}$  spray droplets must be displaced radially outward by the deceleration and expansion of their former gases that are being transferred into the  $k^{\text{th}}$  spray group. But Eq. 22 states that the gas velocity is higher at the increased spray zone radius, so the  $(k-1)^{\text{th}}$  droplets will be accelerated. An influx of gas from the  $(k-2)^{\text{th}}$



spray element is thus required, both to make up for the gas transferred inwardly and to provide the increased liquid oxygen spray momentum. Continuation of this conceptual process leads to the already obvious conclusion that the outermost spray groups require an influx of hydrogen to satisfy their gas mass and momentum requirements.

Spray zone structure was computed by means of a complex portion of the digital computer program. The programmed equations constitute a detailed system for ensuring continuity of mass and energy during the interelement gas exchange processes. Since the accounting system is not of direct interest to the combustion processes per se, only a description of the conceptual bases of the spray zone solution need be developed here. This is accomplished in the next few paragraphs by including this portion in a complete summarization of the computer model calculation scheme for the nonburning region.

#### Summary of Model Calculation Scheme

As previously noted, the digital computer program is based on using knowledge of conditions at a plane  $x_1$  to calculate the conditions at a plane  $x_2$ , a distance  $\Delta x$  downstream. A simple stepwise progression is used; the value of  $\Delta x$  is presumed to be small enough that mathematical instabilities and accumulation of appreciable errors are avoided.

The program first calculates liquid oxygen jet atomization, if the maximum droplet diameter is not calculated to be exceeded. The acceleration (or deceleration) of each group of spray droplets is then computed, followed by calculation of each group's evaporation rate. Next, the momentum changes of the spray droplets and new oxygen vapor are summed to obtain an estimate of how much hydrogen must be decelerated and mixed into the spray zone. That information is used to approximate the new spray



zone radius and boundary velocity which are then used in a single iteration of the procedure to obtain an improved estimate of spray zone radius.

The total spray zone area is apportioned among the individual spray elements on a basis of proportionate combined gas and spray mass flow-rate. The downstream radii of each spray element annulus are calculated, and a new mean gas velocity associated with each element is then computed using its mean downstream radius. The resultant distribution of spray element areas and gas velocities is assumed to be inviolably determined by the downstream spray zone radius and boundary velocity.

The gas exchange and mixing processes shown in Fig. 3 are then calculated, beginning with the last-formed spray group and proceeding radially outward to successively older spray groups. The gas flowing out of an element is presumed to result from mixing gases from three sources: (1) that which flowed into the element from upstream, depleted by the amount required by inlying elements, (2) evaporation of spray flowing through the element, and (3) gases required from outlying elements. Each calculation proceeds as if the first two quantities are invariant; the value of the third is adjusted by iteration until the gas mixture flowrate, temperature, and density satisfy the prescribed exit velocity and area requirements. Equations providing for mixing among the three streams while preserving continuity of hydrogen and oxygen mass flow and energy were required. The physical and thermodynamic properties needed for solving the spray element mixing equations are detailed in Appendix A.

The initial conditions for the spray zone are preserved, so that if the calculation results are unsatisfactory, an appropriate adjustment can be made and the calculations reperfomed. Two types of readjustment are very commonly encountered: (1) a spray element may need to acquire





additional gas flow when there is none available (successively smaller values of spray zone radius must therefore be assumed and the spray element areas, velocities, and gas exchanges be recomputed until the requirements are satisfied and mass balances); and (2) excessive gas flow may be calculated to exist in the spray zone, usually because of deceleration to gas velocities lower than spray element velocities. In this case, the spray zone radius is increased to accommodate more gas at the lower velocities, and the spray element areas, velocities, and gas exchanges are recomputed.

After a satisfactory solution for spray zone structure has been achieved, the external hydrogen stream expansion and deceleration are computed. Changes in spray droplet temperatures are calculated. Finally, an overall momentum balance is used to calculate the change of static pressure across the  $\Delta x$ -increment.

The calculated conditions at the downstream end of the  $\Delta x$ -increment are examined for fulfillment of combustibility criteria. If the criteria are met, the nonburning model is replaced by a combustion region model; otherwise, the calculated results are used as initial conditions for extending the nonburning region over another  $\Delta x$ -increment.

#### CONDITIONS FOR COMBUSTIBILITY

In Ref. 1, it was stated that "at least two criteria must be satisfied before a flame can penetrate the spray zone and combustion can be sustained: first, enough oxygen must have evaporated so that the gases within the spray zone are flammable (perhaps 5 to 7 volume percent



oxygen), and second, the axial gas velocity must be equal to or less than the turbulent flame speed, or else an established combustion would be swept downstream." Further discussion developed the probability that any flame resulting from ignition in the interior of the spray zone is not a steady-state possibility so long as any of the nonburning spray zone gas is flowing at velocities in excess of the turbulent flame speed. This led to the suggestion that a third condition for combustibility might be the existence of a strong stabilized flame source, such as a continuous eddy of recirculating combustion gases surrounding the spray zone.

These three conditions were used in the model formulation for determining combustibility of the spray zone gases. The third condition was satisfied by requiring that the gas velocity in the outermost spray element which still had unevaporated liquid oxygen spray in it not be greater than the calculated turbulent flame velocity. If the gas velocities throughout the spray zone were below the turbulent flame speed, combustibility was considered to be satisfied when the oxygen concentration in any spray zone element satisfied the flammability limit criterion.

The values for the upper flammability limit for gaseous oxygen and hydrogen mixtures used in the model calculations ranged from 5 to 8 volume (or mole) percent oxygen. The turbulent flame velocity was assumed to be dependent only upon pressure:

$$U_t = a p^{1/2} \quad (23)$$

A detailed discussion of the selection of these relationships is given in Appendix C.



## COMBUSTION REGION

At that position in the combustion chamber where the spray zone combustibility requirements are satisfied, the nonburning injection region model is replaced by a combustion region model. Some general features of this region's structure are discussed briefly before the details of the model formulation are developed.

Initial conditions for the combustion region are established, and these are used to calculate conditions one  $\Delta x$ -increment further down the chamber. The model calculations thus continue stepwise along the length of the chamber in the manner previously discussed.

### Flame Spreading

Since the axial gas velocities within the spray zone must be lower than the turbulent flame speed, flame should propagate from the point of ignition across the entire spray zone within an axial distance that is of the order of the spray zone thickness. With injection element spacings on the order of 1/2 inch, spray zone thicknesses of the order of 1/8 to 1/4 inch appear reasonable. The chamber length associated with flame spreading through the spray zone is thus only a very small fraction of the chamber length; simplification to the assumption of a plane flame front across the spray zone at the position of first combustibility thus appears to be justified.\*

---

\*Some model calculations were performed in which ignition was provided for only in the gases directly against the liquid oxygen jet and, even though the oxygen concentrations in the outer elements were too low to satisfy flammability, expansion of hot gases out of the core of the spray zone increased the spray gasification rates such that the combustible region spread radially outward as rapidly as the more likely inward propagation.



### Spray Zone Combustion

Superposition of combustion on the annular-shell structure of the nonburning spray zone appeared to impose insurmountable difficulties. The heterogeneous combustion probably generates intense local turbulence (Ref. 12) that would invalidate such an analysis in any case. The contents of the nonburning spray zone elements, therefore, were considered to be thoroughly mixed upon passage through the standing plane flame front. The mixed gases were presumed to burn, resulting in a one-dimensional flow of combustion gases with all of the sprays uniformly mixed in it.

The combustion process was accounted for in an indirect way similar to that used for liquid oxygen/RP-1 propellants earlier (Ref. 5). At each local axial plane across the spray combustion zone, the flowrates of gaseous hydrogen and gaseous oxygen that had been mixed to form the combustion gas stream were considered to have reacted to thermodynamic equilibrium, stagnation conditions, and then to have been accelerated isentropically to the local flow conditions. This permitted considerable simplification of the combustion model in that all of the desired combustion gas properties could be tabulated (or curve-fitted with polynomials) as simple functions of local gaseous propellant mixture ratio. The results of complete thermochemical performance calculation programs are thus used without introducing the complexity of those calculations into the combustion model. In Appendix D, values of the combustion gas properties so used are given. Other physical, thermodynamic, and transport properties required for the solution of the combustion model are also given in Appendix D.



### Transverse Inhomogeneities

The combustion region model then must account for three concentric flows: (1) any residual liquid oxygen jet that penetrates as far downstream as the combustion region, (2) the spray combustion zone, and (3) any residual hydrogen stream or other gas flow which surrounds the spray combustion zone but does not itself contain liquid oxygen spray. The model formulation consists of expressions for the interaction and mass transfer between the spray combustion zone and the liquid oxygen jet and between the spray combustion zone and the surrounding gas flow, as well as for the internal behavior of the latter two streams.

In general, two kinds of inhomogeneity might be expected to occur and persist for some distance axially into the combustion region. The first is implied by recognition of a gas stream that does not contain spray. Initially, this stream may have been only slightly more fuel rich than the gases in the spray combustion zone. Further downstream, however, its fixed composition will become more and more fuel rich with respect to spray combustion zone gases because of continued oxygen spray gasification.

The second kind of transverse inhomogeneity must develop within the spray combustion zone as a result of accelerated atomization and gasification of the residual liquid jet. The atomization equations, (Eq. 1a and 2a), show that a moderate velocity increase resulting from burning the gases surrounding the liquid oxygen jet will both increase the jet atomization rate and decrease the mean droplet size being produced. Further, the gases surrounding the spray droplets are at elevated temperature so that increased heat transfer to the drops hastens their gasification. A residual liquid oxygen jet containing a large portion of the injection flowrate may thus be atomized and gasified fairly rapidly in only a short segment of chamber length to form a highly oxygen-rich core in the spray combustion zone.



Both of those kinds of inhomogeneity in the propellant combustion field will be degraded, with increasing distance from the injector, by turbulent mixing processes. Whether a completely mixed, fully burned equilibrium combustion chamber exhaust gas (which is desirable for maximizing performance efficiency) is achieved must ultimately be determined by this type of gas-phase mixing.

In formulating a model of the combustion region, an accounting for both kinds of inhomogeneity appeared to be inordinately complex, if not intractable. The further simplification was introduced that the oxygen spray and vapor resulting from liquid oxygen jet atomization is continually mixed uniformly with the other spray and combustion gases in the spray combustion zone. Only turbulent mixing of the surrounding fuel-rich gas stream into that oxygen-rich zone then was considered. As a result of this simplification, it was necessary to provide for accentuating the apparent effect of the latter process by diverting some of the nonburning spray zone gases around the flame front and into the surrounding gas stream. While some such process may actually occur, its accentuation here should be considered as an artifice to compensate for the simplification concerning the absence of an oxygen-rich core in the spray combustion zone.

#### Initial Conditions

The three concentric streams referred to previously were initialized at the end of the nonburning region. The liquid oxygen jet flows from one region into the next without change. Similarly, the liquid oxygen spray elements are unchanged with respect to sizes and numbers of droplets,



but they are no longer presumed to be separated into annular strata. Before initializing the spray combustion zone gas flow, a portion of the gas of each nonburning spray element was diverted radially outward into the surrounding gas stream. The proportion of gas flow to be diverted out of the  $n$ th spray element was arbitrarily taken to be:

$$F_{\text{div},n} = c_7 \left( \frac{k + 1 - n}{k} \right)^2 \quad (24)$$

where  $k$  represents the number of spray elements that still contain unevaporated spray, with the  $k^{\text{th}}$  element lying next to the liquid oxygen jet. The flowrate of gases into the spray combustion zone is then:

$$\dot{w}_{\text{cgl}} = \sum_{n=1}^k \dot{w}_{\text{gnl}} (1 - F_{\text{div},n}) \quad (25)$$

and the amount of oxygen in that gas is:

$$\dot{w}_{\text{O}_2\text{cgl}} = \sum_{n=1}^k X_{\text{O}_2\text{gnl}} \dot{w}_{\text{gnl}} (1 - F_{\text{div},n}) / M_{\text{gnl}} \quad (26)$$

By simple mass continuity relationships, the flowrate and oxygen content of the surrounding gas stream are then determined.



The actual combustion of the spray combustion zone gases is considered to take place across the first combustion region  $\Delta x$ -increment so that the initial conditions are still nonburning. The static pressure, therefore, is most likely the same as that last calculated for the nonburning region. Continuity of momentum then requires that the spray combustion zone's initial gas velocity be:

$$U_{cgl} = \left[ \sum_{n=1}^k \dot{w}_{gnl} (1 - F_{div,n}) U_{gnl} \right] / \dot{w}_{cgl} \quad (27)$$

The cross-sectional area required for this gas flow is then:

$$A_{cgl} = \frac{\dot{w}_{cgl}}{\rho_{cgl} U_{cgl}} \quad (28)$$

where  $\rho_{cgl}$  is obtained from a perfect gas law relationship:

$$\rho_{cgl} = \frac{144 P_1 M_{cgl}}{R T_{cgl}} \quad (29)$$

requiring that additional mixing equations, paralleling Eq. 26, be employed to obtain  $T_{cgl}$  through thermal continuity.

Another set of equations, similar to those used for the spray combustion zone gases, was written for simultaneously obtaining initial values of the surrounding gas stream flowrate, composition, temperature, density, velocity, and flow area.





If the sum of the liquid oxygen jet, spray combustion zone, and gas stream flow areas thus calculated exceeded the total cross-sectional area available, the two gaseous flow areas were reduced proportionately to make that sum equal to the chamber area per injection element. An iterative procedure was then used to lower the static pressure and increase the gas velocities until overall mass and momentum continuity relationships were satisfied.

#### Liquid Oxygen Jet Atomization

The equations presented previously for liquid oxygen jet atomization rate and local mean droplet sizes produced in the nonburning region were used as well in the combustion region. The one-dimensional combustion gas velocity and density replaced  $U_g'$  and  $\rho_g'$  in Eq. 1a and 2a. The previously imposed maximum droplet diameter was also honored in the combustion region, so that atomization could continue (or be resumed) within a particular  $\Delta x$ -increment only if droplets smaller than that maximum were to be formed.

In the Fortran formulation of the computer program, storage locations were reserved for a maximum of 100 individual spray groups. This was believed to be a sufficient number for most practical systems since it would account, for example, for liquid jet penetration to a minimum of 5 inches from the injector if  $\Delta x$  were 0.05 inch, or to 10 inches if  $\Delta x$  were 0.10 inch. If the conditions or controls had been chosen such that some unatomized liquid oxygen jet were computed to survive past the formation of 100 spray groups, all of that remaining jet was dumped into the 100th spray group; while this is certainly unrealistic, it permitted the machine calculations to continue without using values for variables taken from storage corresponding to entirely different variables.

Individual Droplet Behavior

The dynamic behavior of all the droplets in each size group, during their passage through a given  $\Delta x$ -increment, was calculated using equations related to Eq. 6 through 12. Droplet ballistics were determined directly from Eq. 6 through 9 using combustion gas properties wherever the subscript "gnl" occurs there. Similarly, changes in droplet bulk temperature were evaluated by means of Eq. 10 and 11. Droplet mass evaporation rates were calculated by an equation related to Eq. 12 but derived for high evaporation rates into a gas stream that does not contain any of the evaporating species (Ref. 6):

$$w_{dn2} = w_{dn1} - \frac{2 \pi M_L \phi_{vnl} D_{dn1} Nu_{Mnl} P_1 \Delta x}{RT_{g1} (U_{dn1} + U_{dn2})} \left[ \log_e \left( \frac{P_1}{P_1 - P_{vnl}} \right) \right] \quad (30)$$

Noting from Eq. 29 that the terms  $\rho_g/(144 M_g)$  in Eq. 12 and  $P_1/(RT_g)$  in Eq. 30 are equivalent for a perfect gas reveals that these two evaporation equations differ only in their terminal bracketed terms.

If the local static pressure exceeds the critical pressure of oxygen, it has been predicted that nearly all of the heat transferred to the liquid oxygen spray droplets will be absorbed as sensible heat of the liquid rather than being returned to the gas stream as latent heat of vaporization (Ref. 6 and 13). Droplets entering (or formed within) the spray combustion zone thus may be gasified by transient heating through the critical temperature rather than by quasisteady-state surface evaporation. The process was included in the model formulation by abruptly adding to the combustion gas stream the mass flowrate of any spray group calculated to have droplet temperatures exceeding the critical temperature of oxygen.



### Turbulent Gas Mixing

In addition to the liquid oxygen spray gasification, the combustion gas flowrate may be increased by admixture of gases from the surrounding gas stream. A rather gross approximation of the turbulent mixing between these streams was employed in the model formulation: a total turbulent mixing length,  $L_t$ , was selected by examination of the velocity vs chamber length plots of Ref. 1, and the surrounding gas stream flowrate was diminished linearly with distance over that length. The combustion gas flowrate was thus:

$$\dot{w}_{cg2} = \dot{w}_{cg1} + \frac{(\dot{w}_{gs1})_i \Delta x}{L_t} + \sum_{n=1}^k (w_{dn1} - w_{dn2}) \dot{N}_{dn} \quad (31)$$

and the surrounding gas stream flowrate was:

$$\dot{w}_{gs2} = \dot{w}_{gs1} - \frac{(\dot{w}_{gs1})_i \Delta x}{L_t} \quad (32)$$

This type of mixing was presumed not to occur unless the propellant flows filled the available chamber cross section.

Spray Zone Combustion

It was noted earlier that propellant combustion was accounted for in the model formulation by considering the local propellant flowrates to have reacted locally to thermodynamic equilibrium stagnation conditions, dependent (for a given range of chamber pressures) only upon the local gaseous propellant mixture ratio. This requires knowledge of the equivalent flowrates of oxygen and hydrogen that resulted in the combustion gas stream:

$$\dot{w}_{O_2cg2} = \dot{w}_{O_2cg1} + \frac{(\dot{w}_{gs1})_i X_{O_2gs1} M_{O_2} \Delta x}{M_{gs1} L_t} + \sum_{n=1}^k (w_{dn1} - w_{dn2}) \dot{N}_{dn} \quad (33)$$

$$\dot{w}_{H_2cg2} = \dot{w}_{cg2} - \dot{w}_{O_2cg2} \quad (34)$$

$$R_{cg2} = \frac{\dot{w}_{O_2cg2}}{\dot{w}_{H_2cg2}} \quad (35)$$

The stagnation properties of the combustion gas were then found as detailed in Appendix D.



$$\begin{aligned}(T_{cg2})_0 &= \int_{T_0} (R_{cg2}) \\ M_{cg2} &= \int_M (R_{cg2}) \\ \gamma_{cg2} &= \int_\gamma (R_{cg2}) \\ \mu_{cg2} &= \int_\mu (R_{cg2}) \\ k_{cg2} &= \int_k (R_{cg2})\end{aligned}\tag{36}$$

Static conditions for the flowing combustion gas obtained from isentropic flow relationships:

$$T_{cg2} = (T_{cg2})_0 \left[ 1 - \frac{\gamma_{cg2} - 1}{2} \left( \frac{U_{cg2}}{(a_{cg2})_0} \right)^2 \right]\tag{37}$$

$$(a_{cg2})_0 = \left[ \frac{\gamma_{cg2} (T_{cg2})_0 R_{gc}}{M_{cg2}} \right]^{1/2}\tag{38}$$



### Combustion of the Surrounding Gas Stream

The initial oxygen concentration in the gas stream surrounding the spray combustion zone was compared to the upper flammability limit for determining whether this stream would be burned or remain unburned. If the stream were incombustible, the gas stream stagnation temperature and stagnation pressure were assumed to remain constant and equal to their initial values at all downstream positions. This is equivalent to ignoring heat transfer into the gas stream as it flows axially along the chamber.

For the burned gas stream, the stagnation pressure was taken to be the initial value, but the stagnation temperature, stagnation velocity of sound, molecular weight, and ratio of specific heats were determined at the beginning of the combustion region in the same way the spray zone combustion gas properties were obtained. Since no source was provided for mass transfer into this stream, the values for those variables determined upon first combustion were assumed to remain invariant throughout the succeeding flow.

### Area Distribution, Gas Velocities, and Chamber Pressure

Until the total available cross section of the chamber has become filled with flowing propellants and combustion gases, gas generation and heat release can be absorbed by transverse expansion without large gas velocity or pressure changes occurring. Although equations were included in the model formulation for computing the progress of such combustion, only a short segment of a conventional rocket combustor's chamber length is needed to achieve full flow, so the details are omitted.



When the chamber has become filled with axial propellant and combustion gas flow, continued gasification of liquid oxygen and combustion reactions between unlike gas streams must necessarily result in acceleration of the flows and, simultaneously, in lowering of the static pressure. The cross-sectional areas and velocities of the two gaseous streams and the pressure are all unknowns and are all interrelated.

The combustion region model solution was based on approximating the distribution of the chamber cross-sectional area among the liquid oxygen jet, the spray combustion zone, and the surrounding gas stream by assuming initially that the pressure and flow Mach numbers across the  $\Delta x$ -increment are constant. Estimates of downstream gas densities and velocities were thus obtained and, from mass continuity, the required cross-sectional flow areas calculated. In general, the sum of those calculated areas should exceed the total chamber area, so the two gaseous flow areas were reduced proportionately:

$$A_{cg2} = \frac{(A_{cg2})_{est}}{(A_{cg2})_{est} + (A_{gs2})_{est}} (A_{cc2} - A_{lj2}) \quad (39)$$

$$A_{gs2} = A_{cc2} - A_{lj2} - A_{cg2} \quad (40)$$

These approximations were used as starting values which were continuously modified during a subsequent iterative calculation of the two gas stream densities, velocities, and chamber pressure at plane 2.



The iterative procedure began with an estimate that:

$$(P_2)_{\text{est}} = P_1 \quad (41)$$

from which

$$\begin{aligned} \rho_{cg2} &= \frac{144 (P_2)_{\text{est}} M_{cg2}}{R T_{cg2}} \\ \rho_{gs2} &= \frac{144 (P_2)_{\text{est}} M_{gs}}{R T_{gs2}} \end{aligned} \quad (42)$$

and

$$\begin{aligned} U_{cg2} &= \frac{144 \dot{w}_{cg2}}{\rho_{cg2} A_{cg2}} \\ U_{gs2} &= \frac{144 \dot{w}_{gs2}}{\rho_{gs2} A_{gs2}} \end{aligned} \quad (43)$$

which results in a total propellant momentum of:

$$\begin{aligned} \sum I_2 &= (\dot{w}_{cg2} U_{cg2} + \dot{w}_{gs2} U_{gs2} + \dot{w}_{tj2} U_{tji})/g_c + \\ &\frac{\pi}{(6)(1728) g_c} \sum_{n=1}^k \rho_{dn2} D_{dn2}^3 U_{dn2} \dot{N}_{dn} \end{aligned} \quad (44)$$





Therefore,\*

$$P_2 = P_1 + \frac{2 (\Sigma I_2 - \Sigma I_1)}{A_{cc1} + A_{cc2}} \quad (45)$$

The gas stream flow has been assumed to be isentropic. An inversion of the isentropic pressure relationship gives:

$$U_{gs2} = (a_{gs})_o \left\{ \frac{2}{\gamma_{gs} - 1} \left[ 1 - \left( \frac{P_2}{(P_{gs})_o} \right)^{(\gamma_{gs} - 1)/\gamma_{gs}} \right] \right\}^{1/2} \quad (46)$$

Also,

$$T_{gs2} = (T_{gs})_o \left[ 1 - \frac{\gamma_{gs} - 1}{2} \left( \frac{U_{gs2}}{(a_{gs})_o} \right)^2 \right] \quad (47)$$

so that,

$$\rho_{gs2} = \frac{144 P_2 M_{gs2}}{R T_{gs2}} \quad (48)$$

---

\*Derived from the steady-state momentum equation:

$$I_1 + P_1 A_1 + \int_1^2 PdA = I_2 + P_2 A_2$$

with the linear approximation that

$$\int_1^2 PdA = \left( \frac{P_1 + P_2}{2} \right) (A_2 - A_1).$$



and finally:

$$A_{gs2} = \frac{144 \dot{w}_{gs2}}{\rho_{gs2} U_{gs2}} \quad (49)$$

$$A_{cg2} = A_{cc2} - A_{cj2} - A_{gs2} \quad (50)$$

$$U_{cg2} = \frac{144 \dot{w}_{cg2}}{\rho_{cg2} A_{cg2}} \quad (51)$$

$$T_{cg2} = (T_{cg2})_0 \left[ 1 - \frac{\gamma_{cg2} - 1}{2} \left( \frac{U_{cg2}}{(a_{cg2})_0} \right)^2 \right] \quad (52)$$

$$\rho_{cg2} = \frac{144 P_2 M_{cg2}}{R T_{cg2}} \quad (53)$$

All these newly calculated values of combustion and surrounding gas stream properties were then used to re-enter the system of equations at Eq. 44 to obtain modified values of the propellant momentum sum, chamber pressure, etc. Experience showed that the solution usually converged to constant values after four or five iterations; the formulated computer program employed seven iterations.

Values for all parameters of interest having been calculated across an increment of chamber length, they were written out and then used as initial values for calculations across the next increment. This process was continued until either the throat position in the combustion chamber exhaust nozzle was reached or the combustion gas velocity exceeded the local sound velocity. While these two criteria for terminating the model calculations should actually be synonymous, there are valid reasons that they may appear to be different. First, the model computations start



from the injector face with prescribed values of chamber pressure, propellant flowrates, and chamber and nozzle configurations. The prescribed values may be incompatible, e.g., assumption of too high an injection and chamber pressure (or too low a flowrate or too large a throat) would result in calculation of subsonic gas velocity at the geometric throat. Conversely, assumption of too low a chamber pressure, etc., would give sonic gas velocity upstream of the geometric throat. It may thus be necessary to modify the prescribed initial values for the two criteria to come acceptably close to occurring at the same axial location.

#### Combustion Chamber and Nozzle Configuration

The cross-sectional area per injection element of the combustion chamber and nozzle convergence must be specified as a function of distance from the injector. For the transparent two-dimensional combustion chamber employed in the experimental investigation (Ref. 1), these areas are somewhat in doubt because of pyrex liner melting. The initial pretest geometry was modified as detailed in Appendix E to provide input values for the combustion model.



## CALCULATED RESULTS AND DISCUSSION

### BEST-FIT CASES

The selected model calculation results, which have been found to most nearly duplicate the experimental information, are presented and discussed. The reasons for the particular valuation of some parameters are indicated.

#### Initial Model Conditions

The majority of the combustion model cases calculated have been with initial conditions duplicating the experimental injection-end conditions of one of the two experiments that yielded essentially complete experimental information, i.e., tests 417 and 431. The initial model conditions for these two cases are summarized in Table 1.

Injection-end chamber pressure was not measured during either of these tests; the values found to result in model-calculated pressures that match the measured pressures further downstream are given in the table. Further, the pressure listed for test 417 is 100 psia lower than that reported in Ref. 1 because the model calculations corroborated an apparent discrepancy between measured parameters indicated there.

#### Values Selected for Arbitrary Constants

The chamber length increment was taken as  $\Delta x = 0.05$  inch on the basis that 100 increments (and, therefore, 100 spray groups) would permit atomization to proceed over a minimum of 5 inches of chamber length.



The atomization constants were taken as  $B_A = 30$ ,  $C_A = 0.15$ ,  $c_1 = 5.0$  and  $c_2 = 10.0$  (Eq. 1a, 2a, and 3). This value of  $B_A$  is two orders of magnitude larger than that recommended by Mayer (Ref. 2); it was necessary to avoid forming such extremely small spray droplets that their acceleration would result in very abrupt deceleration of the hydrogen stream. Further, it was also necessary to avoid such rapid evaporation of oxygen that combustibility requirements would be satisfied very near the injector. Mayer indicated that in Eq. 1 the importance of liquid viscosity may be overemphasized, i.e., that  $B_A$  may depend upon  $\mu_l^{-1/3}$ . Because the liquid waxes used in Ref. 3 were 20 to 70 times more viscous than liquid oxygen, this effect may partially account for the very large value of  $B_A$  required here. As noted earlier, some additional difference might be expected because Mayer's evaluation of  $B_A$  was based on a mean droplet diameter for the spray, and it is being used here to calculate a local individual droplet diameter. The value of  $C_A$  is toward the high side of the range recommended in Ref. 4.

The rate of decrease of the apparent radius of a hydrogen stream core still having injection velocity was controlled by taking  $c_4 = 0.11852$  in Eq. 13. The subsequent deceleration of the boundary between the spray zone and the surrounding flow was fixed by the exponent in Eq. 18; a value of  $c_6 = 0.65$  was used. As noted earlier, this exponent would be unity for a free jet; a value lower than unity seems likely to result from momentum exchange to the decelerating gases from concurrently decelerating liquid spray.

The maximum spray droplet size was selected as 230 microns, as detailed in Appendix B. Combustibility conditions were taken as 8.0 mole percent oxygen and  $U_t = 12.0 P^{1/2}$ . (This latter equation gives flame speeds approximately 40 percent higher than the turbulent curve in Fig. C-1.)



The fractions of nonburning spray zone gases diverted around the flame-front and into the gas stream surrounding the spray combustion zone (Eq. 24) was determined by  $c_7 = 0.35$ ; the particular value was selected to limit the amplitude of the abrupt combustion gas velocity jump when conditions comparable to test 431 were calculated. The total turbulent mixing length,  $L_t = 9$  inches, was also selected primarily from the experimental velocity profile of that test.

### Nonburning Region

Structure. The propellant flow structure calculated for comparison with test 417 is shown in Fig. 4. (Note that the radial scale is enlarged by 2-1/2 times compared to the axial scale.) As may be inferred from the number of annular gas-spray mixture groups, primary atomization of the liquid oxygen jet was calculated to have proceeded over approximately the first 3/4 inch from the injector and then to have ceased. The first formed spray groups were calculated to have been accelerated rapidly and thus to have decelerated large fractions of the hydrogen stream, with a resultant radial expansion of the decelerated gases. In fact, the entire hydrogen stream flow was very rapidly engulfed by, or drawn into, the expanding spray zone.

It is interesting to compare this calculated structure with nonburning experimental observations of coaxial jet injection. Figure 5 shows two microflash photographs of a cylindrical liquid nitrogen stream injected into ambient air (Ref. 14). Only the 3/16-inch diameter liquid nitrogen jet was flowing in Fig. 5a, while an annular gaseous helium flow (from a 325-psig source tank) surrounded the liquid nitrogen jet in Fig. 5b. The finer atomization imposed by the helium flow is apparent and the correspondence between the observed outer spray boundary there and the calculated



structure in Fig. 4 is striking. It was noted (Ref. 14) that an unatomized liquid core appeared to persist for some inches further downstream with the helium flowing than without it. In another experiment, two parallel cylindrical jets of water, spaced 0.53 inch apart and surrounded by coaxially injected gaseous nitrogen, were observed to maintain their identities as separate liquid jets for about 18 to 20 inches before jet instability eventually led to rather coarse atomization (Fig. 6). These experimental observations lend support to the calculated cessation of surface shear atomization a short distance downstream of the injector.

Liquid Oxygen-Jet Atomization. The calculated mean sizes of spray droplets produced locally by the surface-shear, wave-crest-shedding mechanism (Fig. 7a) remain constant as long as some hydrogen stream persists at injection velocity; it becomes larger as the spray zone boundary velocity decays.

The distributions of spray mass produced among all the droplet sizes are shown in Fig. 7b. The initial sizes and mass atomization rates were used there without accounting for reductions due to vaporization. Figure 7b is plotted on a normalized or reduced diameter basis to facilitate comparisons with standard distribution functions. The three mean diameters noted in Fig. 7b were derived from the calculated droplet masses using the relationship (Ref. 15),

$$(D_{qp})^{q-p} = \frac{\left[ \int_0^{D_{max}} D^{q-3} \left( \frac{dv}{dD} \right) dD \right]}{\left[ \int_0^{D_{max}} D^{p-3} \left( \frac{dv}{dD} \right) dD \right]} \quad (54)$$



Because the volume-number mean diameter,  $D_{30}$ , has been found to compare well with experimentally measured mean diameters in an operating rocket environment (Ref. 16), that mean diameter was used for normalizing the calculated droplet diameters. Ingebo has found that the distributions of spray mass from impinging doublet (Ref. 17) and showerhead injection elements (Ref. 16) were well described by the Nukiyama-Tanasawa distribution equation

$$\frac{dv}{dD} = \frac{b^{6/\delta} D^5}{\Gamma(6/\delta)} \exp[-bD^\delta] \quad (55)$$

The cumulative volume fraction of spray smaller than any arbitrary diameter is shown in Ref. 15 to be given, for this distribution, by the ratio of the incomplete and complete gamma functions:

$$v = \frac{\Gamma_{bD^\delta}(6/\delta)}{\Gamma(6/\delta)} \quad (56)$$

Evaluated at  $\delta = 1$ , this expression gave the indicated Nukiyama-Tanasawa distribution curve in Fig. 7b.

It is seen that, because the relative velocity between the liquid oxygen jet and the hydrogen stream is initially very high, the atomization process produces a spray in which both the numbers of droplets and the spray mass of the smaller droplet sizes predominate. While most rocket injectors produce sprays with  $D_{30}$  between 75 and 150 microns, the surface-wave mechanism produced sprays calculated to have  $D_{30}$ 's between 20 and 40 microns. Because the volume mean diameters of the liquid oxygen sprays are only slightly larger than the smallest droplets being produced, correlation between the calculated results and standard distribution equations is almost





impossible. Another problem arises because the sprays calculated by the coaxial jet model have both maximum and minimum droplet sizes, features that most distribution equations are not capable of describing accurately.

The upper limit distribution function (Ref. 15) accounts for a maximum spray droplet diameter and was used to correlate the spray data in Ref. 3. A dimensionless function of droplet diameter,  $y$ , is assumed to be normally distributed; thus,

$$\frac{dy}{dy} = \frac{\delta}{\sqrt{\pi}} \exp \left[ -\delta^2 y^2 \right] \quad (57)$$

with,

$$y = \log_e \left[ \frac{a D}{D_{\max} - D} \right] \quad (58)$$

The cumulative volume fraction is then given by,

$$v = \frac{\delta}{\sqrt{\pi}} \int_0^{D_{\max}} \exp \left[ -\delta^2 y^2 \right] dy = \frac{1}{\sqrt{\pi}} \int_{-\infty}^{\delta y} \exp \left[ -u^2 \right] du \quad (59)$$

Tables of the "probability integral" may be used to evaluate the latter integral.

For a spray distribution which fits the upper limit function, a plot of  $D (D_{\max} - D)$  vs  $v$  on log-probability paper should yield a straight line. The values of  $\delta$  and  $a$  can be determined from such a plot and, from them, various mean droplet diameters can be calculated (Ref. 15).



The calculated distributions of liquid oxygen spray mass are shown plotted on that basis in Fig. 8. It is seen that about 70 to 80 percent of the spray mass is fairly well fitted by a straight line, and further, that the two sprays are very nearly identical on this basis. Here again, however, the function fails to describe the calculated accentuation of spray mass associated with the smallest droplet sizes. Perhaps this is caused by the arbitrary suppression, in the atomization model, of only the atomization rate (rather than both rate and mean droplet sizes) in the first few  $\Delta x$ -increments. On the other hand, it may be possible that a lower limit/upper-limit distribution function would be required for adequately correlating sprays resulting from this kind of atomization when the relative velocity is initially very high. Such a distribution function is not known at the present time.

The percentages of the liquid oxygen flowrate that were calculated to have been atomized in the nonburning region are shown in Fig. 9; these were obtained by subtracting the percent of liquid oxygen remaining in the liquid jet from 100 percent. The abrupt changes in the atomization rates at 0.6 and 0.9 inch correspond to the cessation of atomization because any further atomization would produce droplets larger than the maximum permitted diameter. Nearly imperceptible increases in "percent atomized" downstream of those positions result from continued evaporation from the surface of the liquid oxygen jets.

Spray Vaporization. Also shown in Fig. 9 are the calculated percentages of the injected liquid oxygen that were vaporized. The comparatively rapid vaporization in the first 1 to 1-1/2 inches from the injector, particularly obvious under the conditions of test 417, was caused by the initially high velocity and concentration gradients. In some cases, a few of the earliest-formed, smallest-diameter spray groups were calculated to have been completely evaporated within this portion of the chamber.



The calculated oxygen concentrations at the outer boundaries of the non-burning spray zones are shown in Fig. 10. The effect of the higher gaseous hydrogen temperature in test 417 is clearly evidenced by the 2 to 3 percent higher oxygen concentration throughout the nonburning region. The bumps in these curves are loosely associated with positions of complete vaporization of the outermost spray groups, with positions where the spray zone boundary velocity falls below the droplet velocities in some of the outermost spray groups and with the completion of engulfing of the hydrogen stream into the spray zone.

Further insight into the spray vaporization phenomena may be gained by studying Fig. 11. Here, at positions fairly close to the injector, the oxygen concentration in the spray zone gases is seen to be highest near the liquid oxygen jet surface. This is because all of the gases drawn into that area have passed through the outlying spray elements and have evaporated part of their liquid. Additionally, those outlying elements are being continually exposed to new hydrogen entering the spray zone. Near the injector, then, the evaporated oxygen tends to migrate in, toward the liquid oxygen jet.

Further downstream, approximately 1 to 1-1/2 inches from the injector, the largest part of the gas deceleration has occurred, no new spray is formed, and little additional momentum is required for accelerating the spray groups. The spray zone gases tend to remain associated with a particular spray group for longer times. Because the heat of vaporization for that liquid oxygen that was vaporized had to come from the gas stream, the coldest gases are those nearest the liquid oxygen jet. These gases also surround the largest droplets. Vaporization near the liquid oxygen jet is thus very slow, while the smaller, outlying spray droplets (surrounded by warmer gases) vaporize at moderate rates. The results are



reflected in Fig. 11 as nearly constant oxygen concentrations in the gases near the liquid oxygen jet and continuously increasing concentrations with increasing radii and distances from the injector.

Velocities and Temperatures. Calculated velocities at the outer boundaries of the spray zones and the velocities of the liquid oxygen spray element droplets formed at a number of specific distances from the injector are plotted in Fig. 12. The diameters of the liquid oxygen droplets when they were formed are indicated on the droplet velocity curves. Under the conditions of test 417 (Fig. 12a), droplets of 20.55 microns initial diameter and smaller were calculated to be completely vaporized within the nonburning region; the positions of droplet consumption are indicated by simply terminating the velocity plots. No spray groups were calculated to have been completely gasified in the nonburning region for the conditions of test 431 (Fig. 12b).

The calculated spray zone droplet and associated mixed gas temperatures are plotted in Fig. 13 for the same spray elements whose velocities were plotted in Fig. 12a. To facilitate comparisons, all curves are labeled with the initial droplet diameters of the spray elements. It is seen that near the injector, as noted earlier, the gases cooled by oxygen evaporating into them are carried radially inward toward the liquid oxygen jet. Beyond 1 inch from the injector, the gas temperatures all decrease gradually as some of their sensible heat is used to supply heat of vaporization. The rate of gas temperature change is highest in the outermost elements, i.e., those which contain the smallest, fastest-evaporating droplets.

The liquid oxygen droplets are calculated to be heated to equilibrium temperatures and undergo quasisteady-state evaporation. Some of the



largest droplet size groups had not yet reached an equilibrium temperature before they entered the combustion region. The equilibrium temperatures are seen to vary slightly with differences in droplet sizes, gas temperatures, and convective conditions.

Qualitatively similar results were calculated for conditions of test 431. The equilibrium droplet temperatures were clustered around 200 to 210 R as opposed to the 220 to 230 R range shown in Fig. 13. The 160 R lower gas temperature was the largest factor in causing this difference.

Combustibility. Examination of Fig. 10, 11, and 12 reveals that the ultimate satisfaction of the combustibility conditions was controlled by different criteria under the two different sets of test conditions. For test 417, with high hydrogen injection temperature and velocity, enough oxygen was evaporated approximately 2 inches from the injector to fulfill the flammability criterion, but the spray zone boundary gas velocity was nearly 400 ft/sec. The proportionality constant in Eq. 23 was thus selected to force  $U_t$  to be equal to the calculated spray zone boundary velocity at the position of abrupt velocity changes observed in the experimental data (Ref. 1).

For test 431, just the opposite situation was obtained. The spray zone boundary velocity dropped below the calculated turbulent flame speed at about 2 inches from the injector, but the oxygen content of the spray zone gases was only about 5 to 6 mole percent. The value of the flammability limit was thus set equal to the spray zone boundary oxygen concentration at the position of abrupt experimental velocity change of this test.



Evaporation of a liquid droplet will cease when the partial pressure of the liquid species in the gas stream becomes equal to that species' vapor pressure at the droplet temperature (Eq. 12). If oxygen/hydrogen rockets are operated with very high chamber pressures and/or with relatively low propellant injection temperatures, it may not be possible to satisfy the combustibility conditions. The pertinent relationships are shown in Fig. 14, a plot of the maximum achievable oxygen mole fraction in gaseous hydrogen as determined from equilibrium liquid oxygen droplet temperature and chamber pressure. The maximum equilibrium droplet temperature is equal to the gas temperature, even if the liquid were injected at a higher temperature than the gas. For the purposes of this discussion then, the abscissa of Fig. 14 may be entered using hydrogen injection temperature.\* Coaxial jet injection of liquid oxygen and gaseous hydrogen with injection temperatures of 185 R into a rocket operating at 700 psia chamber pressure, for example, could not meet the combustibility requirements used in the current model. Figure 14 shows 6.5 mole percent oxygen to be the maximum attainable. This situation can be ameliorated only by augmenting the liquid oxygen vaporization by supplying heat from some other source not considered in this model.

Two heat sources not accounted for in the model are radiation from the chamber full of high-temperature gases and recirculation of combustion gases. Radiant energy transfer to the nonburning region was examined for the conditions of test 417 in a simplified manner; it was calculated that as much as 1 percent of the liquid oxygen injection rate could be

---

\*Figure 13 suggests that a value of gas temperature 10 to 20 R lower than hydrogen injection temperature would be more realistic. This temperature drop provides the sensible heat of the warming droplets, latent heat of vaporization, and superheat for the vapors.



evaporated by radiation. At an injection mixture ratio of 5, however, the oxygen content of the spray zone gases would be raised by an average of only 0.3 mole percent. Under other operating conditions, this effect could conceivably have more influence and needs to be taken into account.

The likelihood of combustion gas recirculating was indicated by the value of the Craya-Curtet number, previously described. The calculated values of that variable for the two tests analyzed are shown in Fig. 15. In both cases, the Craya-Curtet number exceeded the critical value of  $3/4$  well before the combustibility conditions had been satisfied; the omission of combustion gas recirculation from the model thus appears to be a valid simplification for these cases.

Chamber Pressure. The majority of decrease in gas stream momentum as the gases are decelerated is absorbed in accelerating the liquid oxygen spray. The remainder results in increasing chamber pressure along the axial length. The model calculations showed a rapid rise in chamber pressure in the first  $1/2$  inch of the chamber and a gradual rise in pressure throughout the remainder of the nonburning region. Certainly some pressure rise should be expected, but in the absence of direct experimental evidence, it is not possible to state how realistic the model predictions are in this regard. Possibly, the model overestimates the amount of gas needed to be decelerated for providing spray momentum, and thus overemphasizes the pressure rise in this region. This subject will be discussed further in the next section.





### Combustion Region

The nonburning regions were replaced by combustion regions at 3.25 and 3.20 inches from the injector in model calculations based on the conditions of tests 417 and 431, respectively.

Structure. The combustion region model resulted in structural characteristics shown in Fig. 16 for test 417. This figure is a direct follow-on to Fig. 4. Comparison with Fig. 1 shows the calculated structure to be roughly similar to that initially hypothesized; the calculated spray zone spreading is more abrupt and the nonspray-bearing gas mantle is much less prominent than anticipated.

The abrupt, rapid spreading of the propellant streams to completely fill the elemental chamber flow channel is an idealization required by the stepwise, downstream-progression model employed. In an actual subsonic flow, the propellant flow structure upstream of the flame front should be affected by the impending combustion region expansion and the spreading made less abrupt than that calculated.

Intuitively, the structure shown in Fig. 16 suggests that the choice of this combustion region model based on a well-mixed, one-dimensional spray combustion zone being surrounded by a nonspray-bearing gas mantle is probably much less realistic than one based on a very oxygen-rich, dense spray core being surrounded by combustion gases having decreasing spray population with increasing distance from the axial centerline. Having selected the former basis for the model formulation, however, other calculated results will be examined before critical conclusions are drawn.





Combustion Gas Velocity. Immediately upon passing through the flame front at the leading edge of the combustion region, the spray zone gases were reacted. An abrupt increase of volumetric flowrate resulted; this, in turn, caused radial expansion until the propellant/combustion gas flow completely filled the flow channel. Then, higher axial gas velocities were attended by decreased chamber pressure. The existing liquid oxygen droplets' vaporization rates were greatly enhanced as a result of both higher gas temperatures and greater convection. This further raised the combustion gas velocity. The gas velocity soon became high enough so that liquid oxygen jet atomization by the surface shear mechanism was resumed. These processes are thus seen to be interrelated in a manner that causes escalation or bootstrapping to quite high combustion gas velocities.

Comparison With Experimental Velocity Data. The experimentally derived velocity and pressure data presented in Ref. 1 for tests 417 and 431 are reproduced in Fig. 17a and 17b, respectively. The calculated combustion gas velocities (and other parameters which are discussed below) are also plotted to facilitate direct comparisons. It is seen that the calculated combustion gas velocity jumps agree quite well with those observed experimentally. This suggests that the early portions of the combustion model adequately describe the initial bootstrapping processes.

Liquid Oxygen Jet Atomization. Under the conditions of test 417, the atomization process was calculated to be resumed immediately downstream of the flame front. The initially high combustion gas velocity resulted immediately in quite small liquid oxygen droplets; less than 1/4 inch into the combustion region, the produced spray was calculated to be wholly vaporized and reacted within the same  $\Delta x$  increment that it was atomized.



The residual liquid oxygen jet, containing 45 percent of the liquid oxygen injection rate, was thus found to be completely atomized in only 1/2 inch.

Because of the lower hydrogen injection rate and the lower proportion of oxygen evaporated in the nonburning region of test 431, a lesser jump in gas velocity was calculated to occur at the beginning of the combustion region than was found for test 417. The resumption of liquid oxygen jet atomization was delayed, therefore, until accelerated droplet vaporization increased the combustion gas velocity even more. Droplet sizes near the maximum were thus produced at first.

Continued vaporization led to a gradual reduction in the produced droplet sizes, but it was nearly 1 inch into the combustion region before the atomization rate became comparable with that found in the combustion region for test 417. These relationships are seen in Fig. 18. The calculated ends of the residual liquid oxygen jets correspond well with the experimentally observed distances to which velocity as low as liquid oxygen injection velocity penetrated in Fig. 17.

Two representative examples of the droplet weight distributions are shown in Fig. 19. The first, Fig. 19a, is for the sprays traversing the flame fronts the second, Fig. 19b, is for the sprays remaining just after completions of liquid oxygen jet atomization. Comparing Fig. 19a with Fig. 7b reflects the complete evaporation of several liquid oxygen spray group sizes in the nonburning region for test 417, so that  $D_{30}$  increased and the distribution favored the larger drop sizes, but there was only partial vaporization of all spray group sizes for test 431, so that  $D_{30}$  simply decreased. These changes do not appear to be predictable, a priori, from the injection conditions.



Comparing Fig. 19a and 19b, it is seen that the spray throughout the combustion region for test 417 can be described by the Nukiyama-Tanasawa distribution function. Because the new spray atomized from the jet was found to evaporate as soon as it was formed, all the spray shown for test 417 in these figures had its origin in the nonburning region. Ingebo (Ref. 16) has observed experimentally that a burning ethyl alcohol spray similarly fits the Nukiyama-Tanasawa function at several distances from a rocket injector. The liquid oxygen spray in the combustion region for test 431 was not nearly so simply behaved: nearly 85 percent of its spray shown in Fig. 19b originated in the combustion region. Again, neither the distributions nor mean droplet sizes of these sprays appear to be predictable by any means other than this model.

Spray Droplet Behavior. Calculated velocities for some droplet size groups are plotted in Fig. 17a and 17b. The velocities were comparable with those calculated in Appendix B and were well behaved. The largest formed droplet's velocities described a lower boundary for the experimental velocity data points.

Droplet equilibrium temperatures of 240 R were calculated for the conditions of both tests in the early portions of the combustion regions. These gradually dropped to 235 R at the beginning of nozzle convergence, in direct agreement with the behavior predicted in Appendix B, Fig. B-1 and B-2.

Nonspray-Bearing Gas Mantle Behavior. The gaseous flow diverted out of the nonburning liquid oxygen spray zone and around the flame front contained enough oxygen to be flammable under the conditions of test 417, but not under the conditions of test 431. The model calculations thus



ascribed reacted, combustion-gas properties to this gas stream in the former case and unreacted, mixed-gas properties in the latter case. The calculated gas stream velocities were correspondingly high for test 417 and low for test 431, as seen in Fig. 17. Because there were no experimental velocity data points as high as the calculated gas stream velocity for test 417, it must be concluded that either the radiation from that thin, reacted mantle was too weak to affect the streak film exposures or the mantle is fictitious.

Mixing of the model-calculated gas stream flowrate into the spray combustion zone at a linear rate with increasing distance from the injector, however, resulted in a combustion gas velocity profile that modeled the highest experimental velocity data very well. This is seen in the chamber length between 5 inches from the injector and the beginning of the nozzle convergence (Fig. 17).

To determine whether the gas velocity profile might be determined by unevaporated oxygen spray distributed along the chamber (Fig. 18), model calculations were made with no spray zone gases diverted into a gas stream mantle. The results (Fig. 20) suggest that the observed gradual approach to the nozzle inlet combustion gas velocity is almost wholly attributable to turbulent mixing of unlike gas streams. As noted before, the actual situation might require mixing a strongly oxidizer-rich core radially outward rather than a fuel-rich mantle radially inward. The overall effect would be the same: Over a sizeable fraction of the chamber length, the propellant combustion is controlled by turbulent mixing processes.

This result of the present model calculations is in direct agreement with the results of related experimental and analytical studies at NASA, Lewis Research Center (Ref. 18 and 19).



Chamber Pressure. The calculated chamber pressures are seen to decrease rapidly immediately downstream of the flame fronts. These drops result from continuity of momentum. The increasing momenta of accelerating gases and spray can come only from a decreasing chamber pressure.

Following that precipitous drop, the calculated chamber pressures agree well with the measured pressures. Too few pressures were measured in the nonburning region and early combustion region to define the actual pressure profile, but those obtained suggest smoother pressure profiles than those calculated. Perhaps the apparent disagreement stems from the experimental measurements, e.g., the pressure tap geometry or flow patterns may have affected the data and (because the data are time and location averaged) fluctuations in individual flame front position and variations in those positions among all the jets would tend to smooth and flatten the pressure profile. On the other hand, the model could be forced to give a more nearly constant pressure profile by assuming more drastic suppression of atomization near the injector, considerably higher turbulent flame speeds and different flammability limits than those used. The calculated gas velocities would no longer match the experimental streak velocities upstream of the flame front, however. More quantitative knowledge in this regard will probably be dependent upon both refined pressure measurements and determination of flammability limits and flame velocities under appropriate rocket conditions.

#### Conclusions From the Best-Fit Cases

The integrated atomization and spray behavior formulation permits description of the entire propellant flow structure from specifications of the injector and chamber configurations and propellant injection conditions.



The potential utility of the combustion model is thus greatly enhanced. Further, the formulation should be directly applicable to studies of similar atomization processes with other fluids, whether or not evaporation is significant. For extension to other rocket combustors, the formulation may need to be expanded to include nonreacting gas circulation, combustion gas recirculation, and continued atomization by other processes, such as jet instability and centrifugal forces imposed by swirlers.

The model calculations offer definitive, convincing evidence for the existence of the hypothesized plane flame front standing at a fixed (or quasi-fixed) position in the liquid oxygen spray zone. Under the imposed model conditions, any penetration of combustion gases or flame into this zone at some upstream position would either be swept downstream (by the gas flow velocity exceeding the local turbulent flame speed) or would rapidly escalate through increased spray vaporization, chamber filling, gas acceleration and enhanced liquid oxygen jet atomization to the same phenomena described by the model but at the upstream position. This seemingly adamant interpretation is dictated by the model conditions of relatively low contraction ratio (which permits moderately high combustion gas velocities even though only fractional amounts of the liquid oxygen have been vaporized, and leads to combustion reaction and atomization mutually augmenting each other) and unappreciable combustion gas recirculation.

This interpretation is not believed to be incompatible with nor to refute other investigators' interpretations of their experimental observations in which it is suggested that the atomizing liquid oxygen jet and liquid oxygen spray zone are intimately surrounded by reacting combustion gases all the way upstream to the injector (Ref. 19 and 21). Their experiments were carried out in relatively high-contraction-ratio combustors and under conditions conducive to combustion gas recirculation, so that the bootstrapping phenomena should not have occurred.





The combustion region model appears to constitute an adequate although somewhat simplified representation of the spray gasification and transverse mixing processes. The one-dimensional model of the nozzle flow processes appears to describe them accurately to the nozzle throat when a nozzle erosion factor is applied to account for the cross-sectional area variation resulting from pyrex melting.

#### MODEL PREDICTIONS FOR OTHER MAINSTAGE CONDITIONS

Model calculations were carried out in which controlled variations were made in the initial conditions, while holding the values of all arbitrarily evaluated variables equal to those used in the best-fit cases. Chamber pressure, mixture ratio, hydrogen injection temperature, and liquid oxygen injection temperature were individually varied from those listed in Table 1 for test 431. The major comparison bases for evaluating the predicted effects were the location in the chamber where the combustibility criteria were satisfied, and which of those criteria was the last to be fulfilled.

Raising the chamber pressure by increasing both propellant flowrates at constant injection mixture ratio resulted in the calculated position of the flame front being closer to the injector face, i.e., 3.2 inches at 455 psia, 2.8 inches at 500 psia, 2.5 inches at 700 psia, and 1.7 inches at 800 psia. At the lower pressures, this effect resulted from somewhat finer atomization because of the increased gas density at higher pressures. At 800 psia, supercritical heating of the smallest liquid oxygen droplets was encountered. Their abrupt gasification caused the combustibility criteria to be satisfied appreciably earlier than they were at 700 psia. Hydrogen injection temperature was high enough to avoid altogether the vaporization difficulties noted earlier in relation to Fig. 14. Calculated



boundary velocities dropped below the turbulent flame speeds earlier than the flammable oxygen concentrations were reached in all of these cases. The Craya-Curtet number at the flame front was less than its critical value in the 800 psia case, implying that combustion gas recirculation could invalidate the model predictions at that and higher pressures.

The injection mixture ratio was varied by raising the hydrogen flowrate and lowering the liquid oxygen flowrates by amounts that would give total flowrate satisfying 100 percent  $c^*$  efficiency at a fixed chamber pressure. The flame front position moved downstream with increasing mixture ratio and was controlled by the attainment of flammable mixtures. The flame front moved upstream with decreasing mixture ratio, in general, but at mixture ratios of approximately 5, flammability could be achieved only at sizable distances (10 to 12 inches) downstream of the injector. The reason for this anomalous behavior was not discerned. Three position values were: (1) 2.5 inches at  $MR = 3$ , (2) 3.2 inches at  $MR = 7$ , and (3) 3.9 inches at  $MR = 12$ . Combustibility was controlled at that lowest mixture ratio by the velocity criterion.

Liquid oxygen injection temperature was varied from 160 to 210 R and the calculated position of the flame front moved steadily upstream as the temperature was increased. Some values were: approximately 6 inches at 160 R, 3.4 inches at 175 to 180 R, 2.4 inches at 190 R, and 1.9 inches at 210 R. Reaching flammable oxygen concentrations controlled combustibility at temperatures below 200 R, while deceleration to turbulent flame velocity controlled those cases having 200 R or warmer liquid oxygen.

The flame front position similarly moved upstream with hydrogen injection temperature increases. At 400 R, the combustibility was controlled by the velocity criteria, which was satisfied at 2.7 inches. The computer





model encountered computational difficulties in the nonburning spray zone with 500 R hydrogen and would not converge on a solution. With hydrogen colder than that reported for test 431, the flame front moved downstream. While 200 R hydrogen should eventually produce a combustible mixture (Fig. 14), the liquid oxygen evaporation was so slow that it is questionable whether combustibility could be achieved in the available chamber length; the highest spray zone oxygen concentration at 5 inches from the injector was only about 3 percent.

#### Comparison With Experimental Data

Several other tests were reported in Ref. 1 to have been conducted with the coaxial jet injector. While the combustion field velocity data were incomplete and a flame front position cannot be ascribed to each of those tests, comparisons can be based on the lengths of the liquid oxygen jet/spray visible in the high-speed Fastax motion pictures. The experimental condition for all the tests, together with estimates of the liquid oxygen jet lengths, are summarized in Table 2.

Chamber pressure variation among the tests was quite modest and most likely did not influence the observed liquid oxygen jet lengths appreciably. Liquid oxygen injection temperatures were not measured and so cannot be discussed. The combustor starting procedure was such, however, that the steady-state mainstage liquid oxygen temperatures should have been comparable among the tests.

Regarding the other parametric variations, the experiments do not appear to support the predicted anomalous behavior at mixture ratios in the vicinity of 5, nor the predicted difficulty in achieving combustible



mixtures with 200 R hydrogen. There may, of course, be an interplay between the two effects masked by the particular combinations of experimental temperatures and mixture ratios encountered. However, in view of the predicted sensitivity of the flame front position to liquid oxygen injection temperature, a few degrees difference in that variable among the tests may have exhibited an unexpectedly large influence on the results. For that reason, it was thought impossible to examine the existing experimental data satisfactorily with a comprehensive parametric model study.

#### MODEL PREDICTIONS FOR PRESTAGE CONDITIONS

It was reported in Ref. 1 that the liquid oxygen jet/sprays were visible during prestage for only about  $1/2$  to  $3/4$  inch from the injector, and that strong combustion gas recirculation was evident in the motion pictures. Because the prestage start transient lasted for about 0.4 to 0.5 second and approached steady-state conditions near the end of that time, model calculations were programmed for two sets of prestage conditions to see if their predictions would correspond with the experimental observations.

Altering the propellant flowrates from those of test 431 to obtain an injection mixture ratio of 3 at 260 psia chamber pressure resulted in a predicted flame front at 3.9 inches from the injector without recirculation of combustion gases. Similarly, an oxygen flowrate increase to obtain a mixture ratio of 5 at 365 psia chamber pressure (corresponding to the midpoint between prestage and mainstage) gave a predicted flame front at 3.05 inches without recirculation. In both cases, deceleration to turbulent flame velocity controlled the positions of the combustion fronts.



These results are diametrically opposed to the experimental observations. They apparently can only be explained by assuming that one or both of the propellant streams were actually much warmer than assumed in the model calculations so that the liquid oxygen was atomized, accelerated, and vaporized considerably faster than calculated. Again, it is unfortunate that liquid oxygen manifold temperatures were not measured. Also, fast-response instrumentation would have been required.

#### PREDICTED OSCILLATORY COMBUSTION

A possibility that the flame front might fluctuate, rather than stand at a fixed position was suggested by model calculations for a combustor having a different shape and contraction ratio than the transparent two-dimensional combustor. Results with 200 R hydrogen predicted a flame front standing several inches from the injector, but the expansion-deceleration-chamber area relationships were such that strong combustion gas recirculation was indicated. The model prediction with 300 R hydrogen was that the flame front would be appreciably closer to the injector, but recirculation would not be likely. Thus, recirculation of enough combustion gas to warm the hydrogen by 100 R would not only permit the flame front to move upstream but would simultaneously disrupt the combustion gas recirculation. The continued injection of fresh, cold hydrogen would then push the flame front back downstream and reopen the recirculation paths. Such an oscillating combustion process has not been observed in current combustors of conventional design.



## CONCLUSION

It has been found possible, using conceptual hypotheses derived from transparent model rocket combustor experiments, to construct a semiempirical, analytical model of the steady-state combustion processes following coaxial jet injection of liquid oxygen and gaseous hydrogen. Further, by judicious selection of assumptions and particular arbitrary constants, it has been possible to obtain substantial agreement between the model's predictions and experimental results from two of the experiments. The other experimental results have not fully corroborated the accuracy of analytically predicted trends, but insufficient data were obtained to establish or deny the model's validity.

Several aspects of the developed rocket combustion model are unique. Perhaps the most striking feature is the interpretation of the experimental results in terms of a standing, plane flame front. This concept has been determined conclusively to be inappropriate for systems in which both propellants are injected as liquids, but appears from this work to be valid for liquid-gas combinations if combustion gas recirculation is insignificant.

The use of fundamental combustion parameters (flammability limits and turbulent flame speeds) in rocket combustion models is unusual; they are here related directly to the flame-front phenomenon. If continued uses are to be made of coaxial jet injectors under conditions similar to those studied here, it would prove very helpful to analytical model studies to have more accurate knowledge of these parameters under appropriate rocket pressure, temperature, and flow conditions.



Another unique feature of the current model is the quantitative inclusion of the atomization process. This is the first time to our knowledge that this has been attempted. The significance of this accomplishment was somewhat reduced by the necessity of using arbitrary constants. Currently, the nonburning region model is being programmed to calculate liquid wax atomization by an airstream in anticipation that a single set of constants can be found to reproduce the variety of atomization data in Ref. 3, and that those can be related to the constants used here for liquid oxygen/gaseous hydrogen.

One reason for developing a steady-state combustion model is to determine if combustion efficiency will be degraded by large propellant droplets passing through the nozzle without being evaporated. By including the atomization process in the model, direct knowledge is gained of what the largest droplet sizes are, how much of the spray mass is associated with them, and equally important, where they are formed. Thus, if undesirably coarse spray is encountered, a much more enlightened injector modification program can be undertaken than if only the undesirable droplet sizes were known.

Turbulent mixing processes between unlike gas streams in the combustion region, although treated in an approximate manner, have been shown to limit the propellant combustion rates through much of the chamber length. The selected turbulent mixing of a gas mantle into a well-mixed spray combustion zone is possibly less factual than is the mixing of an oxygen-rich, dense-spray core into a surrounding fuel-rich, dilute-spray flow. Further, a more rigorous quantitative treatment of turbulent mixing would be required for studying effects on combustion efficiency of element spacing or injection density changes.



Radiant energy transfer and combustion gas recirculation, neglected in this model, appear to be important, if not controlling processes, with some injector and chamber geometries and under some operating conditions. While these phenomena might profitably be included in future model developments, the fact that such a statement can be made demonstrates one area of usefulness of the present model. Comparison between analytical predictions and experimental observations with a variety of systems can increase greatly the current understanding of the combustion processes. Such qualitative contributions are of value through indirect influence on problem solution across a broad range of problems.

Another area of combustion model utility is in predicting the effects of making parametric changes in a particular combustor system. Quantitative effects can be observed. Of course, extension to conditions very much different from those previously found to agree with the model will be subject to some doubt unless limited experimental confirmation is undertaken.

APPENDIX APHYSICAL, THERMODYNAMIC, AND TRANSPORT PROPERTIES FOR THE  
NONBURNING REGION

Data for selected properties of hydrogen and oxygen were curve fitted to obtain relationships for use in the combustion model solutions. Unless a specific indication is made of pressure or pressure dependence, the equations were derived for properties at 500 psia and the properties were assumed not to vary appreciably with pressure within the ranges of pressure encountered in the model calculations.

## PROPERTIES OF LIQUID OXYGEN

Density

$$\rho_{\text{LOX}} = 39.88 + 0.479 T_L - 0.001733 T_L^2 \quad (\text{A-1})$$

$(T_L < 275\text{R})$

Surface Tension

$$\sigma_{\text{LOX}} = 2.485 \times 10^{-3} - 0.975 \times 10^{-5} T_L \quad (\text{A-2})$$

$(126\text{R} < T_L < 160\text{R})$



### Viscosity

The viscosity at zero pressure was arbitrarily multiplied by two as an approximation of the effect of pressure.

$$\mu_{\text{LOX}} = 2 \exp \left[ \frac{352}{T_l} - 11.13 \right] \quad (\text{A-3})$$

$$(140\text{R} < T_l < 220\text{R})$$

### Specific Heat (Constant Pressure)

$$(c_p)_{\text{LOX}} = 0.3726 + 2.0482 \times 10^{-4} T_l \quad (\text{A-4})$$

### Vapor Pressure

$$P_{v, O_2} = \exp \left[ 11.961 - \frac{1476.49}{T_l - 3.568} \right] \quad (\text{A-5})$$

$$(160\text{R} < T_l < 278.6\text{R})$$

### Heat of Vaporization

The values at saturation pressures were curve-fitted;

$$H_{v, O_2} = 128.23 \left( 1 - \frac{T_l}{278.6} \right)^{0.38} \quad (\text{A-6})$$





## GASEOUS OXYGEN PROPERTIES

Specific Heat (Constant Pressure)

$$(c_p)_{\text{gO}_2} = 1.16 - 0.00275 T, \quad (T < 300 \text{ R})$$

$$(c_p)_{\text{gO}_2} = 0.2134 + \left( \frac{5.2404}{T - 256.9} \right), \quad (300\text{R} < T < 740\text{R}) \quad (\text{A-7})$$

$$(c_p)_{\text{gO}_2} = 0.2489 + 0.964 \times 10^{-5} T - \frac{1.555 \times 10^4}{T^2}, \quad (740\text{R} < T)$$

Diffusivity into Hydrogen

An expression recommended in Ref. 22 was used for extrapolating from a value of  $\mathcal{D}_{12}^P$  at 273 K and 1 atmosphere:

$$\mathcal{D}_{\text{O}_2, \text{H}_2} = \frac{1.4083 \times 10^{-6} T^{5/2}}{P (T + 192.6)} \quad (\text{A-8})$$

## GASEOUS HYDROGEN PROPERTIES

Viscosity

$$\mu_{\text{H}_2} = 1.213 \times 10^{-3} + 9.55 \times 10^{-9} T \quad (\text{A-9})$$

$$(70\text{R} < T < 500\text{R})$$



The expressions for the following three parameters should not be used at temperatures lower than those indicated.

Thermal Conductivity

$$k_{H_2} = 0.019 + 1.675 \times 10^{-4} T \quad (A-10)$$

$$(170R < T < 500R)$$

Specific Heat (Constant Pressure)

$$(c_p)_{g H_2} = 2.095 + 5.08 \times 10^{-3} T - 4.93 \times 10^{-6} T^2 \quad (A-11)$$

$$(150R < T < 500R)$$

Ratio of Specific Heats

$$\gamma_{H_2} = \frac{T + 2.7}{0.8012T - 44.4} - \left( \frac{T + 2.7}{0.8012T - 44.4} - 1.4 \right) \left( \frac{100 - P/14.69}{198} \right)$$

$$(T > 160R)$$

$$(A-12)$$



## GASEOUS MIXTURES OF HYDROGEN AND OXYGEN

Mole Fraction Oxygen

$$X_{O_2} = \frac{\dot{w}_{O_2}}{\dot{w}_{O_2} + 15.873 \dot{w}_{H_2}} = \frac{\dot{w}_{O_2}}{15.873 \dot{w}_g - 14.873 \dot{w}_{O_2}} \quad (A-13)$$

Molecular Weight

$$M_g = \frac{32 \dot{w}_g}{15.873 \dot{w}_g - 14.873 \dot{w}_{O_2}} \quad (A-14)$$

Heat Capacity (at Constant Pressure)

$$(c_p)_g = \frac{32 X_{O_2} (c_p)_{O_2} + 2.016 (1 - X_{O_2}) (c_p)_{H_2}}{M_g} \quad (A-15)$$

Viscosity

The viscosities of mixtures containing 3, 5, and 7 mole percent oxygen were calculated by a method recommended in Ref. 22 and fitted with the following:

$$\mu_g = \mu_{H_2} \left( 1 + 8.5 X_{O_2} - 30 X_{O_2}^2 \right) \quad (A-16)$$



### Thermal Conductivity

A correlation method recommended in Ref. 22 for predicting the thermal conductivity of gaseous mixtures was used to estimate values for 3, 5, and 7 mole percent oxygen. These were curve-fitted by,

$$k_g = k_{H_2} (1 - 6.98 X_{O_2} + 32.5 X_{O_2}^2) \quad (A-17)$$

### PROPERTIES OF GAS FILM AROUND A DROPLET

The appropriate preceding properties were evaluated in the gas film surrounding a liquid oxygen droplet by using an assumed arithmetic mean film temperature,

$$T_f = \frac{T_d + T_g}{2} \quad (A-18)$$



## APPENDIX B

### DETERMINATION OF A MAXIMUM DROPLET SIZE FOR LOX-JET ATOMIZATION

The liquid oxygen/gaseous hydrogen propellant combustion field was reported in Ref. 1 to have been observed by simultaneous motion and streak photographic techniques. Velocity data reduced from luminous traces on the streak films exhibited characteristics that supported the hypothesis that the highest velocities measured at any particular distance from the injector were representative of local combustion gas velocity. Considerable doubt was expressed concerning the physical significance of the lowest observed velocities, particularly at distances several inches downstream of the photographically observed disappearance of a discrete liquid oxygen jet/spray. At approximately the end of the visible liquid oxygen jet, however, the lowest velocities approximated liquid oxygen injection velocities, and further downstream more or less abrupt velocity increases were noted. It was stated (Ref. 1) that "The inflections to increasing lower boundary velocities probably correspond with completion of liquid oxygen jet atomization. For a short distance downstream of that point, the lower boundary must reasonably be attributed to large liquid oxygen droplet trajectories."

Droplet ballistic equations show that a large, massive droplet will be accelerated more slowly by a given gaseous flow around the droplet than will a small droplet. If the lowest velocity streaks correspond with large droplets, then (neglecting initial velocity and gas inhomogeneity effects) those must be the largest droplets; otherwise, even lower velocity streaks would have been observed. This observation has been used before (Ref. 5) in combustion model calculations as an indication of the maximum size droplets that might occur in a burning spray.



Even if the lowest streak velocities are not known to result from large droplets, it can be hypothesized that if an arbitrarily large droplet were formed, it would produce streak velocities even lower than those actually observed. If that arbitrary diameter were then successively reduced, a particular size might be found that would accelerate so that its velocity history would duplicate (or approximate) the lowest observed velocities. That particular size could then be considered to be the maximum droplet size produced in the experiment under investigation.

That concept was applied in determining the maximum liquid oxygen droplet size that the atomization process model should be permitted to produce. It was assumed that the rocket combustion gas flow field could be prescribed throughout an appropriate length of the combustion chamber. Parameters of interest include velocity, pressure, composition, molecular weight, density and the transport properties (viscosity and thermal conductivity). These were derived from construction of an upper boundary around the experimental streak velocity data and from an assumption that the combustion gas at every axial position corresponded to the injection mixture ratio.

A single droplet of liquid oxygen was then imagined to be inserted into that flow field at some point and its subsequent history was calculated under the assumption that its evaporation/combustion had no discernible effect on the massive combustion gas flow. Because this is an initial value problem, the calculations must begin from assumed values of droplet diameter, temperature, and velocity as well as from a particular position in the chamber. Here, interest lies in droplets of arbitrary diameter and having liquid oxygen injection velocity and temperature, being first exposed to the combustion gas stream at about the point of complete primary atomization.



The equations used in this study are the same as those used in the complete combustion model, i.e. Eq. (7), (8a), (8b) and (9) for droplet ballistics, Eq. (10) and (11) for droplet temperature change, and Eq. (30) for droplet evaporation. The physical and transport properties employed were similarly evaluated (as discussed in Appendix D). The equations were programmed for solution with an IBM 7094; the solution was based on simple stepwise progression down the length of the chamber from the droplet insertion point. Portions of the read-in data and of the computed results were machined plotted to give direct visualization of how closely the velocities matched.

The calculated behaviors of six sizes of liquid oxygen droplets with initial temperatures of 180 R and initial velocities of 180 ft/sec, which were assumed to have been inserted 3.0 inches downstream of the injector into a combustion gas flow field based on the experimental data of run 417, PETER, PRA (Ref. 1), are shown in Fig. B-1 a, b and c. Comparable results are shown in Fig. B-2 a, b and c for similar liquid oxygen drops inserted 4.5 inches from the injector at 200 ft/sec into a combustion gas flow field prescribed from run 431, PETER, PRA.

Examination of these calculated results suggests that droplets having diameters between 175 and 200 microns might correspond to the maximum size droplets that could have produced the lowest velocity streaks. Comparison with other calculated results, in which droplets formed closer to the injector were considered, and recognition that the actual gas densities over the first few inches of calculation must be higher than those used in the calculations, led to the selection of 230 microns as the maximum liquid oxygen droplet diameter for use in the model.



## APPENDIX C

### FLAMMABILITY LIMITS AND FLAME VELOCITIES FOR FUEL-RICH HYDROGEN/OXYGEN MIXTURES

The flammability limits of hydrogen/oxygen gas mixtures at low temperatures and high pressures and under relatively high-velocity flow conditions have not been systematically determined. Values for combustibility evaluation in the combustion model calculations were derived from examination of the effects of these variables on the limits for less severe conditions than those encountered in the rocket experiments.

At atmospheric pressure, values ranging from 92 to 96 mole percent hydrogen have been reported (Ref. 23) for the upper, fuel-rich flammability limit. Variability in the limit composition arises from differences in type and size of apparatus employed, strength of the ignition source, direction of flame propagation, purity of reactants, and initial mixture temperature. A reasonable base value appears to be 94 percent hydrogen at 291 K and 1 atmosphere.

Constantine (Ref. 24) has used a concept attributed to Zabetakis to calculate the effects of reactant temperature on the upper flammability limit. The limit mixture is said to occur at compositions such that combustion product temperature remains a constant. The lowered initial enthalpy that results from mixing liquid oxygen with gaseous hydrogen was calculated to narrow the upper limit (i.e., lower the hydrogen concentration) by only about 0.2 percent. Varying the initial hydrogen temperature had a much more pronounced effect. Mixing liquid oxygen with hydrogen at 80 K gave a calculated limit of 92.8 percent hydrogen, which broadened linearly with increasing hydrogen temperature to 95.5 percent at 580 K.





Raising the pressure apparently broadens the upper limit for these reactants; an increase from about 92.5 percent hydrogen at atmospheric pressure to about 95.5 percent at 15 atmospheres has been reported (Ref. 25). This trend has been interpreted as supporting a thermal flame propagation mechanism rather than a chain branching mechanism (Ref. 26).

The superposition of a flow velocity on limit mixtures of hydrogen and oxygen apparently has not been studied. There is some evidence (from comparing quiescent tube and flat-flame burner results for other fuels) that suggests that broadened limits may be experienced (Ref. 26). For a purely thermal propagation mechanism, however, turbulence of the flowing stream may enhance local quenching and result in narrowed limits (Ref. 27).

For lack of more definitive information, values of upper flammability limit were selected for model computations with an assumed simplification that the effect of pressure is offset by the effects of flow and turbulence. Thus values of 92 to 95 percent hydrogen were used.

Quantitative information regarding the turbulent flame velocities through hydrogen/oxygen mixtures are even less abundant than flammability limit data. Most investigators have measured laminar flame speeds and the majority of the available data are for oxidizer-rich or near stoichiometric mixtures. For laminar flames, the highest velocities have been observed with mixtures that are slightly fuel-rich, e.g., about 70 to 75 percent hydrogen (Ref. 28 and 29). These highest laminar velocities increase with pressure; data of Ref. 28 and 29 for pressures of 0.5 to 15 atmospheres are quite well fit by an exponential equation of a form given in Ref. 28,

$$S_u \text{ (cm/sec)} = 1200 + 315 \log_e [P \text{ (atm)}] \quad (C-1)$$



Flame speeds at 90 atmospheres, however, exceeded that given by Eq. (C-1) by about 75 percent so that extrapolation to pressures greater than 15 atmospheres is certainly questionable. A more often reported relationship between laminar flame speed and pressure is,

$$S_u = a P^b \quad (C-2)$$

Values of the pressure exponent apparently range from about  $-1/2$  to  $+1$ , depending upon the specific reactants involved and on the presence and concentration of diluents. Some investigators have suggested that the exponent is related to the order of reaction,  $n$ , through  $b = 1/2 (n - 2)$ ; experimental data should then favor values of  $b = -1/2, 0, +1/2$ , etc.

The laminar burning velocities of Ref. 28 and 29 are reproduced in a log-log plot in Fig. C-1. It is seen that an equation of the form (C-2) can include the data at 90 atmospheres, but does not fit the low-pressure data nearly so well as did Eq. (C-1).

Turbulent flame velocities through a stoichiometric hydrogen/oxygen mixture have been determined at two pressures using an extension of a Bunsen burner method (Ref. 30). These two data points are also shown in Fig. C-1. While the turbulent value at 14.6 atmospheres is  $1-3/4$  times the laminar value, considering them to be  $\pm 30$  percent away from the equation shown, which correlates the laminar data, makes the difference seem of dubious significance.

In Ref. 1, however, the velocity data reduced from luminous streak photographs indicated that the maximum gas velocities just upstream of the position of abrupt velocity increase were very appreciably higher than the laminar or turbulent data in Fig. C-1. This is roughly indicated by



a circled triangle on that graph. Considering that symbol as a valid turbulent flame-velocity point permits the approximation shown, i.e.,  $U_t \propto p^{1/2}$ . This relationship was applied in the model calculation, but the proportionality constant was selected arbitrarily to force the position of achieving combustible conditions to match the observed velocity jump position.

Other variables that are probably influential in determining flame speed have not been included, simply because no data were found. The laminar flame speed is known to decrease sharply with increasing hydrogen concentration, above about 70 percent (Ref. 29), but apparently no determinations with near-limit mixtures have been obtained. Similarly, the effect of lowering the reactant mixture temperature is not known.



## APPENDIX D

### PHYSICAL, THERMODYNAMIC, AND TRANSPORT PROPERTIES FOR THE COMBUSTION REGION

#### PROPERTIES FOR EQUILIBRIUM COMBUSTION GASES AT VARIOUS MIXTURE RATIOS

The computed results of frozen thermodynamic equilibrium performance calculations using the Rocketdyne n-element program (Ref. 31) were used. Properties were calculated for mixture ratios ranging from 0.5 to 48 pound  $O_2$ /pound  $H_2$  at 550 psia pressure. The properties needed in the combustion model computations are presented in Fig. D-1, D-2, and D-3 as functions of gas mixture ratio.

Values were read from these graphs at 18 selected mixture ratios (10 of which were between 0 and 9) and were made available to the computer as tabular arrays. At times in the model program when gas properties at a particular location in the chamber were required, the equivalent gas mixture ratio at that location was used to enter and search the table. Properties were determined by linear interpolation between the tabulated values corresponding with the mixture ratios immediately above and below the local mixture ratio. If the local effective mixture ratio exceeded the highest tabulated mixture ratio, the properties at the highest tabulated value were used.



## PROPERTIES OF GAS FILM AROUND A DROPLET

Evaluations of the Reynolds, Prandtl, Schmidt, and Nusselt numbers in Eq. 10 and 11 were based on mean values of the appropriate properties within the gas/vapor film around a droplet. In the nonburning region, the properties were approximated simply by assuming the free-stream composition and an arithmetic mean film temperature. In the combustion region, such an approach is not at all realistic because the combustion gases are reactive with the oxidant droplet vapors; much greater deviations from free-stream composition may be required before such a mean temperature can be effected.

For that reason, mean film properties were determined in the combustion region by the following method. The vapors evolved from a droplet were assumed to react instantaneously with the surrounding combustion gases to thermodynamic equilibrium. The oxidant concentration, however, must decrease with increasing distance from the droplet surface. At some point, the composition can conceivably be such that the local adiabatic flame temperature is the arithmetic mean temperature between the droplet and free-stream temperatures; the mean film properties were evaluated at that point. This was accomplished in the combustion model program by cross-plotting some of the desired properties against adiabatic flame temperature from the n-element performance program computations at several oxidizer-rich mixture ratios and then curve-fitting those cross plots. The resultant equations were:

$$\mu_{fg} = (4.4311 \times 10^{-5}) \log_e (T_{fg}) - 3.1570 \times 10^{-4} \quad (D-1)$$



$$k_{fg} = \exp \left[ (2.979 \times 10^{-4}) T_{fg} - 3.5967 \right] \quad (D-2)$$

Oxygen diffusivity was related to the combustion gas mixture ratio:

$$\begin{aligned} \mathcal{D}_{O_2, cg} &= (0.01421 + 0.09 R_{cg}) / P_1 \quad ; R_{cg} < 3.5 \\ &= (0.35444 - 0.007382 R_{cg}) / P_1 \quad ; R_{cg} > 3.5 \end{aligned} \quad (D-3)$$

Specific heat of oxygen vapor was evaluated by Eq. (A-7) using  $T_{fg}$ .



## APPENDIX E

### CROSS-SECTIONAL AREAS VS DISTANCE FROM INJECTOR FOR TRANSPARENT TWO-DIMENSIONAL MODEL ROCKET

The transparent two-dimensional model rocket combustion chamber, from which experimental results are used in this report ".....had a constant 1.00- by 21.63-inch cross section from the injector face to 12.5-inches downstream of the injector, then converged to a 1.00- by 13.50-inch cross section nozzle throat at 22.7-inches downstream of the injector. The initial chamber contraction ratio was thus 1.60;.....During the mainstage portions of the experiments with hydrogen/oxygen propellants, however, melting of the pyrex walls began a few milliseconds after full chamber pressure was achieved. Small globules of molten glass were continuously shed from the chamber exhaust so that the nozzle area gradually increased throughout each test and the contraction ratio gradually decreased." (Ref. 1).

The effective contraction ratio,  $\mathcal{A}_{\text{eff}}$ , at the time during a particular firing that the streak velocity data were reduced was inferred from the apparent combustion gas Mach number  $m_x$  at the beginning of nozzle convergence. Isentropic acceleration of a completely reacted, frozen-equilibrium combustion gas stream from a cross-sectional area  $A_x$  to sonic velocity at the nozzle throat, with area  $A_t$ , is given (Ref. 32) by,

$$\mathcal{A}_{\text{eff}} = \frac{A_x}{A_t} = \frac{1}{M_x} \left[ \frac{1 + \frac{\gamma_x - 1}{2} m_x^2}{1 + \frac{\gamma_x - 1}{2}} \right]^{\frac{\gamma_x + 1}{2(\gamma_x - 1)}} \quad (\text{E-1})$$



The melting and erosion of the Pyrex was seen photographically to occur fairly generally downstream of about 7 inches from the injector, both the motion pictures and posttest inspection suggested that the major configuration changes probably occurred in the nozzle section. The chamber cross-sectional area per injection element was calculated for combustion model input, therefore, with a wall erosion factor applied only in the nozzle. This factor was assumed to have a value of unity near the beginning of nozzle convergence and to increase linearly to a maximum value of  $1.60/A_{eff}$  at the nozzle throat.

The equations used were:

$$A_{cc} = A_{cci} \quad , \quad 0 < x \leq 12.50 \quad (E-2)$$

$$A_{cc} = F_{erosion} A_{cci} \left[ 0.538 + 0.0924 \sqrt{25 - (x-12.50)^2} \right] ,$$

$$12.50 < x < 14.82 \quad (E-3)$$

$$A_{cc} = F_{erosion} A_{cci} \left[ 1.059 - 0.0483 (x - 12.50) \right] ,$$

$$14.82 < x < 20.47 \quad (E-4)$$

$$A_{cc} = F_{erosion} A_{cci} \left[ 1.741 - 0.1482 \sqrt{25 - (22.7-x)^2} \right] ,$$

$$20.47 < x < 22.70 \quad (E-5)$$

where:

$$F_{erosion} = 1 + \frac{(1.6 - A_{eff})(x - 12.50)}{A_{eff}(22.70 - 12.50)} \quad (E-6)$$





## NOMENCLATURE

$a$	= velocity of sound, ft/sec or an arbitrary constant
$A$	= area, sq in.
$A_s$	= surface area, sq ft
$\mathcal{R}_{eff}$	= effective chamber contraction ratio
$b$	= spray characterization parameter or an arbitrary constant
$B_A$	= spray drop size parameter (Eq. 1)
$c$	= arbitrary constants
$c_p$	= specific heat at constant pressure, Btu/lbm-R
$C_A$	= spray atomization rate parameter
$C_D$	= drag coefficient
$Ct$	= Craya-Curtet number
$D$	= diameter, inches or microns
$D_{20}$	= surface-number mean droplet diameter for a spray
$D_{30}$	= volume-number mean droplet diameter for a spray
$D_{32}$	= volume-surface (Sauter) mean droplet diameter for a spray
$\mathcal{D}_v$	= diffusivity of one gas into another, sq ft/sec
$e$	= base of Napierian logarithms = 2.71828
$f( )$	= functional symbol
$F_{div}$	= fraction of spray element gas flow diverted out of the spray combustion zone
$F_I$	= fraction of initial gas momentum still associated with gaseous propellants
$F(n)$	= factor for suppressing atomization just downstream of the injector
$g_c$	= gravitational constant = 32.17 lbm-ft/lbf-sq sec
$H_v$	= heat of vaporization, Btu/lbm



ROCKETDYNE • A DIVISION OF NORTH AMERICAN AVIATION, INC

I	=	momentum, lbf
k	=	thermal conductivity, Btu/ft-hr-R
K	=	a defined droplet drag parameter (Eq. 7)
$L_t$	=	chamber length to accomplish turbulent mixing, inches
M	=	molecular weight, lbm/lb-mole
$m$	=	mach number
$\dot{N}$	=	number flowrate of spray droplets, $\text{sec}^{-1}$
Nu	=	Nusselt number
$Nu_H$	=	$2 + 0.6 Re^{1/2} Pr^{1/3}$
$Nu_M$	=	$2 + 0.6 Re^{1/2} Sc^{1/3}$
p	=	spray mean drop diameter variable (Eq. 54)
P	=	pressure, lbf/sq in.
$P_v$	=	liquid vapor pressure, lbf/sq in.
Pr	=	Prandtl number = $3600 c_p \mu/k$
q	=	spray mean drop diameter variable (Eq. 54)
r	=	radius, inches
R	=	universal gas constant = 1544 ft-lbf/lb-mole-R or gas mixture ratio, if subscripted
Re	=	Reynolds number, $\rho D U/(12 \mu)$
Sc	=	Schmidt number = $\mu/(\rho \mathcal{D})$
$S_u$	=	laminar flame speed, ft/sec
t	=	time, seconds
T	=	temperature, R
u	=	an integrating parameter (Eq. 59)
U	=	velocity, ft/sec
$U_k$	=	kinematic or space-mean velocity, ft/sec
v	=	cumulative volume fraction of spray smaller than diameter D
w	=	droplet weight, lbm



**ROCKETDYNE** • A DIVISION OF NORTH AMERICAN AVIATION, INC

- $\dot{w}$  = weight flowrate, lbm/sec  
 $\dot{W}$  = local spray production rate, lbm/sec  
 $x$  = distance along the direction of flow, inches  
 $\Delta x$  = incremental distance, inches  
 $X$  = mole fraction  
 $y$  = a dimensionless droplet diameter function (Eq. 58)  
 $z$  = heat transfer factor (Eq. 11)

#### Greek Letters

- $\gamma$  = ratio of specific heats ( $c_p/c_v$ )  
 $\delta$  = spray characterization parameter  
 $\mu$  = viscosity, lbm/ft-sec  
 $\pi$  = 3.14159  
 $\rho$  = density, lbm/cu ft  
 $\sigma$  = surface tension, lbf/ft  
 $\Gamma(p)$  = Gamma function =  $\int_0^{\infty} u^{p-1} e^{-u} du$ ,  $p \geq -1$   
 $\Gamma_{u_1}(p)$  = incomplete Gamma function =  $\int_0^{u_1} u^{p-1} e^{-u} du$ ,  $p \geq -1$   
 $\Sigma$  = summation symbol

#### Superscripts

(prime) = gas properties evaluated at an effective atomization distance away from the liquid jet surface



Subscripts

A	=	local surface atomization
b	=	gas, spray zone boundary value
cc	=	combustion chamber value
cg	=	combustion product gas value
cr	=	critical state value
d	=	droplet value
def	=	value within the mixing zone between a gas jet and its surroundings, referred to as a velocity defect zone
est	=	estimated value
f	=	value within the gas film surrounding a droplet
final	=	value at completion of combustion
g	=	value associated with a gas
gs	=	value associated with the non-spray-bearing gas stream in the combustion region
H <sub>2</sub>	=	gaseous hydrogen value
i	=	initial value
j	=	jet value
l	=	liquid (subcritical temperature, condensed state) value
max	=	maximum value
mean	=	average value
n	=	value associated with the nth spray group
o	=	stagnation value
O <sub>2</sub>	=	oxygen value
p	=	value at or preceding the position furthest from the injector to which a portion of a gas jet penetrates with injection velocity maintained or spray mean drop diameter variable
q	=	spray mean drop diameter variable



**ROCKETDYNE** • A DIVISION OF NORTH AMERICAN AVIATION, INC.

- r** = relative value or value at an arbitrary radius
- sz** = spray zone value
- t** = turbulent flame value
- v** = vapor state value
- w** = wall value
- x** = value at an arbitrary axial position
- 1** = value at the beginning of a  $\Delta x$ - increment
- 2** = value at the end of a  $\Delta x$ - increment
- 1-2** = value produced within a  $\Delta x$ - increment



## REFERENCES

1. Combs, L. F. and F. W. Hoehn, "Steady-state Rocket Combustion of Gaseous Hydrogen and Liquid Oxygen. Part I: Experimental Investigation." Research Report RR 64-24, Rocketdyne, a Division of North American Aviation, Inc., Canoga Park, California, June 1964.
2. Mayer, E., "Theory of Liquid Atomization in High Velocity Gas Streams." ARS Journal, Vol. 31, No. 12, December 1961, 1783.
3. Weiss, M. A. and C. H. Worsham, "Atomization in High Velocity Airstreams," ARS Journal, Vol. 29, No. 4, April 1959, 252.
4. Dickerson, R. A. and M. D. Schuman, "Atomization Rates of Droplets and Jets," AIAA Preprint No. 63-498, December 1963.
5. Lambiris, S., L. P. Combs and R. S. Levine, "Stable Combustion Processes in Liquid Propellant Rocket Engines," Combustion and Propulsion. Fifth AGARD Colloquium: High Temperature Phenomena, The MacMillan Co., New York, N. Y., 1963, 569-634.
6. Wieber, P. R., "Calculated Temperature Histories of Vaporizing Droplets to the Critical Point," AIAA Journal, Vol. 29, No. 11, December 1963, 2764-2770.
7. Bird, R. B., W. N. Stewart and E. N. Lightfoot, Transport Phenomena. John Wiley and Sons, Inc., New York, N. Y., 1960, 636-649.
8. Schlichting, H., Boundary Layer Theory, McGraw Hill Book Co., New York, N. Y., 4th Edition, 1960, 607.
9. Becker, H. A., "Concentration Fluctuations in Ducted Jet Mixing." Sc. D. Thesis, Department of Chemical Engineering, Massachusetts Institute of Technology, Cambridge, Mass., 1961.



10. Becker, H. A., H. C. Hottell and G. C. Williams, "Mixing and Flow in Ducted Turbulent Jets," Ninth Symposium (International) on Combustion, Academic Press, New York, N. Y., 1963, 7-19.
11. Schlichting, H., op. cit., 242.
12. Lewis, B. and G. vonElbe, Combustion, Flames and Explosion of Gases, Academic Press, New York, N. Y., 2nd Edition, 1961, 414-428.
13. Combs, L. P., "Calculated Propellant Droplet Heating Under F-1 Combustion Chamber Conditions," Research Report RR64-25, Rocketdyne, a Division of North American Aviation, Inc., Canoga Park, California, December 1964.
14. Carlson, L. W., Personal communication of unpublished experimental information, Rocketdyne, a Division of North American Aviation, Inc., Canoga Park, California, 1962.
15. Mugele, R. A., and H. D. Evans, "Droplet Size Distribution in Sprays," Ind. and Eng. Chem., Vol. 43, No. 6, June 1951, 1317-1324.
16. Ingebo, R. D., "Heat Transfer and Drag Coefficients for Ethanol Drops in a Rocket Chamber Burning Ethanol and Liquid Oxygen," Eighth Symposium (International) on Combustion, Williams and Wilkins Co., Baltimore, Maryland, 1962, 1104-1112.
17. Ingebo, R. D., "Drop-Size Distributions for Impinging-Jet Break-up in Airstreams Simulating the Velocity Conditions in Rocket Combustors," TN 4222, National Advisory Committee for Aeronautics, Washington, D. C., March 1958.
18. Hersch, M., "Effect of Interchanging Propellants on Rocket Combustor Performance with Coaxial Injection," TN D-2169, National Aeronautics and Space Administration, Washington, D. C., February 1964.



19. Burrows, M. C., "Radiation Processes Related to Oxygen-Hydrogen Combustion at High Pressures," a paper presented at the Tenth Symposium (International) on Combustion, Cambridge, England, August, 1964. To be published by The Combustion Institute, Pittsburgh, Penna., 1965.
20. Combs, L. P., "Mixing Processes in Liquid Propellant Rocket Combustion Chambers: A Review," a paper to be presented at the Joint Meeting of the American Institute of Chemical Engineers and the Institution of Chemical Engineers, London, England, June 1965. (August 1964).
21. Heidmann, M. F., "Oxygen-Jet Behavior During Combustion Instability in a Two-Dimensional Combustor," TND-2735, National Aeronautics and Space Administration, Washington, D. C., March 1965.
22. Reid, R. C., and T. K. Sherwood, The Properties of Gases and Liquids, McGraw-Hill Book Co., New York, N. Y., 1958.
23. Coward, H. F. and G. W. Jones, Limits of Flammability of Gases and Vapors, Bulletin 503, U.S. Bureau of Mines, Washington, D. C., 1952.
24. Constantine, M. T., "Flammability Limits of Hydrogen in Oxygen," unnumbered internal memorandum, Rocketdyne, a Division of North American Aviation, Inc., Canoga Park, California, 30 October 1962.
25. Edse, R. and W. A. Strauss, "Research on Combustion Phenomena at High Pressures," ARL TN 60-152, Ohio State University Research Foundation, Columbus, Ohio, February, 1961.
26. Linnett, J. W., and C.J.S.M. Simpson, "Limits of Inflammability," Sixth Symposium (International) on Combustion, Reinhold Publ. Corp., New York, N. Y., 1957, 20-27.
27. Mullins, B. P. and S. S. Penner, Explosions, Detonations, Flammability and Ignition, Pergamon Press, London, 1959, 123.





28. Agnew, J. T. and L. B. Graiff, "The Pressure Dependence of Laminar Burning Velocity by the Spherical Bomb Method," Combustion and Flame, Vol. 5, No. 3, September 1961, 209-219.
29. Strauss, W. A. and R. Edse, "Burning Velocity Measurements by the Constant-Pressure Bomb Method," Seventh Symposium (International) on Combustion, Butterworths Scientific Publ., London, 1959, 377-385.
30. Edse, R., Bull. Enging. Exper. Sta., Ohio, Vol. 149, 1952, 441; quoted by G. A. McD. Cummings: "Stationary Flames at Pressures Above One Atmosphere," Combustion Researches and Reviews 1957, Butterworths Scientific Publ., London, 1957, 4.
31. Gerhouser, J. M. and R. J. Thompson, Jr., "Theoretical Performance Evaluation of Rocket Propellants," Report No. R-5802, Rocketdyne, a Division of North American Aviation, Inc., Canoga Park, California, August 1964.
32. Sutton, G. P., Rocket Propulsion Elements, John Wiley and Sons, New York, N. Y., 3rd Edition, 1963, 41.



TABLE 1

INITIAL MODEL CONDITIONS FOR CASES  
COMPARABLE WITH EXPERIMENTAL DATA

Initial Value of Parameter	Experiment for Comparison (Ref. 1)	
	Test No. 417	Test No. 431
$P_i$ , psia	457	455
$A_{cci}$ , sq in./element	0.483	0.525
$\lambda_{eff}$	1.312	1.344
$\dot{w}_{O_2i}$ , lb <sub>m</sub> /sec-element	0.592	0.655
$T_{O_2i}$ , R	185	185
$A_{O_2i}$ , sq in./element	0.01368	0.01368
$U_{O_2i}$ , ft/sec	89.6	99.1
$\dot{w}_{H_2i}$ , lb <sub>m</sub> /sec-element	0.1200	0.0921
$T_{H_2i}$ , R	~ 465	~ 305
$A_{H_2i}$ , sq in./element	0.03452	0.03452
$U_{H_2i}$ , ft/sec	2670	1360
$R_i$	4.93	7.11



TABLE 2

SUMMARY OF EXPERIMENTAL CONDITIONS  
AND VISIBLE LOX JET LENGTHS

Test No.	Injector End $P_c$ , psia	Mixture Ratio, o/f	Hydrogen Injection Temperature, $R^*$	Approx. Visible LOX-Jet Length, inches
417	[470]**	4.9	~ 500	2.8 to 3.2
418	516	5.0	[chilled]	3.5 to 3.8
419	516	5.0	[chilled]	3.5 to 3.7
431	[450]**	7.1	315	4.1 to 4.3
432	516	4.1	205	3.0 to 3.2
433	522	5.2	210	4.1 to 4.3
452	459	5.8	200	3.8 to 4.1

\*The temperatures measured in the injection manifold were considered in the combustion model to be stagnation values.

\*\*Extrapolated from downstream pressure data by comparison with measured values from the other tests.

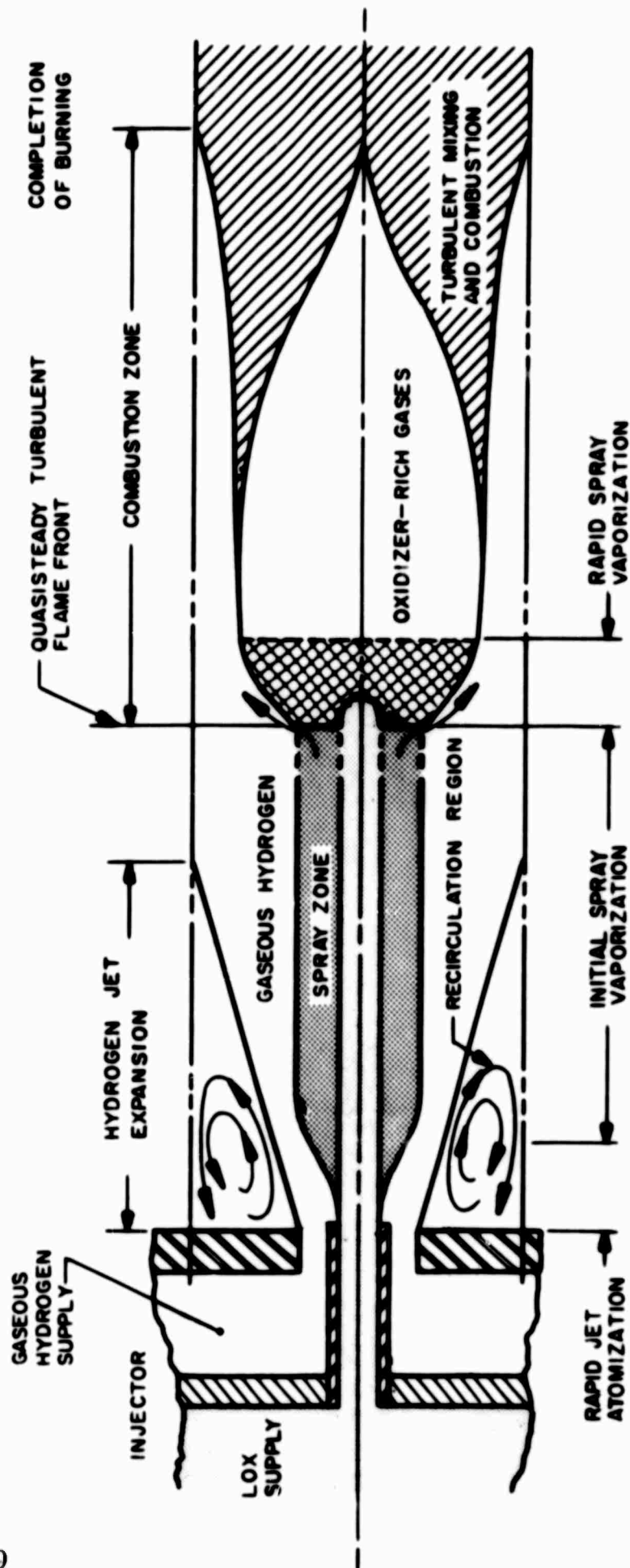


Figure 1. Schematic Representation of the Combustion Processes for Coaxial Jet Injection of Gaseous Hydrogen and Liquid Oxygen (Ref 1)

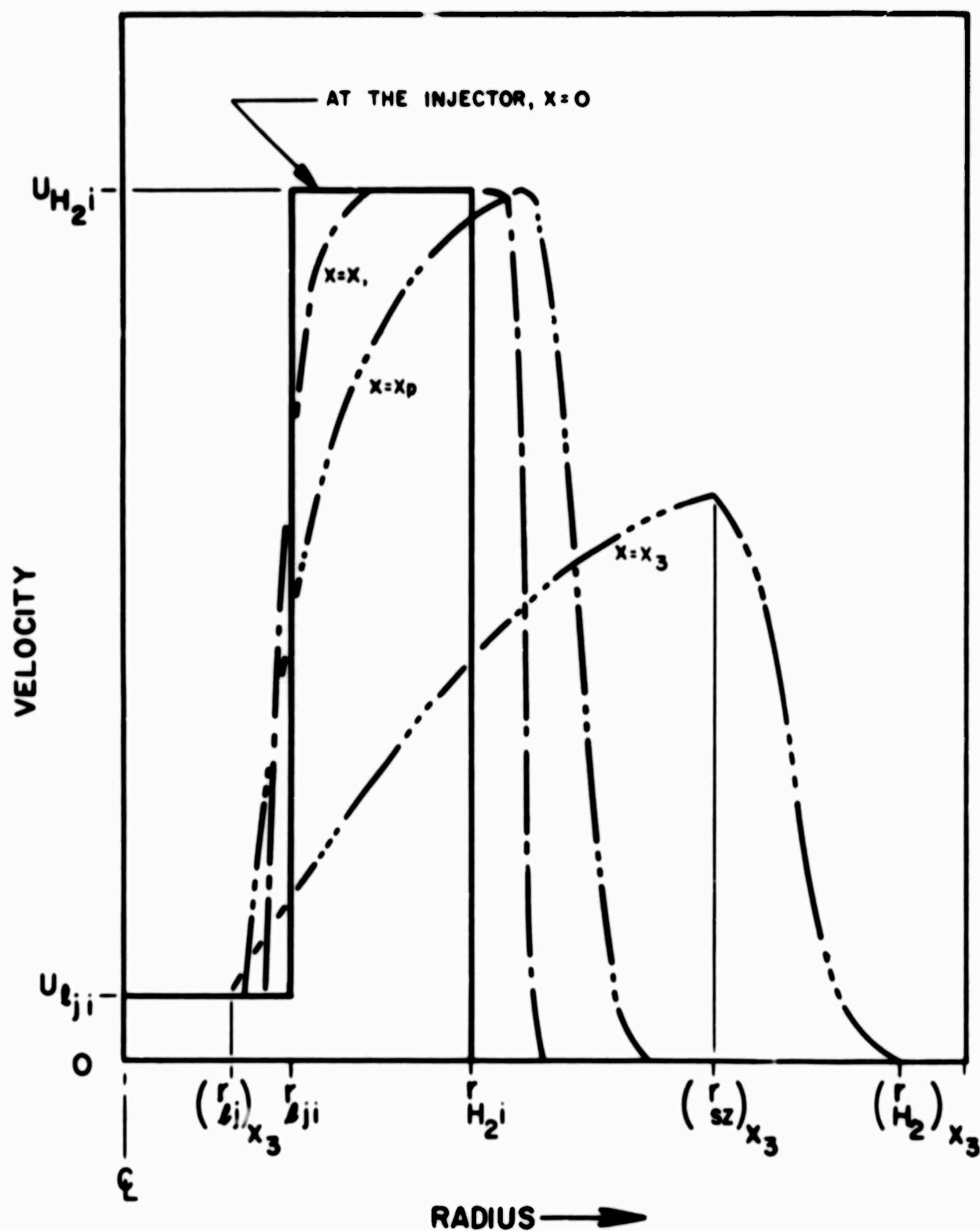


Figure 2. Velocity Profiles at Various Distances Downstream from a Coaxial Jet Injection Element (Conceptual)

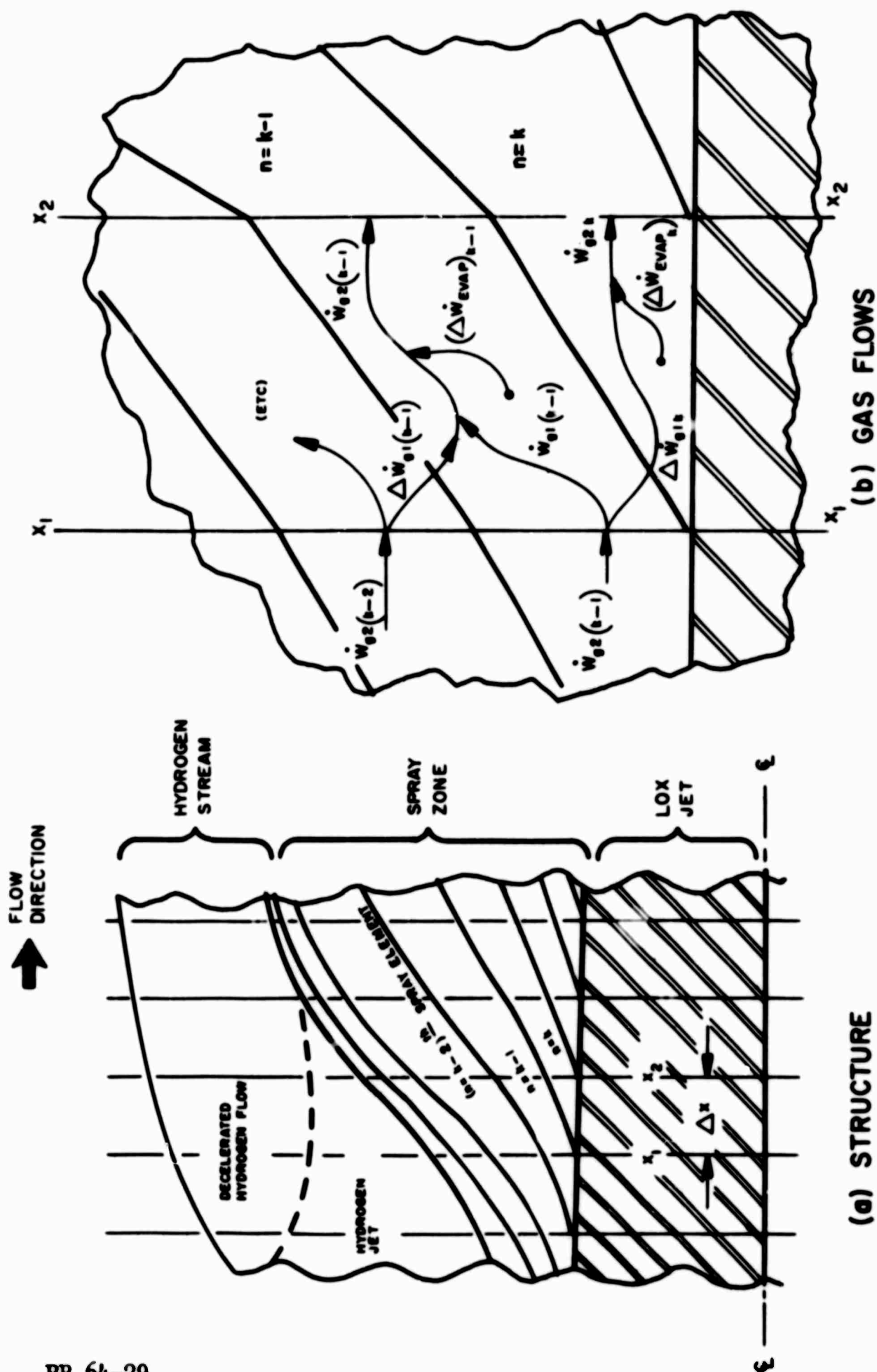


Figure 3. Spray Zone Elemental Structure and Gas Flows (Conceptual)

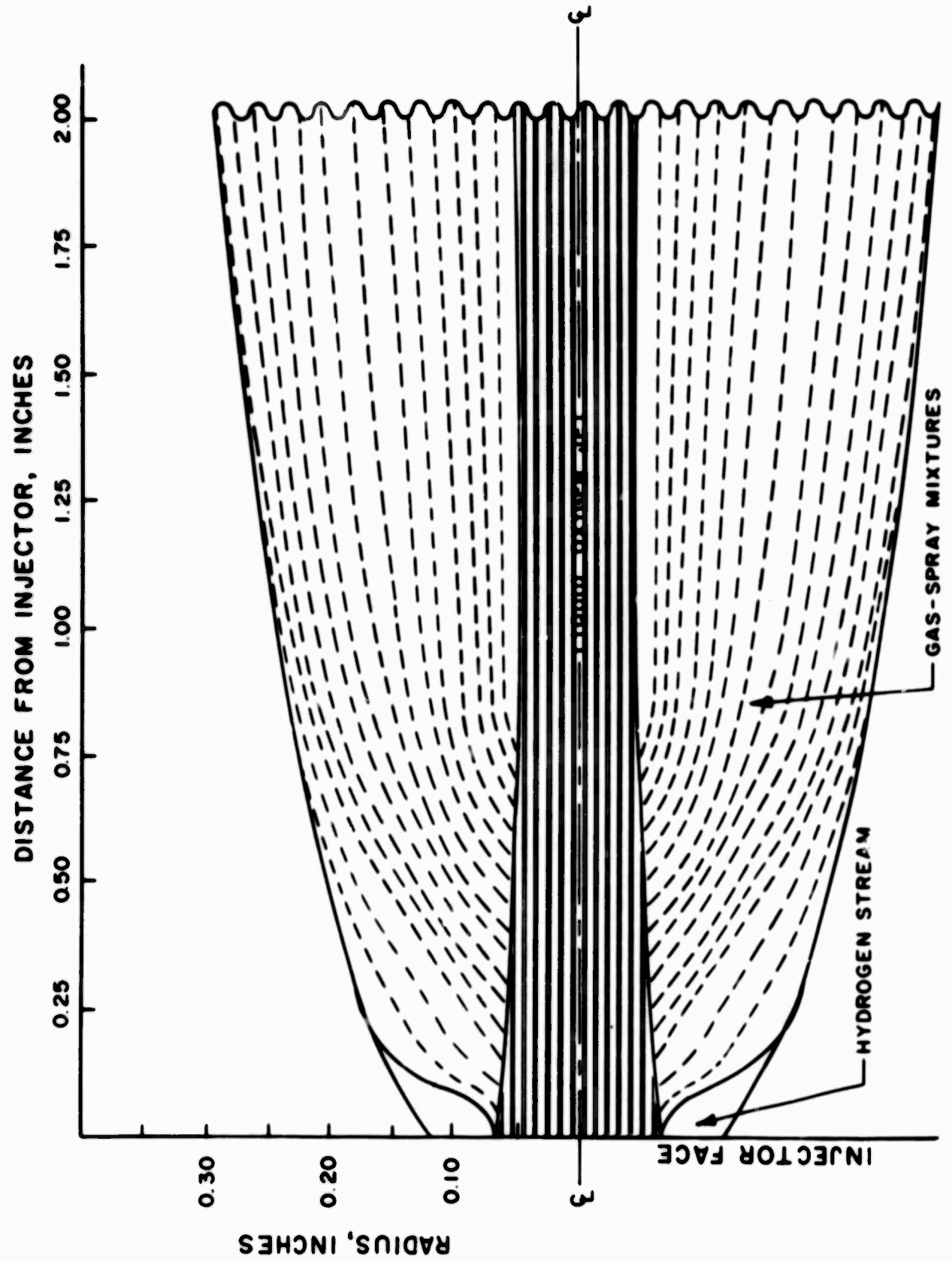


Figure 4. Calculated Nonburning Region Structure for Conditions of Test 417



(a) Without Surrounding Gas Flow

1260-8/7/61-S1A



(b) With Surrounding Flow of Helium

1260B-8/7/61-S1F

Figure 5. Coaxial Jet Injection of Liquid Nitrogen Into Ambient Air (Ref. 14)



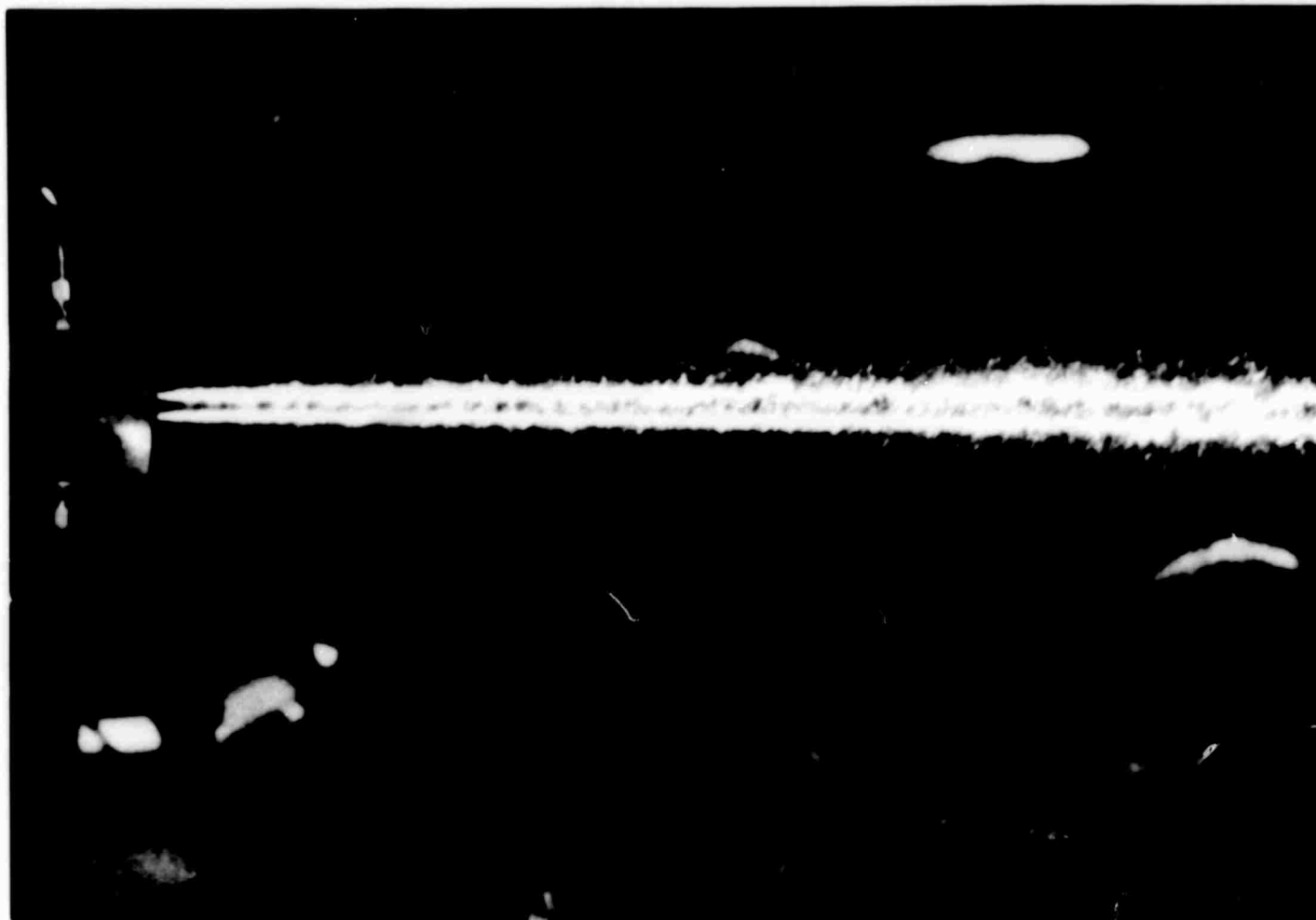


Figure 6. Photograph of Water Jet Atomization From Two Coaxial Jet Elements With Gaseous Nitrogen

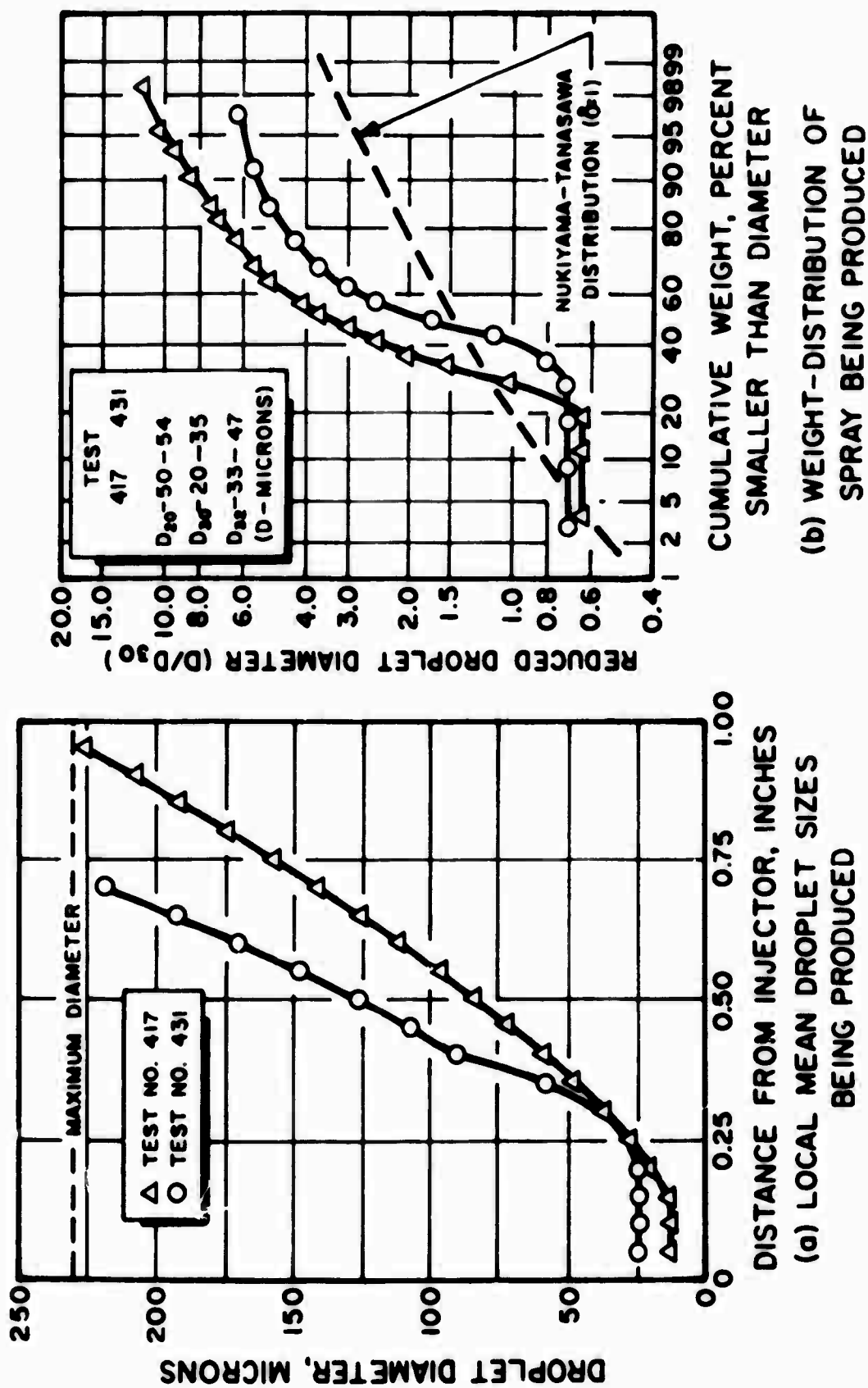


Figure 7. Calculated LOX Spray Characteristics (Nonburning Region)

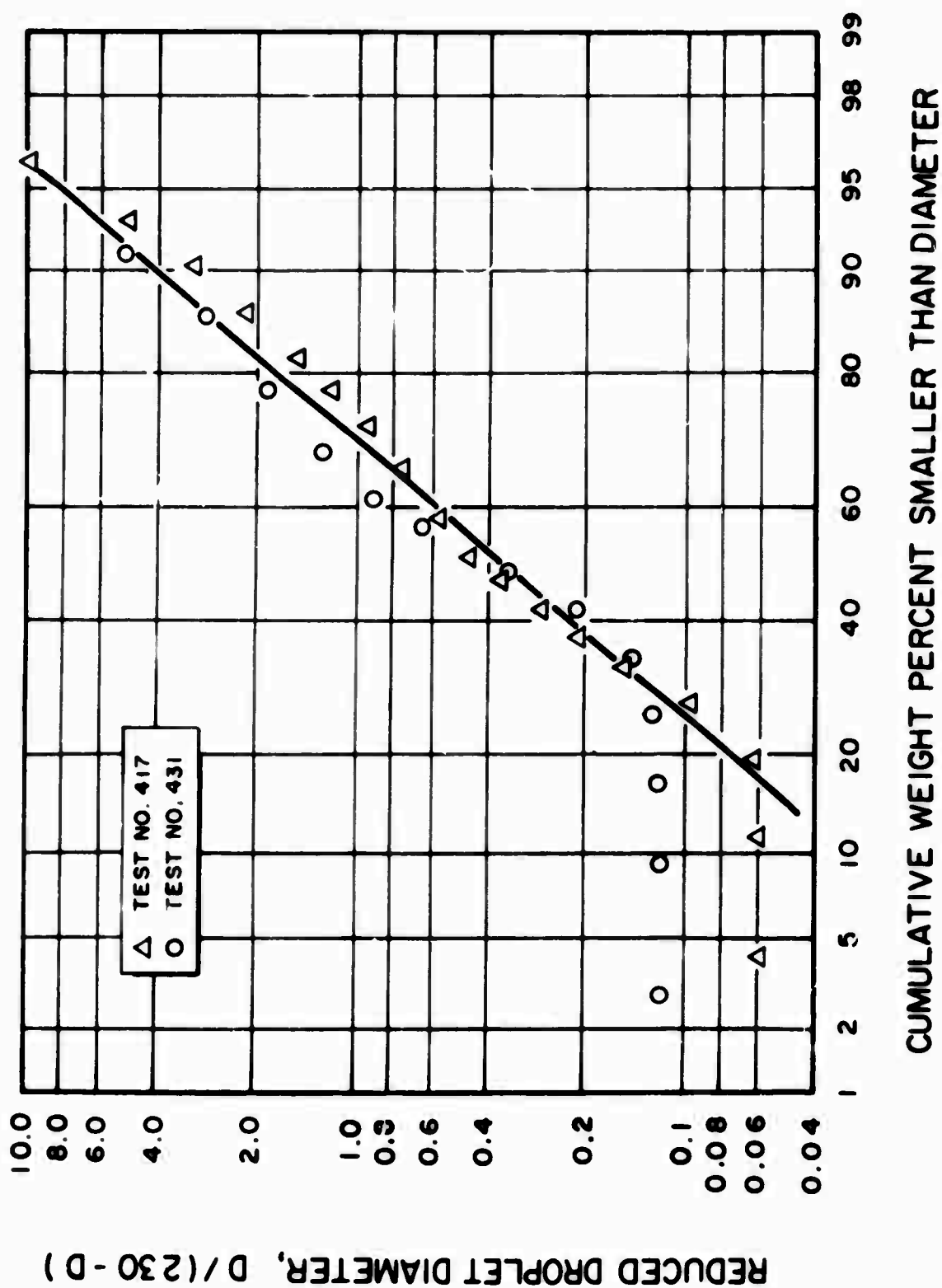


Figure 8. Weight Distribution of Spray Being Produced

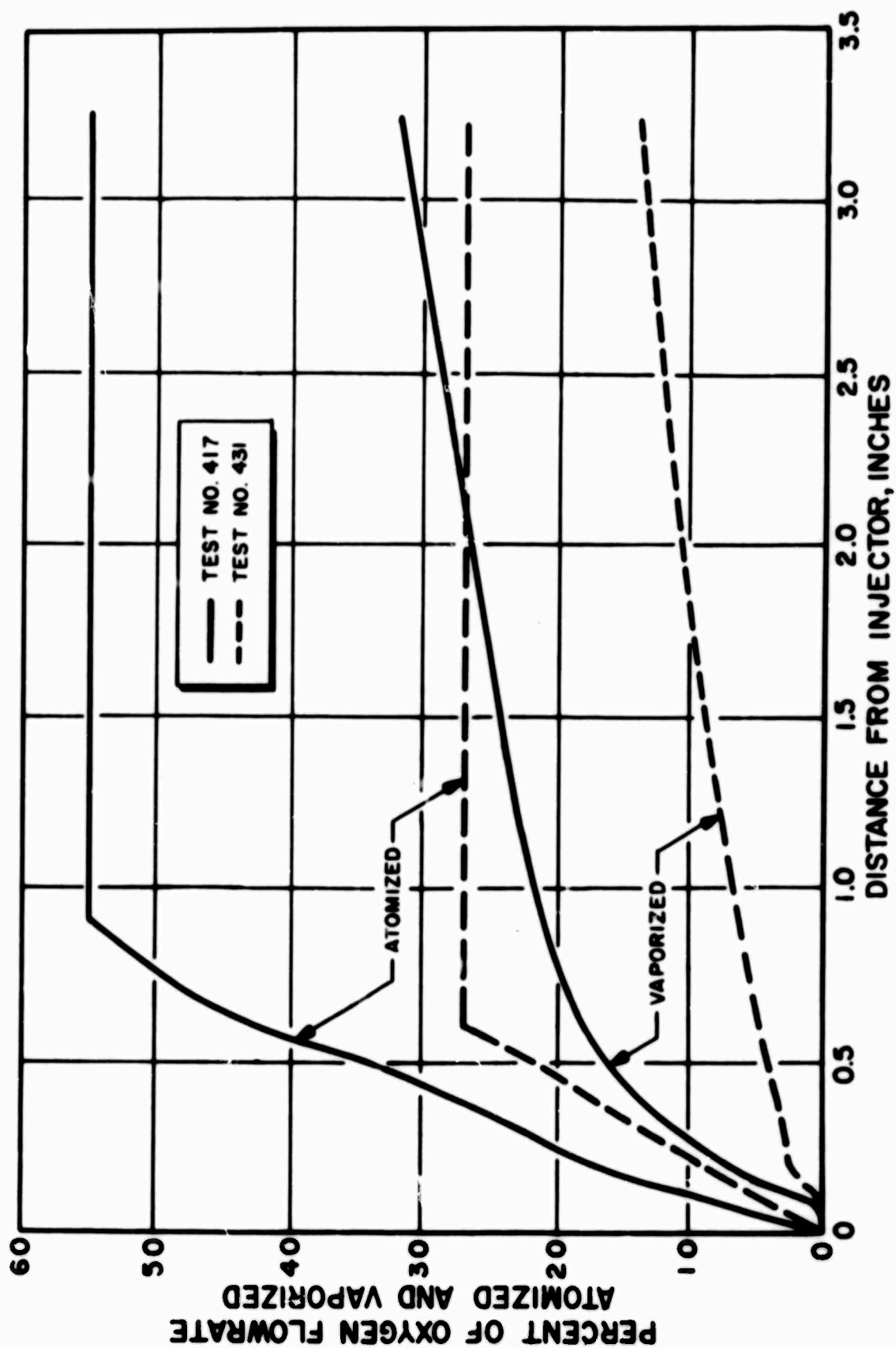


Figure 9. Lox-Jet Atomization and Spray Vaporization in the Nonburning Region

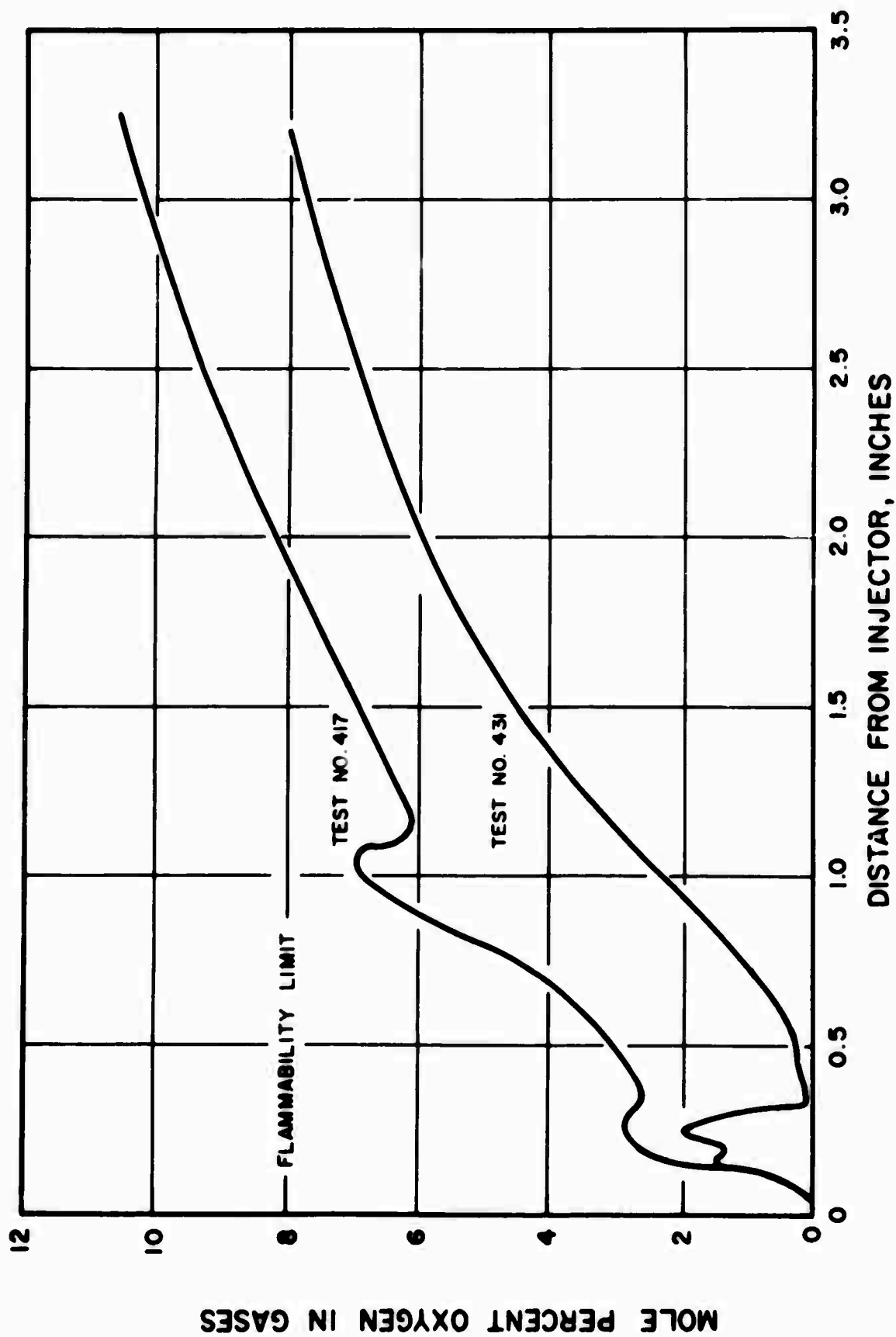
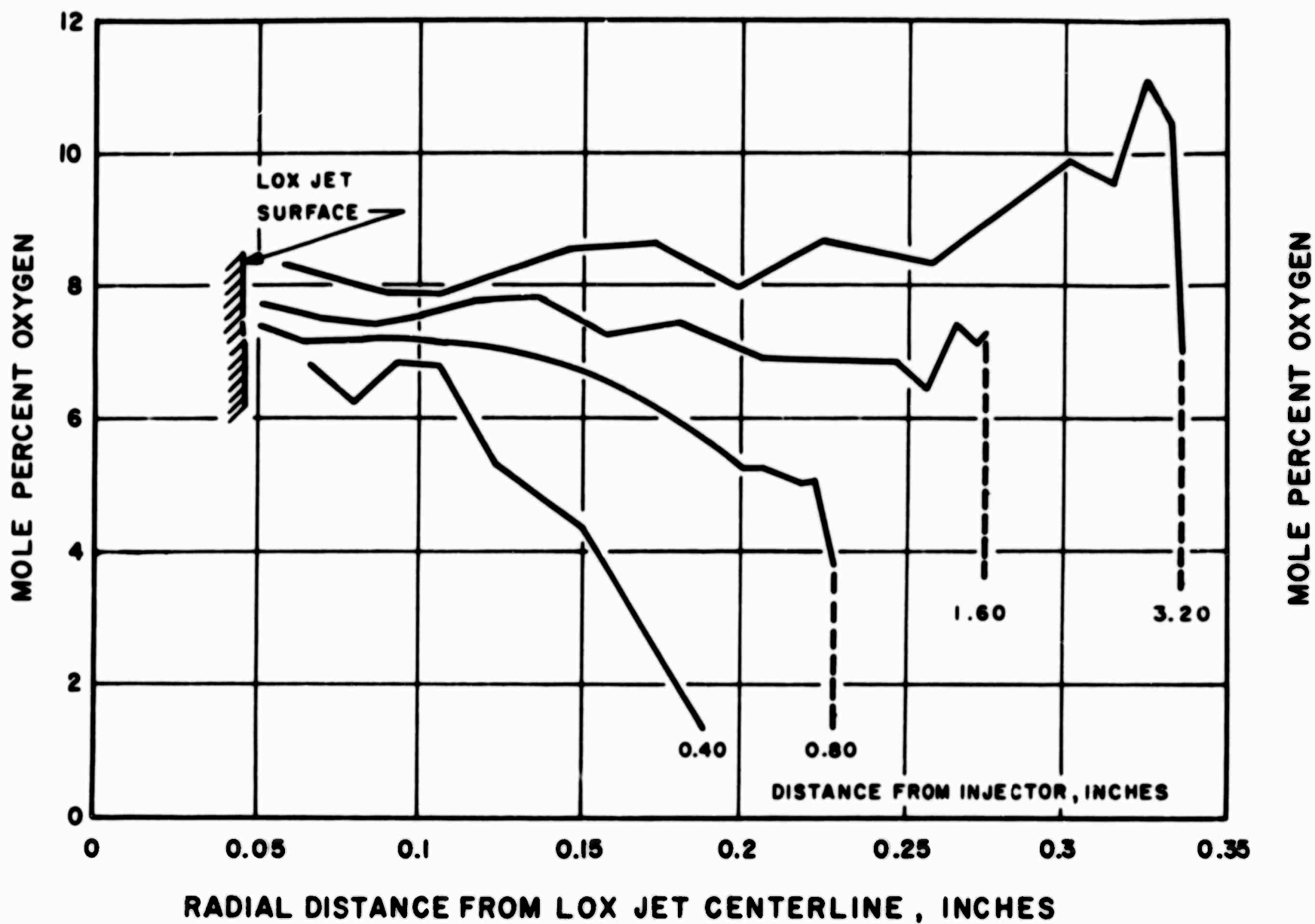


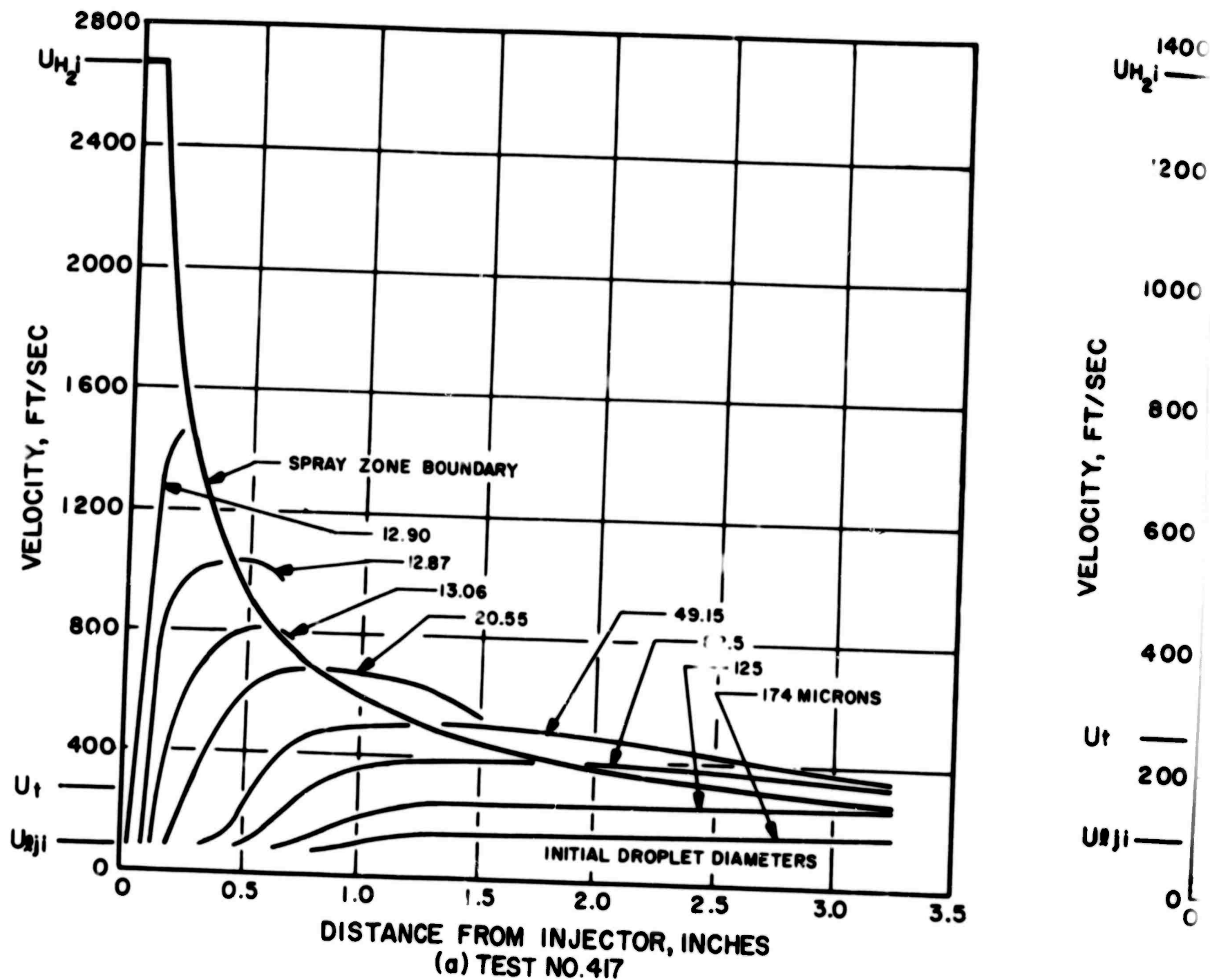
Figure 10. Oxygen Concentration in Gases at the Spray Zone Boundary, Nonburning Region





**Figure 11. Oxygen Concentration Profiles in the Nonburning Spray Zone at Various Distances From the Injector**

**B**







ROCKETDYNE



A DIVISION OF NORTH AMERICAN AVIATION, INC.

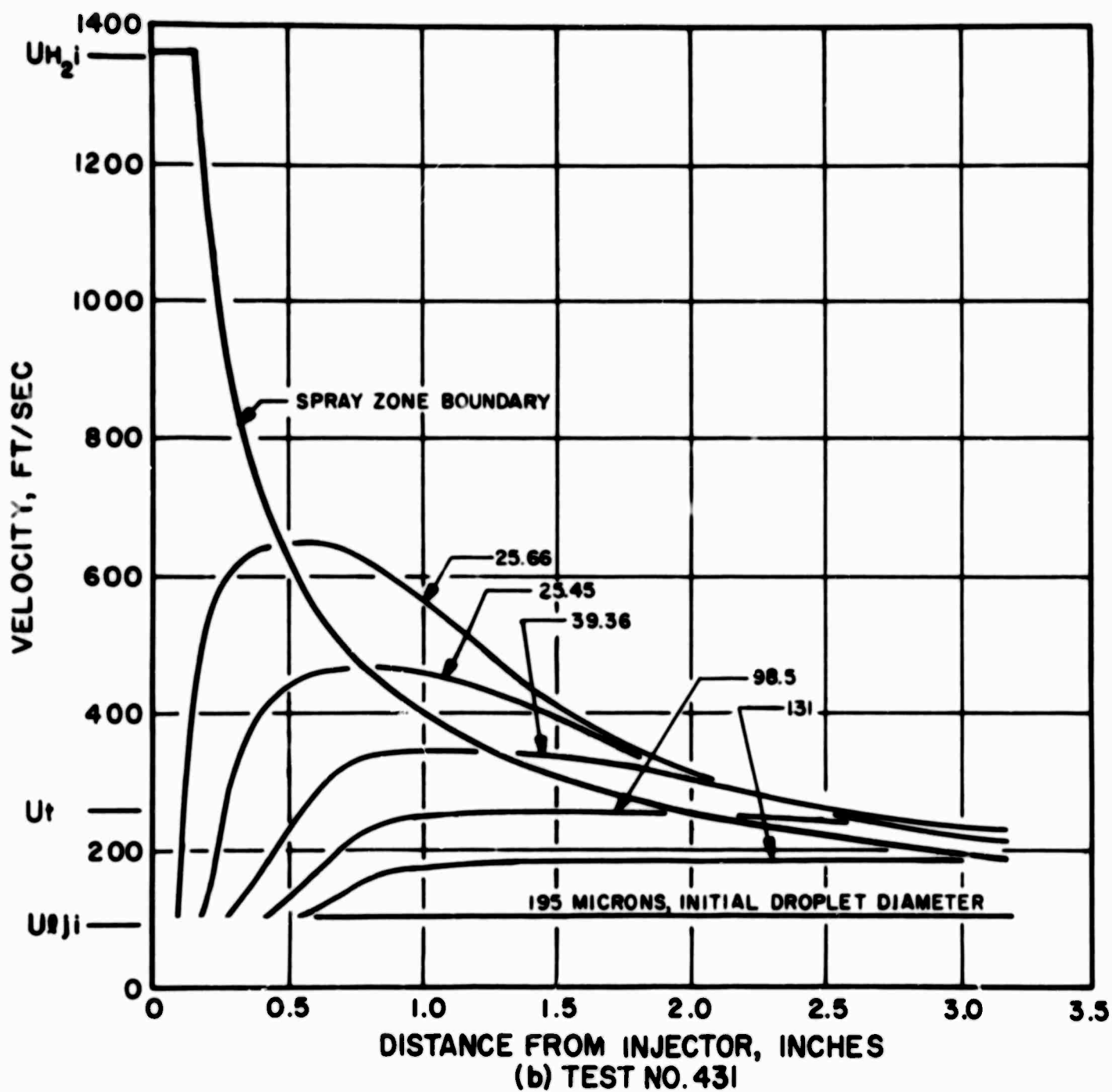


Figure 12. Velocities of the Spray Zone Boundary Gases and Selected Droplet Size Groups in the Nonburning Spray Zone

RR 64-29

B

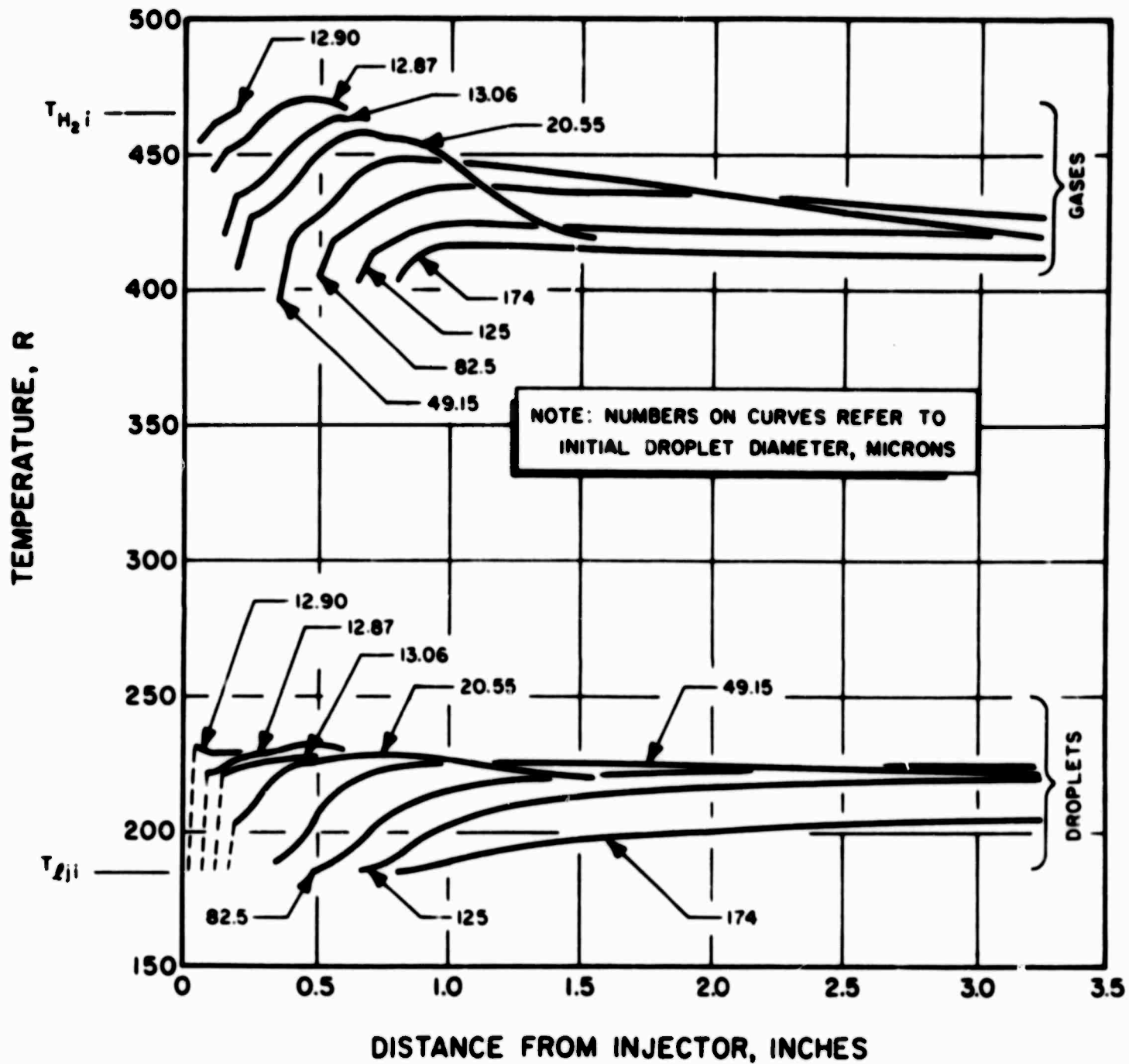


Figure 13. Spray Element Droplet and Gas Temperatures in the Nonburning Region (Test 417)

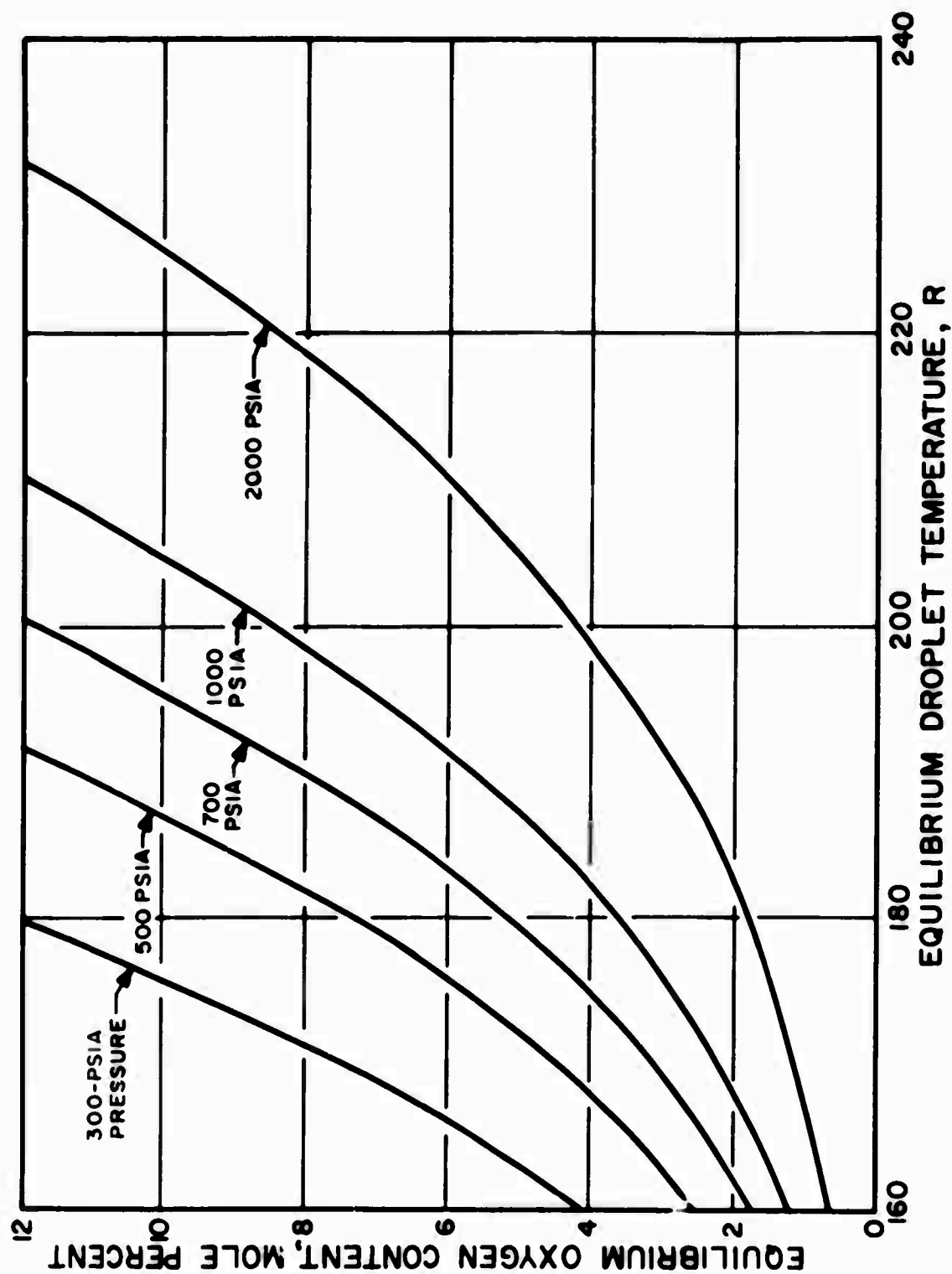


Figure 14. Maximum Equilibrium Oxygen Concentration in Hydrogen-Oxygen Gas Mixtures That Contain LOX Spray

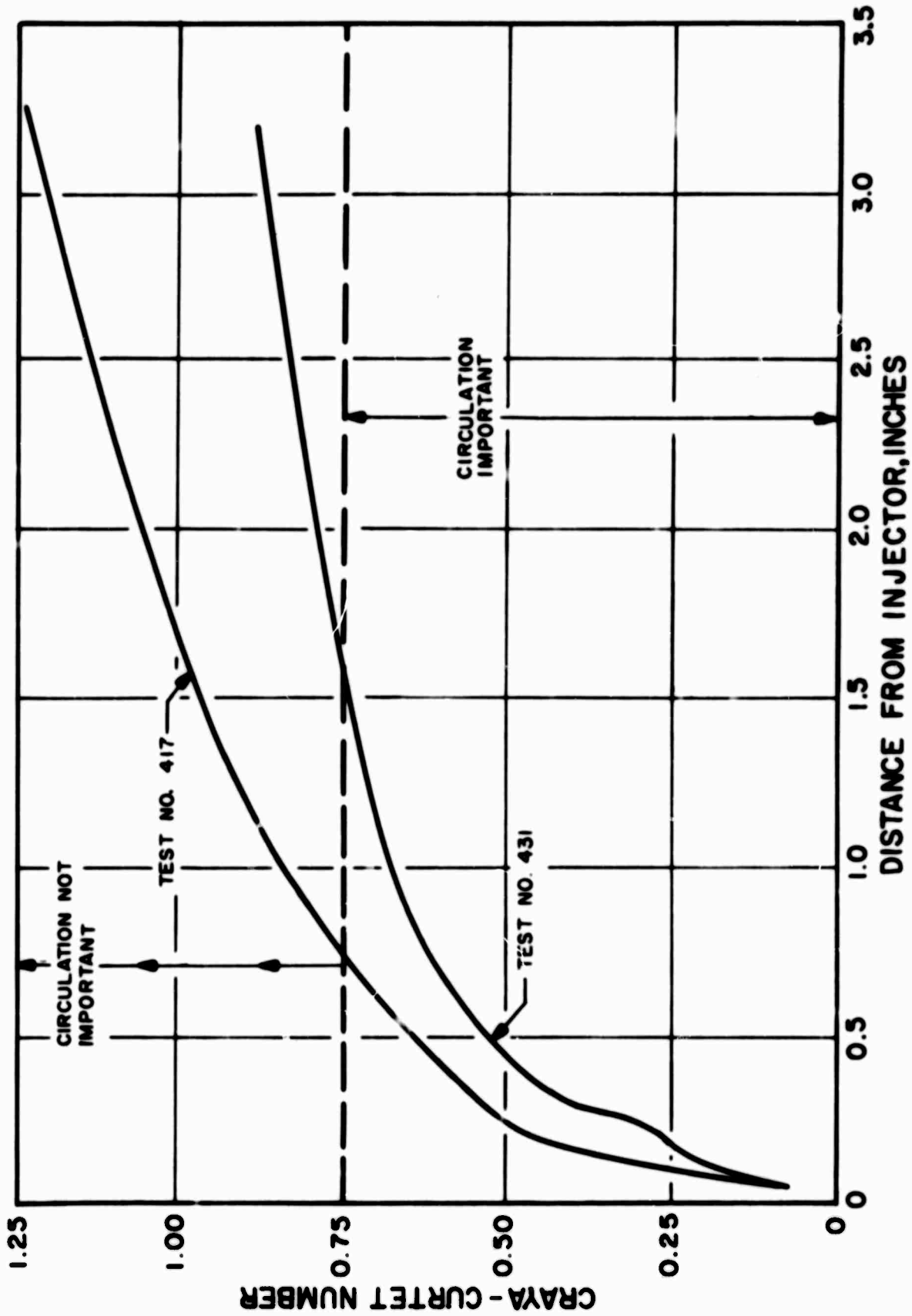


Figure 15. Calculated Craya-Curtet Number

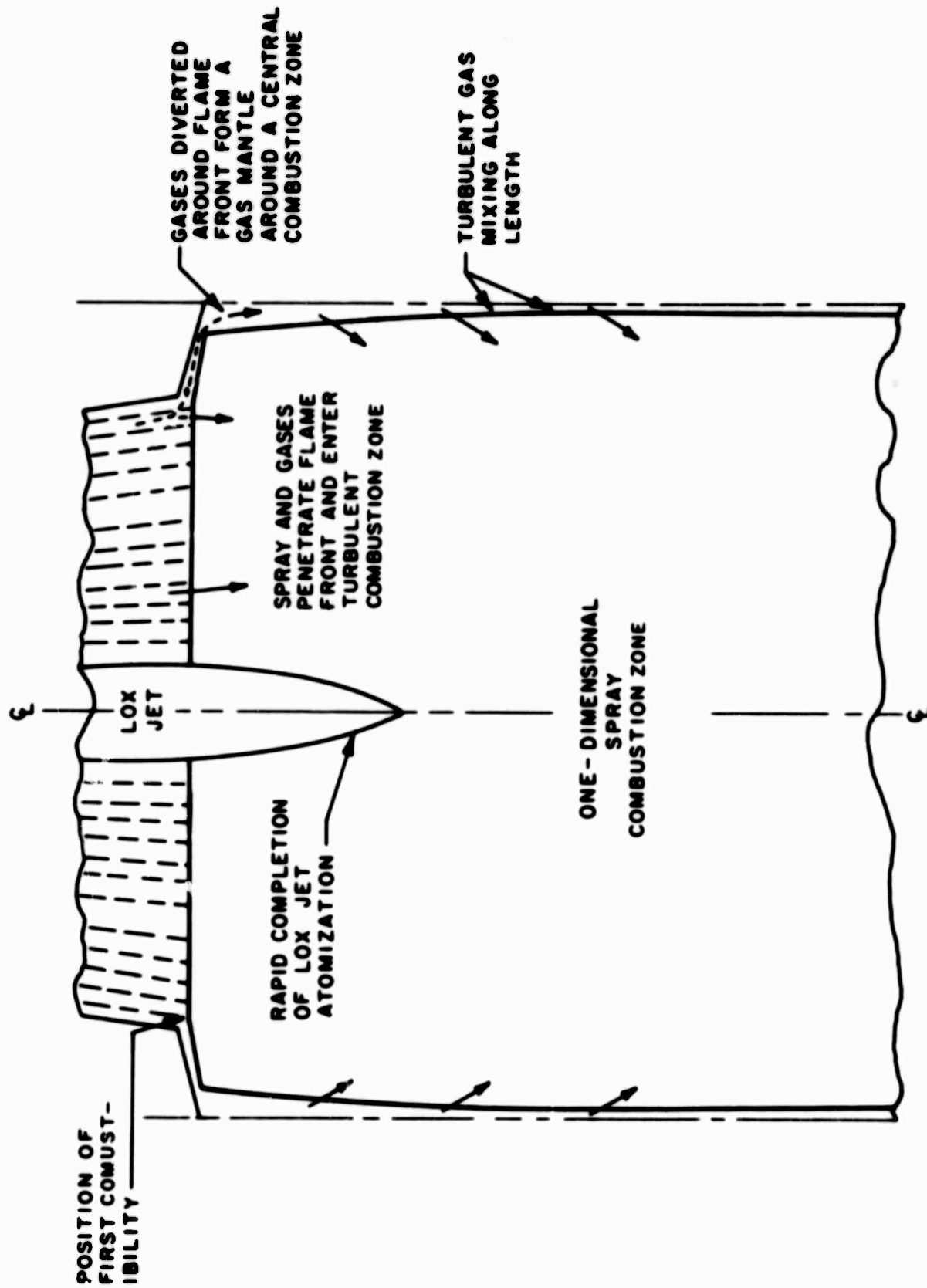
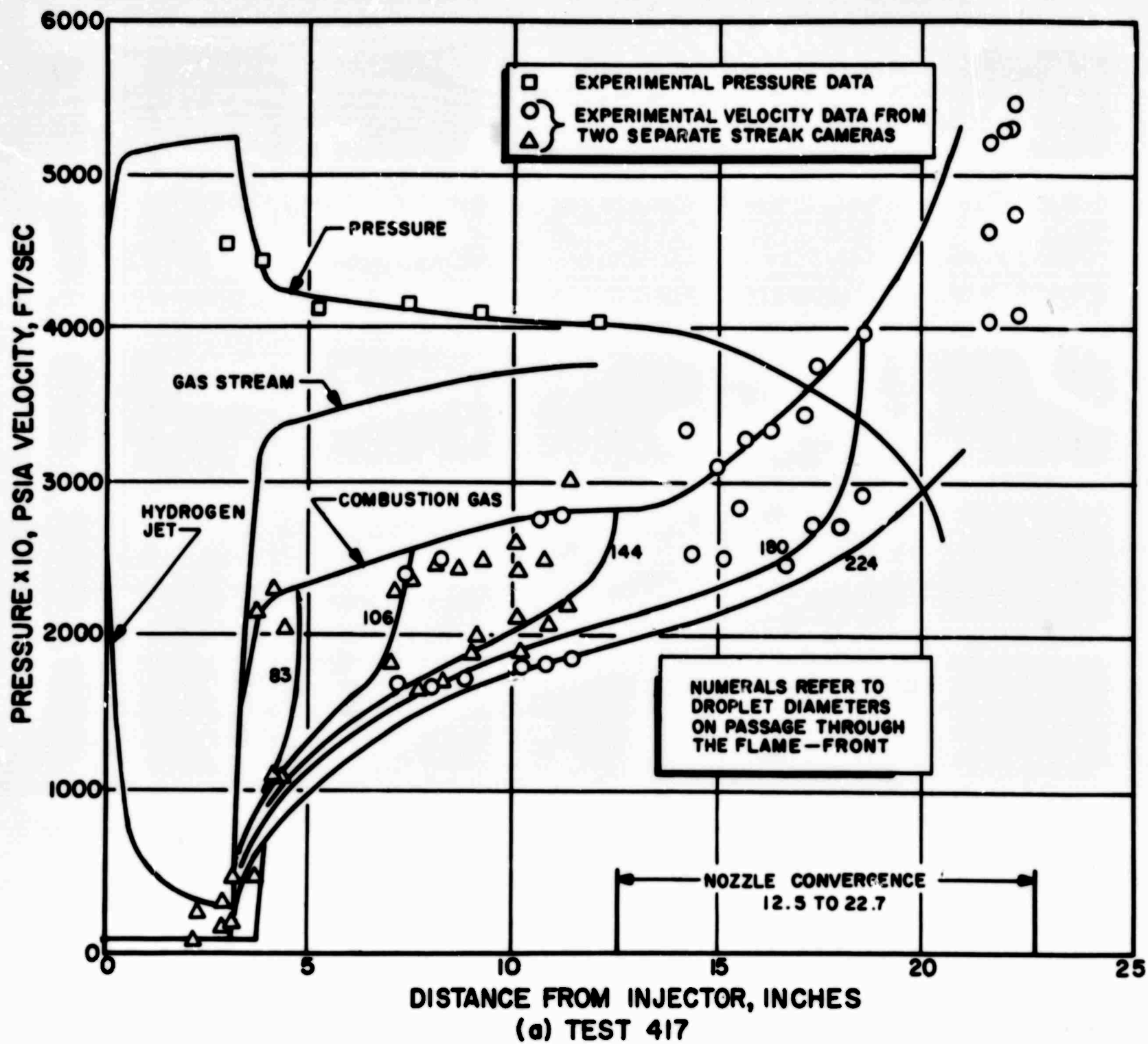


Figure 16. Calculated Combustion Region Characteristics, Test 417



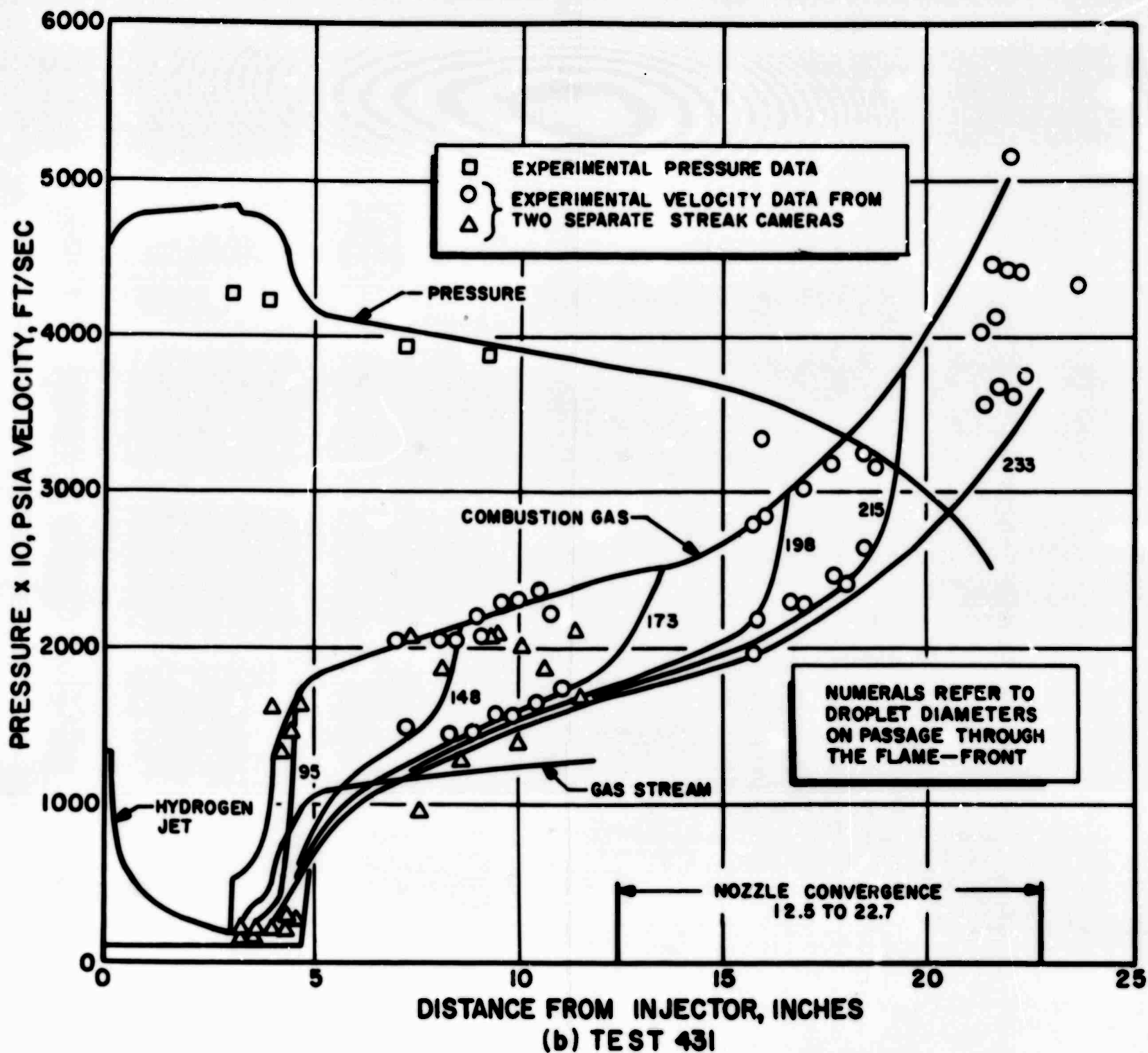


Figure 17. Comparison Between Experimental Data and Calculated Velocities and Pressures of the Best-Fit Cases

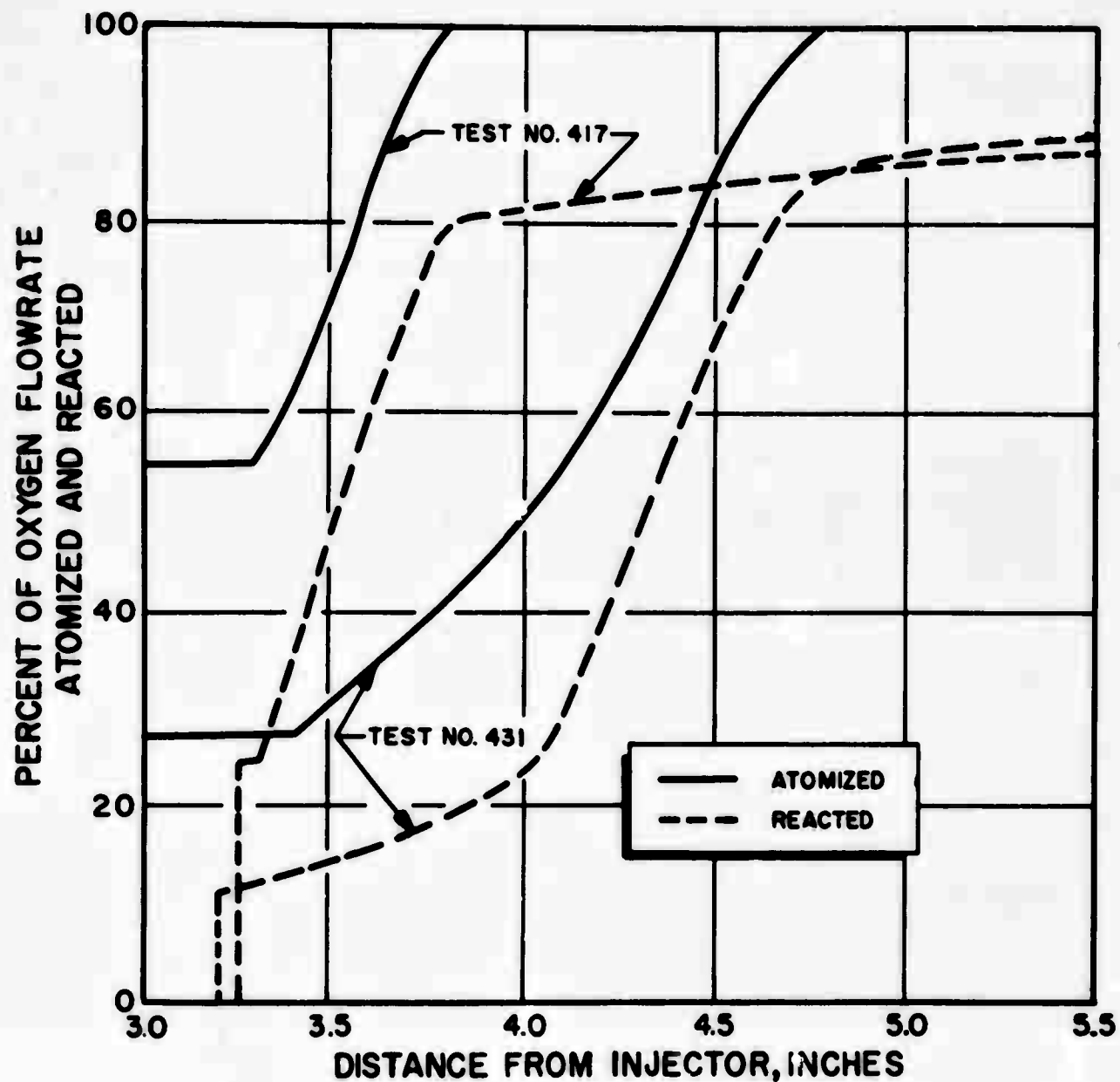


Figure 18. Progress of Oxygen Atomization and Reaction in the Combustion Region



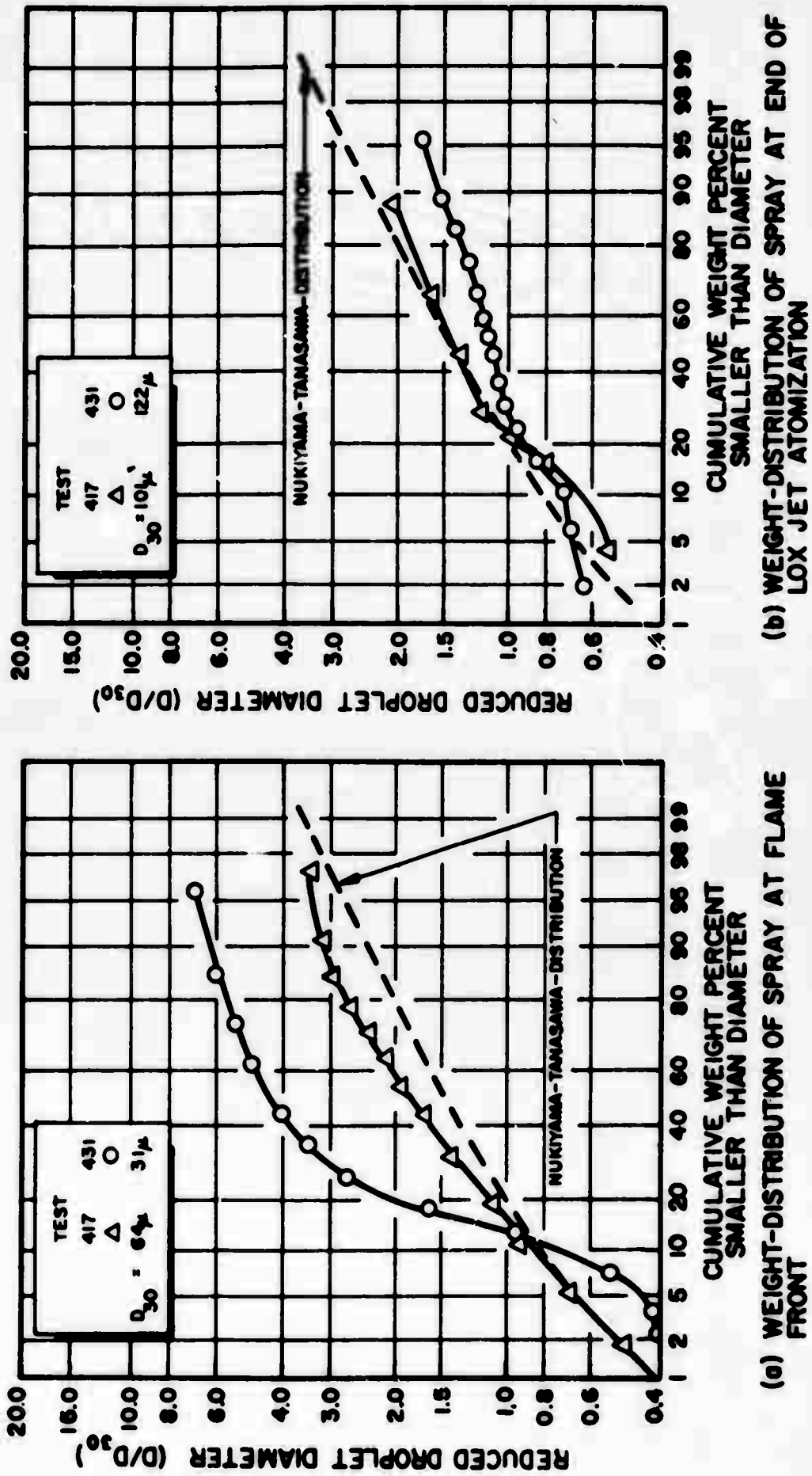
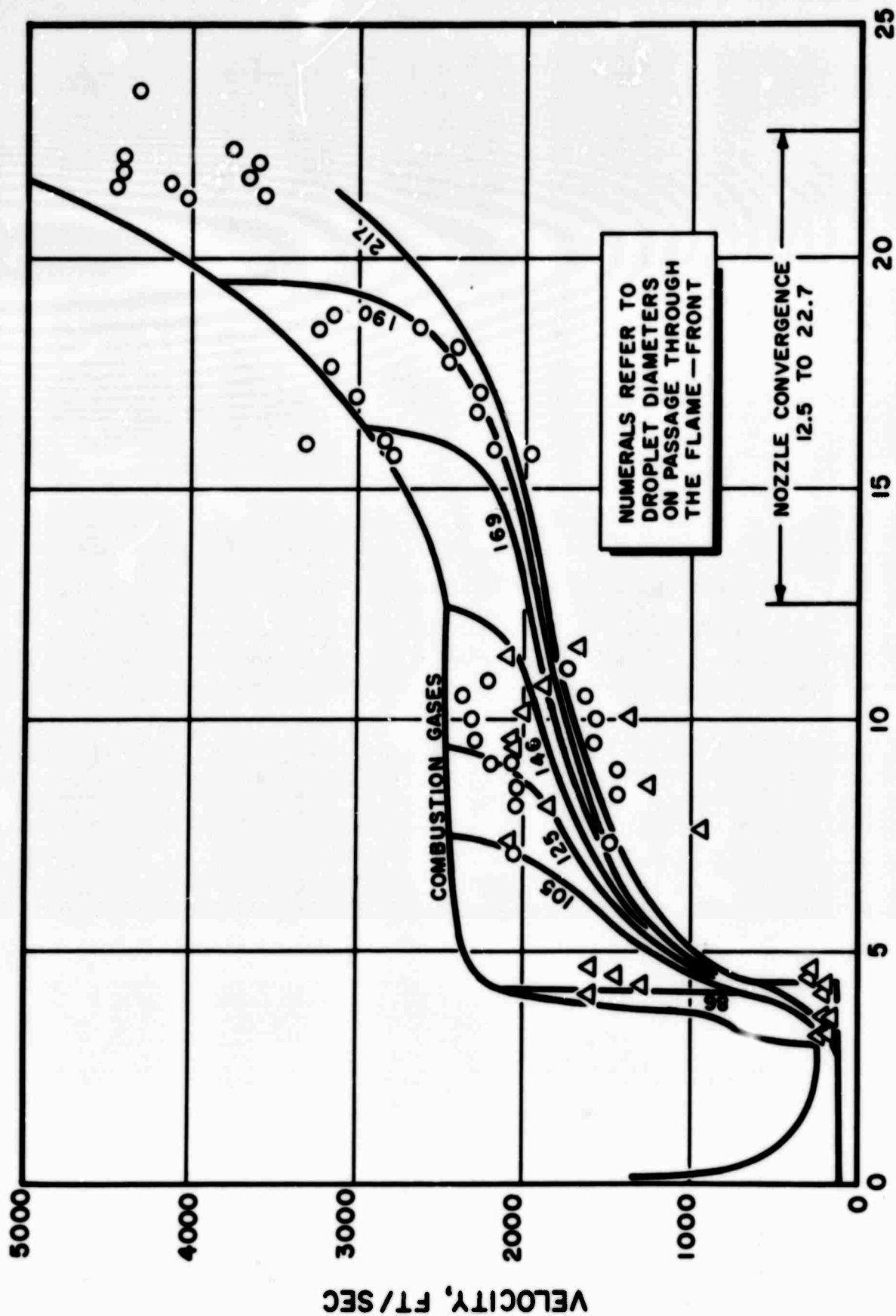
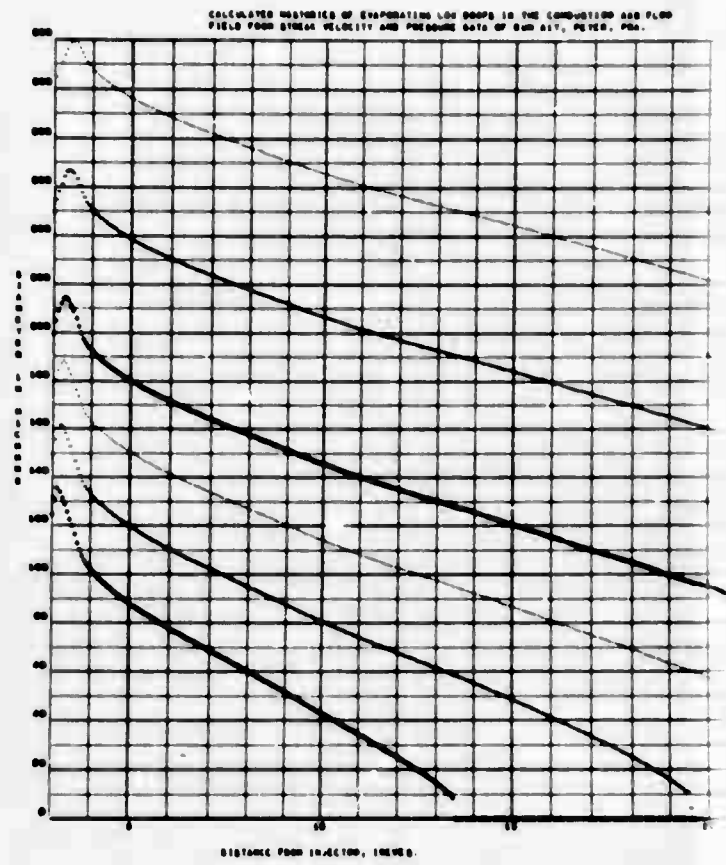
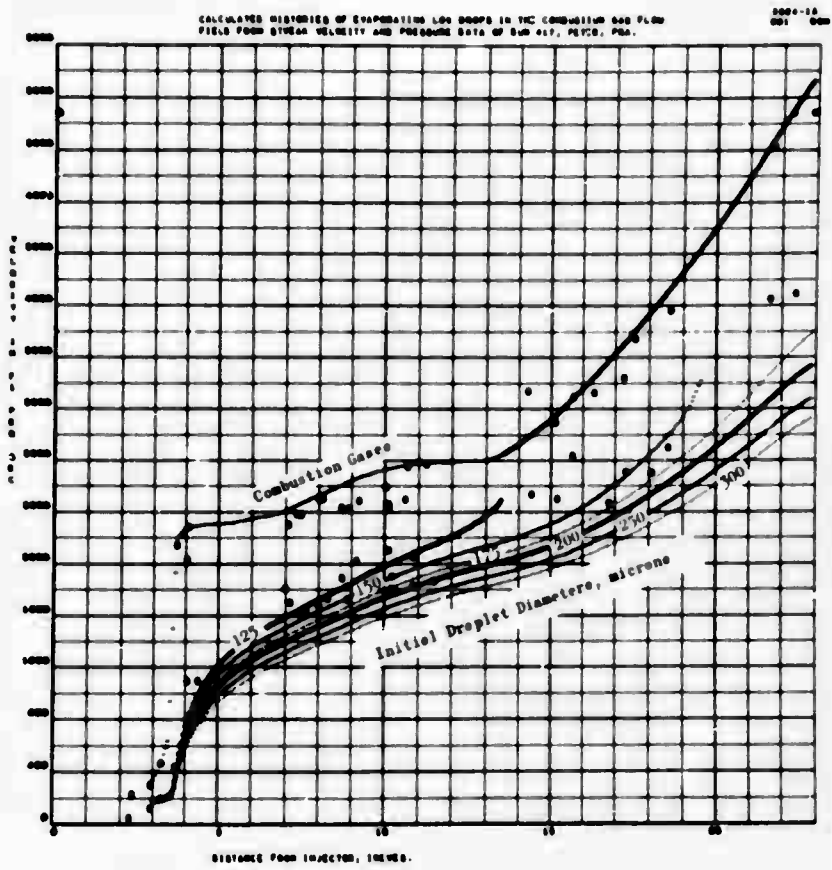


Figure 19. Calculated LOX Spray Characteristics (Combustion Region)



### DISTANCE FROM INJECTOR, INCHES

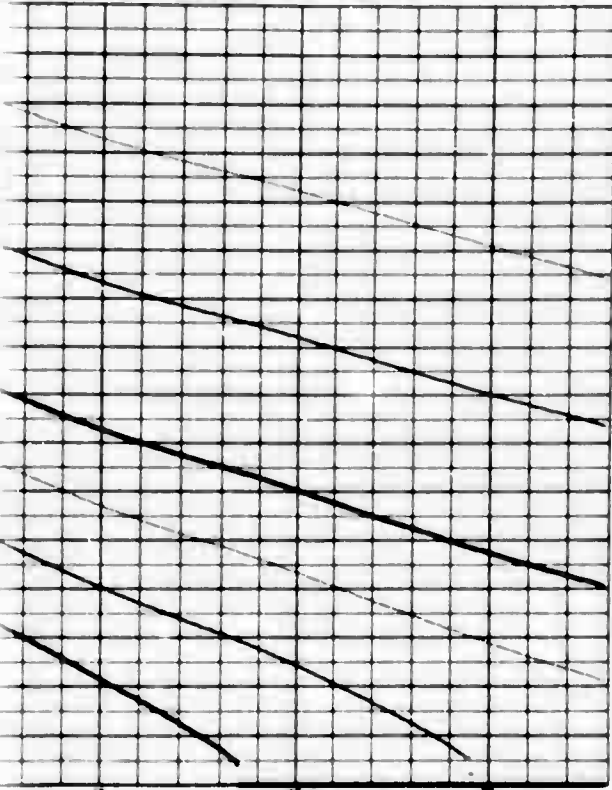
Figure 20. Comparison Between Experimental Data and Calculated Velocities When No Gaseous Mantle Flow was Provided (Test 431)





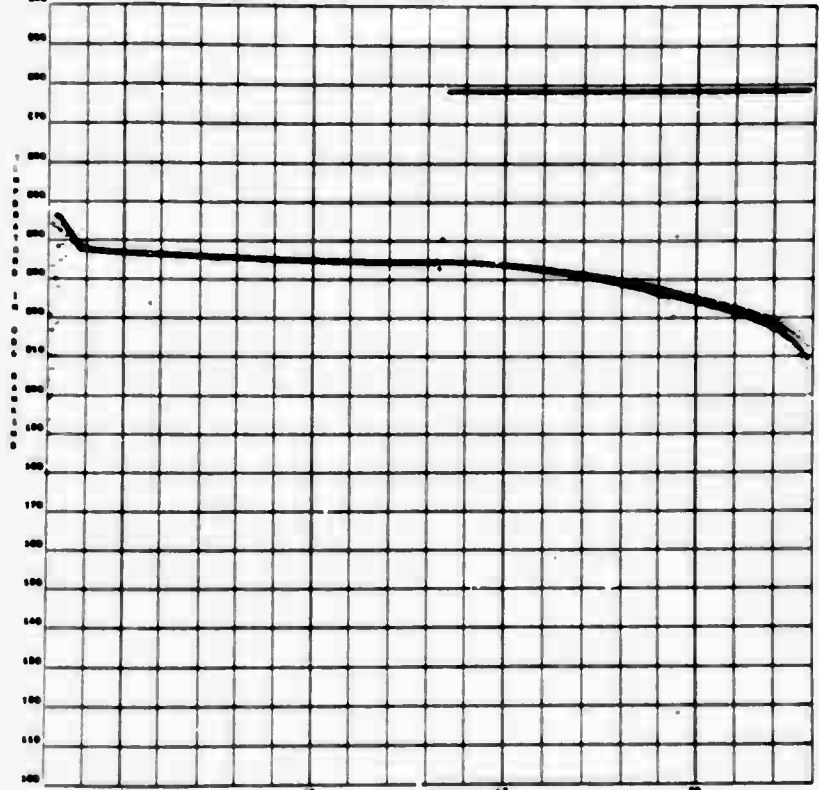
ROCKETDYNE • A DIVISION OF NORTH AMERICAN AVIATION, INC.

0007-10  
000 000  
CALCULATED BEHAVIORS OF EVAPORATING LIQ DROPS IN THE COMBUSTION GAS FLOW  
FIELD FROM STREAM VELOCITY AND PRESSURE DATA OF RUN 417, PETE, PRA.



DISTANCE FROM INJECTOR, INCHES.

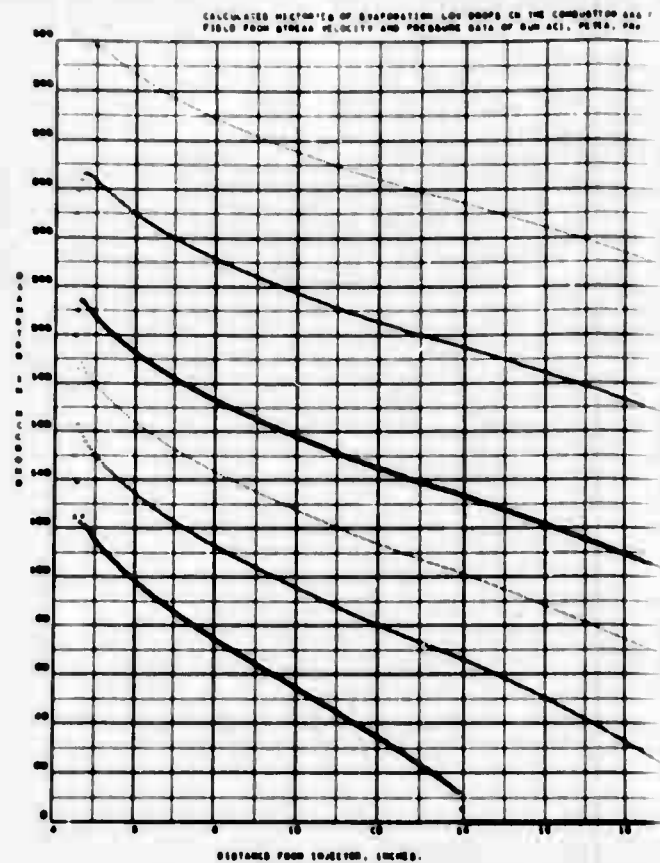
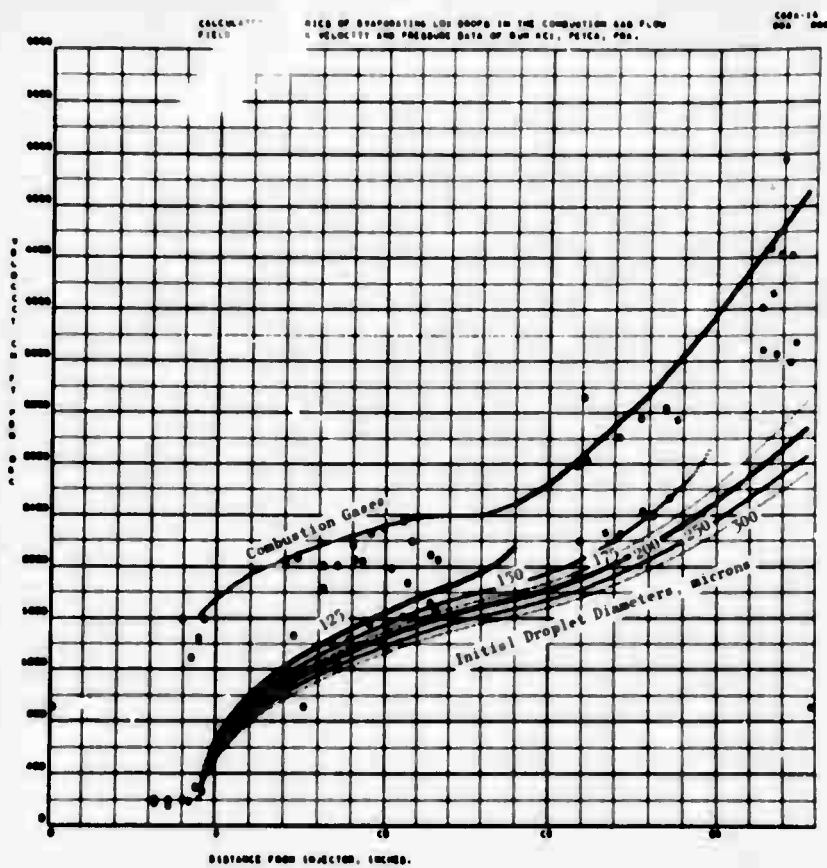
0007-10  
000 000  
CALCULATED BEHAVIORS OF EVAPORATING LIQ DROPS IN THE COMBUSTION GAS FLOW  
FIELD FROM STREAM VELOCITY AND PRESSURE DATA OF RUN 417, PETE, PRA.



DISTANCE FROM INJECTOR, INCHES.

Figure B-1. Calculated Behaviors of Various Sizes of Liquid Oxygen Droplets in a Combustion Gas Flow Field Prescribed from Run 417, PETE PRA

B





ROCKETDYNE • A DIVISION OF NORTH AMERICAN AVIATION, INC.

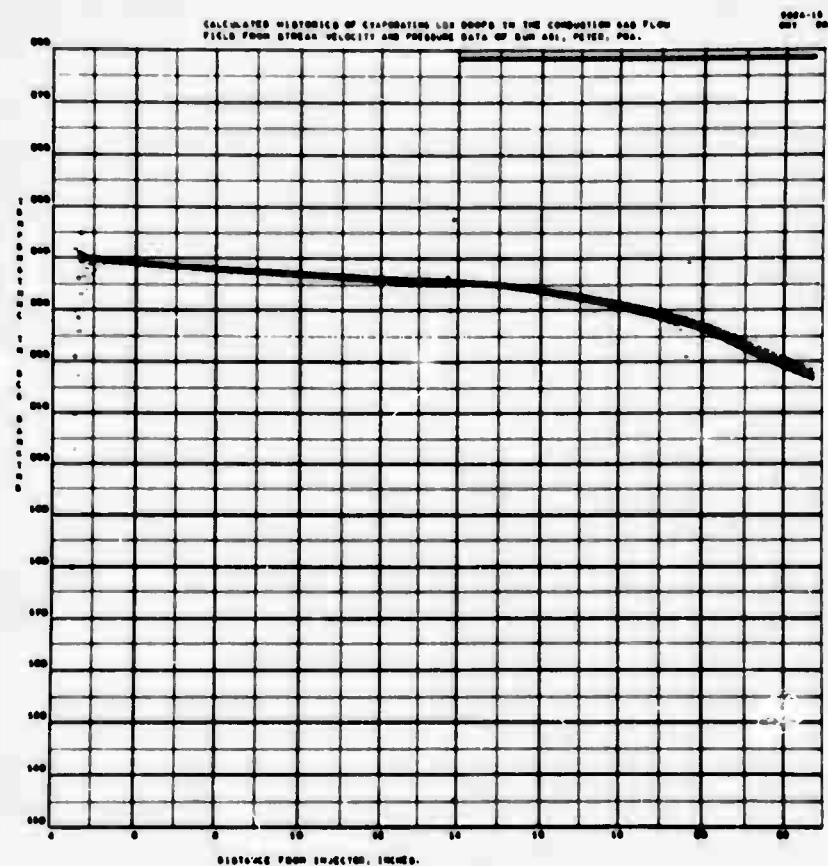
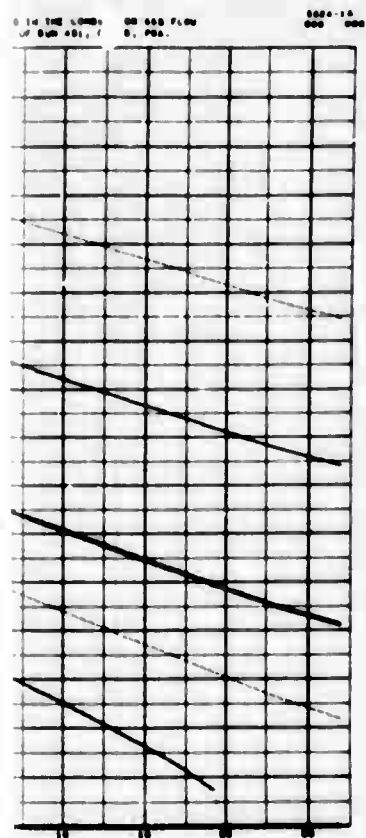


Figure B-2. Calculated Behaviors of Various Sizes of Liquid Oxygen Droplets in a Combustion Gas Flow Field Prescribed from Run 431, PETER, PRA

**B**

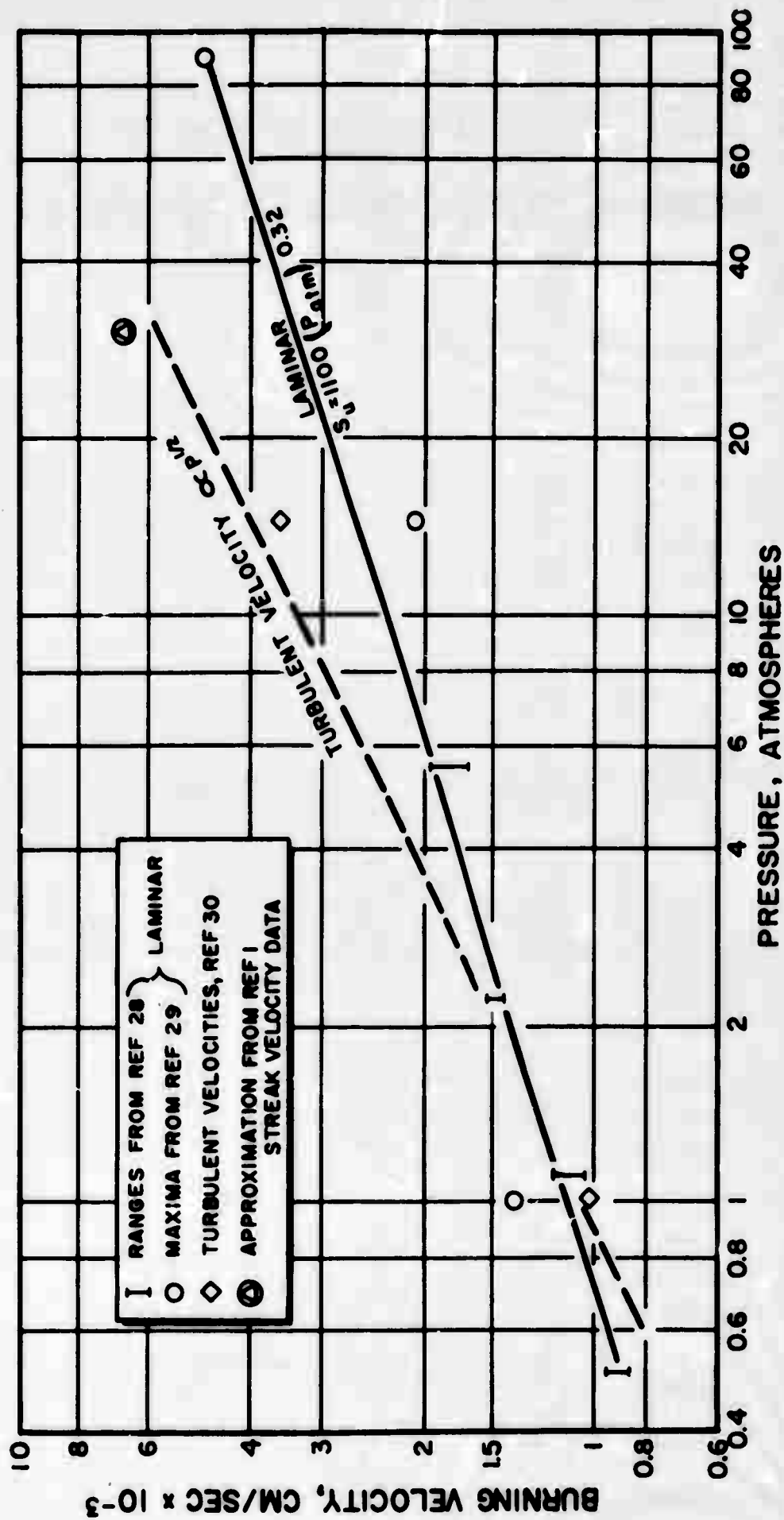


Figure C-1. Burning Velocities for Gaseous Mixtures of Hydrogen and Oxygen (Near Stoichiometric)

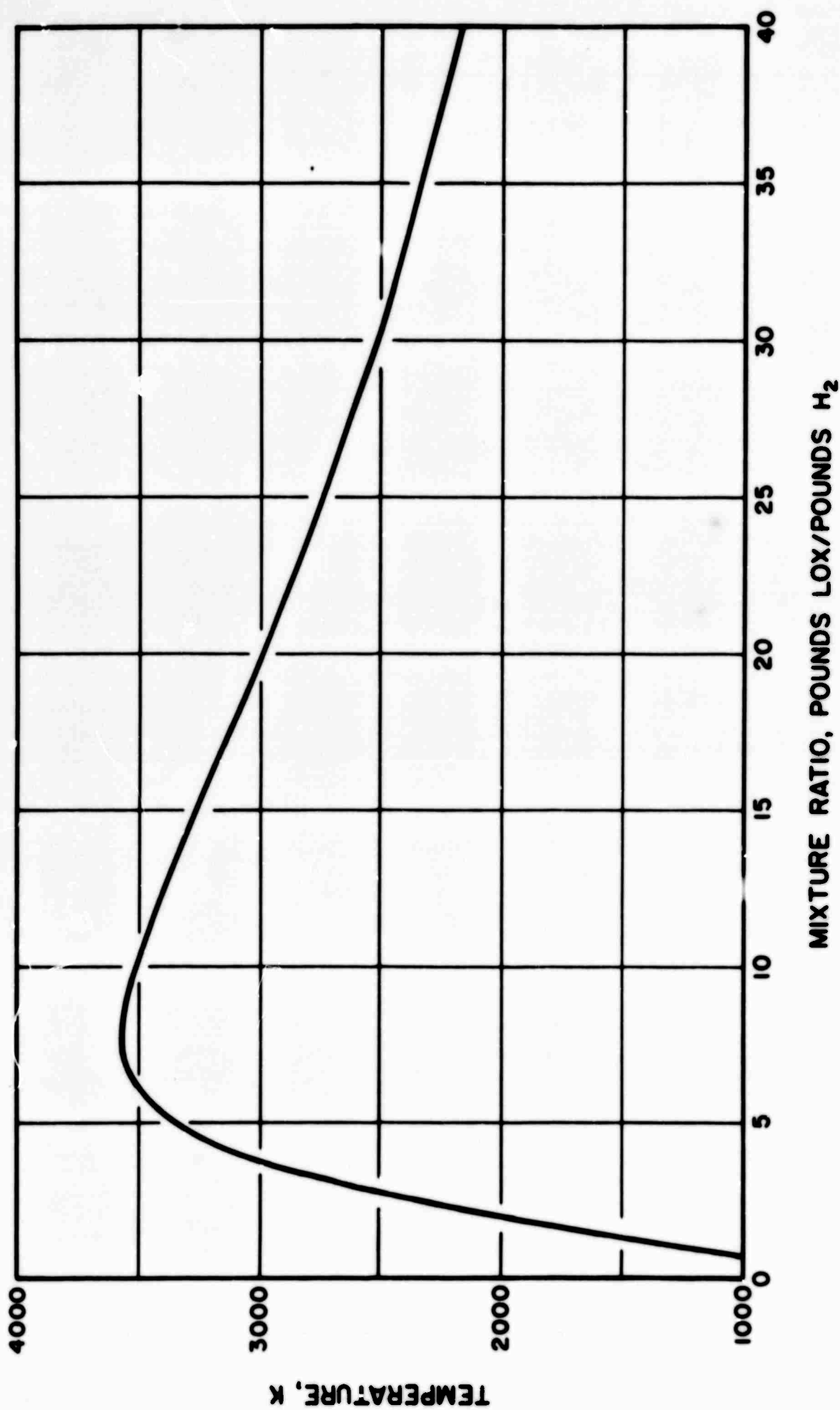


Figure D-1. Equilibrium, Stagnation Temperature for LOX/H<sub>2</sub> Combustion Product Gases at 550 Psia



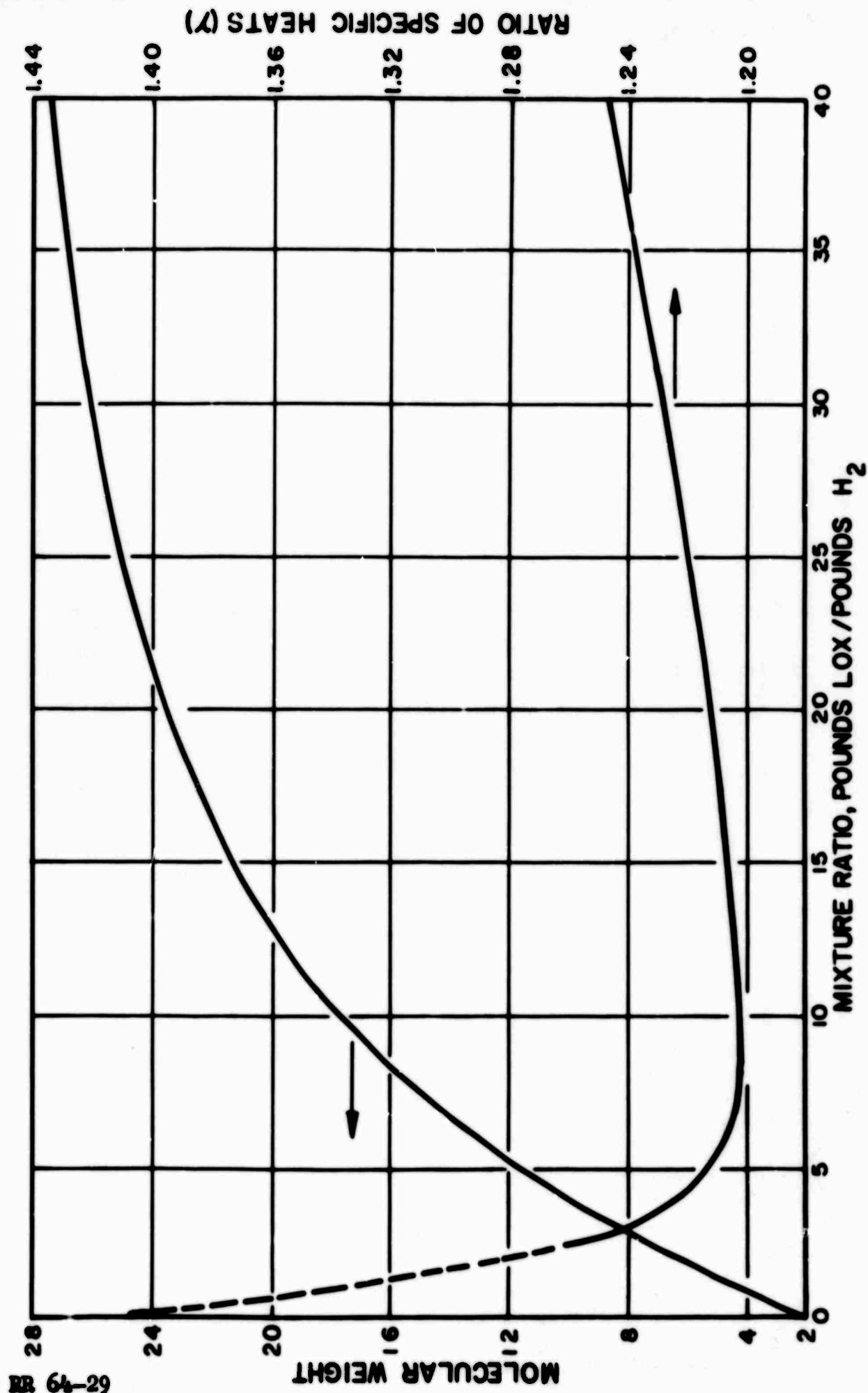


Figure D-2. Equilibrium Molecular Weight and Ratio of Specific Heats for LOX/ $H_2$  Combustion Product Gases at 550 Psia

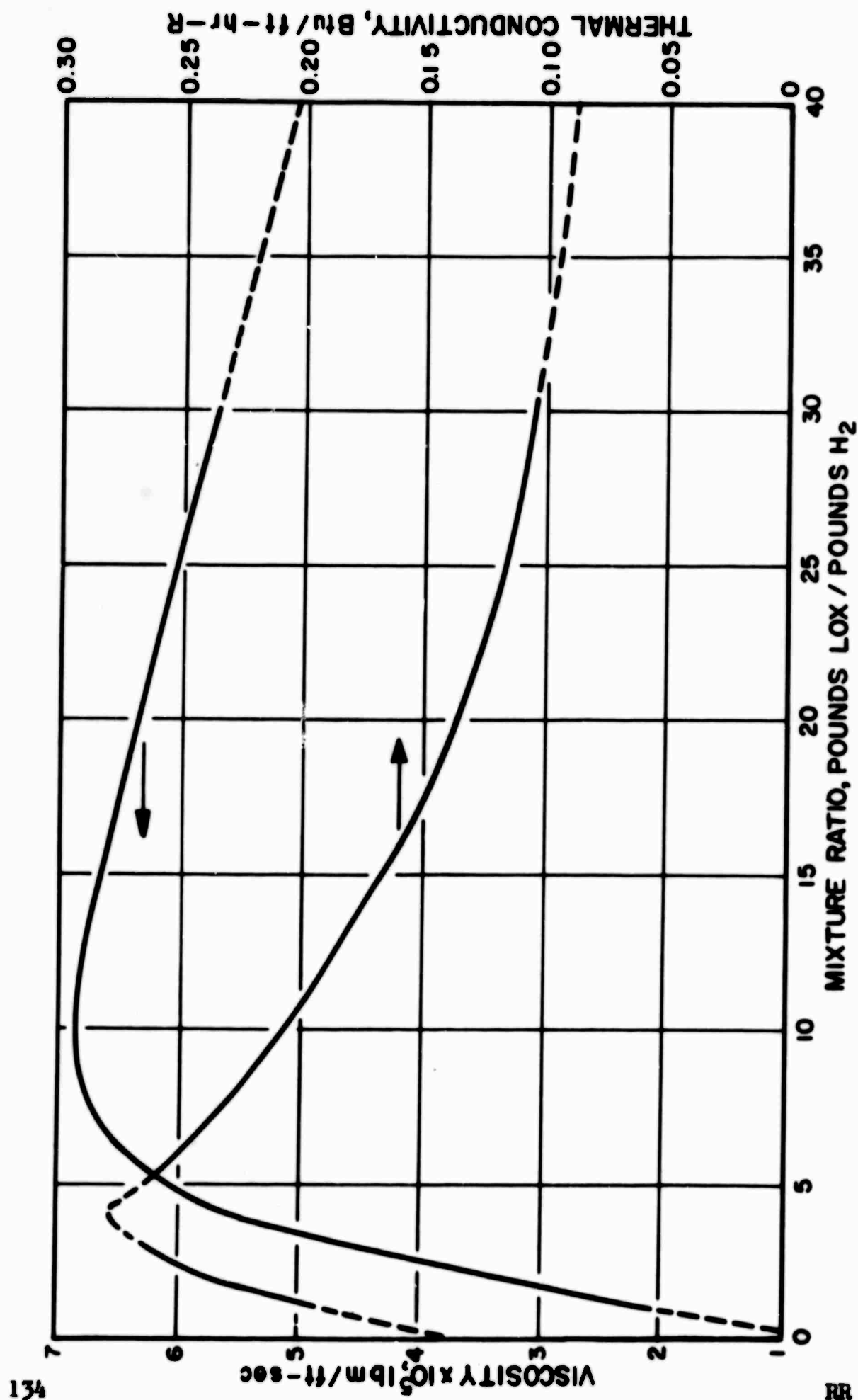


Figure D-3. Equilibrium Viscosity and Thermal Conductivity for LOX/H<sub>2</sub> Combustion Product Gases at 550 Psia

UNCLASSIFIED  
Security Classification

DOCUMENT CONTROL DATA - R&D

(Security classification of title, body of abstract and indexing annotation must be entered when the overall report is classified)

1. ORIGINATING ACTIVITY (Corporate author) ROCKETDYNE, a Division of North American Aviation, Inc., 6633 Canoga Avenue, Canoga Park, Calif.		2a. REPORT SECURITY CLASSIFICATION UNCLASSIFIED	
		2b. GROUP N/A	
3. REPORT TITLE Steady-State Rocket Combustion of Gaseous Hydrogen and Liquid Oxygen. Part II: Analysis for Coaxial Jet Injection			
4. DESCRIPTIVE NOTES (Type of report and inclusive dates) N/A			
5. AUTHOR(S) (Last name, first name, initial) Combs, L. Paul and Schuman, Merlin D.			
6. REPORT DATE March 1965		7a. TOTAL NO. OF PAGES 126 + vi	7b. NO. OF REFS 32
8a. CONTRACT OR GRANT NO. AF49(638)-817		8a. ORIGINATOR'S REPORT NUMBER(S) Research Report No. 64-29	
A. PROJECT NO. 9751		8b. OTHER REPORT NO(S) (Any other numbers that may be assigned this report) N/A	
9. AVAILABILITY/LIMITATION NOTICES <del>Qualified requestors may obtain copies of this report from DDC.</del> <del>Foreign announcement and dissemination of this report by DDC is not authorized.</del>			
11. SUPPLEMENTARY NOTES N/A		12. SPONSORING MILITARY ACTIVITY Air Force Office of Scientific Research Directorate of Engineering Sciences United States Air Force Washington 25, D. C.	
13. ABSTRACT  Simultaneous equations describing rocket propellant injection, atomization, mixing, vaporization, and combustion are formulated for a cylindrical liquid oxygen jet surrounded by an annular gaseous hydrogen stream. The formulation is based on division of the combustion chamber into a nonburning region near the injector and a combustion region further downstream. Processes in the non-burning region are required to satisfy certain combustibility criteria before combustion is possible. The propellants then pass through a plane flame front into the combustion region. A simplified treatment of turbulent mixing between unlike reacting gas streams, one of which contains a liquid oxygen spray, characterizes the combustion region model. Solutions of the system of equations, obtained with a digital computer program, are detailed, discussed, and compared favorably with experimental information from Part I.			

DD FORM 1473  
1 JAN 64

UNCLASSIFIED  
Security Classification